MODELING OF PERMAFROST AND GAS HYDRATE STABILITY ZONE WITHIN ALASKAN ARCTIC SHELVES AND CONTINENTAL MARGINS

By

Sergei I. Pokrovsky

RECOMMENDED:

Advisory committee Chair

Department Head

APPROVED:

Dean, College of Science, Engineering and Mathematics

Dean of Graduate School

December 8, 2003

Date

MODELING OF PERMAFROST
AND GAS HYDRATE STABILITY ZONE
WITHIN ALASKAN ARCTIC SHELVES AND CONTINENTAL MARGINS

A

THESIS

Presented to the Faculty

of the University of Alaska Fairbanks

in Partial Fulfillment of the Requirements

for the Degree of

MASTER OF SCIENCE

By

Sergei I Pokrovsky, B.S.

Fairbanks, Alaska

August 2003

ABSTRACT

A mathematical model was used to determine the behavior of the thermal regime and temperature and pressure conditions due to climate and sea level variations of the gas hydrate stability zone formation at four sites within the Alaskan Arctic Shelf.

Two soil types, coarse-grained and fine-grained, and three types of programs were used. The programs were distinguished by whether or not they took unfrozen water and latent heat into account.

Simulations suggest the presence of subsea permafrost in a vast area of shelf near Prudhoe Bay. Near Barrow and Lonely subsea permafrost extends up to several tens of kilometers offshore, while subsea permafrost near Cape Thompson almost completely disappeared during the last marine transgression. Distribution of subsea permafrost varies with soil type, thermal properties and geothermal heat flow. The possible presence of methane gases in a pore space of the material influences the thermal regime and permafrost distribution. Simulations indicate that a Gas Hydrate Stability Zone can exist at depths from 220 m to 1100 m. Possible formation and presence of gas hydrates in the sediments changes the thermal regime significantly; therefore the shape of subsea permafrost depends on whether or not gases are present in the sediments.

TABLE OF CONTENTS

LIST OF FIGURES

LIST OF TABLES

ACKNOWLEDGEMENTS

I would like to thank my advisor Professor Vladimir Romanovsky for the guidance, support, encouragement, and giving me the opportunity to conduct the exciting research.

Professor Tom Osterkamp, being my co-advisor, helped me tremendously by providing his expertise in modeling of thermal regime of subsea permafrost and gas hydrates investigations.

I specially want to thank the members of the advisory committee, Professor Yuri Shur and Jim Beget for their guidance and encouragement.

I was very fortunate to work with my colleague Dr. Gennadiy Tipenko, who helped me with mathematical modeling.

This research was sponsored by National Science Foundation and State of Alaska.

CHAPTER 1

Introduction

1.1 General

Past sea level history indicates that the continental shelves of the Arctic Ocean were exposed to cold air temperatures, which caused permafrost to form. Subsequent increases in sea level have resulted in the ocean transgression on land. As a result, the permafrost, that has been formed during shelf exposure, was covered by the ocean during this transgression. Generally, permafrost has not had enough time to fully respond to the new thermal and salt boundary conditions at sea bed. In addition, the sea bed temperatures within most of the Alaskan Arctic shelf appear to be negative (Osterkamp and Harrison, 1976). After submergence, subsea permafrost degrades, thawing from the seabed downward by the influx of salt and heat as a result of the new boundary conditions and from the bottom by geothermal heat. The thawing rates at both top and bottom are slow. Northwest of Prudhoe Bay at distances up to several kilometers or more offshore, thawing rates are of the order of a centimeter per year (Lachenbruch et. al., 1982). Consequently, the time required to thaw several hundred meters of subsea permafrost after submergence may approach tens of thousands of years.

The presence of subsea permafrost on the Siberian Arctic shelf was established by Are (1976). In North America, early observations were based on studies made near Barrow, Alaska (Lachenbruch et. al., 1962) that suggested that ice-bearing permafrost could be found near shore. Since the discovery of large petroleum reserves at Prudhoe Bay in the 1960's, offshore areas have been the sites of intense geophysical exploration and of exploratory drilling and production.

Negative temperatures have been observed in the several holes drilled in the coastal waters of the Chukchi Sea (Osterkamp and Harrison, 1982). The study of soil temperatures and limited borehole data indicates that ice-bearing subsea permafrost is probably thin or absent in some areas of the continental shelf except near the coast and beneath the northernmost area of the Chukchi shelf (Osterkamp and Harrison, 1982; Osterkamp et. al., 1987b).

Because the definition of permafrost is stricly based on the temperature of the material being below 0°C, the sea bed can be considered as subsea permafrost even though it is not ice-bonded due to a depressed freezing point of the soil solution caused by the presence of salts (Osterkamp et. al., 1989). Therefore, areas with presence of subsea permafrost on continental shelves of Alaska can exist and should be investigated by different methods including mathematical modeling.

Gas hydrates (clathrate hydrates of natural gases) are solids that consist of water and gas molecules. The water molecules are arranged in nearly spherical, cage-like structures that are hydrogen bonded and contain, at most, one guest molecule bound by Van der Waals forces (Sloan, 1990). While methane, propane and other gases can form gas hydrates, methane gas hydrates appear to be most common in nature (Kvenvolden, 1988). Methane hydrates may occur wherever methane and water exist in close proximity at low temperature and elevated pressures. These conditions are present in permafrost regions and beneath the sea in outer continental margins. Methane hydrates are thought to be widespread in both onshore permafrost regions and in the shallow continental shelves of the Arctic Ocean, where subsea permafrost is found (Kvenvolden, 1988).

In saturated methane hydrate, the molar ratio of methane to water is about 1:6,

which leads to a volumetric ratio af about 164:1 (Davidson et. al., 1978). Hence, decomposition of a gas hydrate can lead to the generation of relatively large volumes of gas at atmospheric pressure. The total reservoir of methane carbon sequestered in gas hydrates associated with permafrost is about 540 Gt (Kvenvolden and Grantz, 1990),which exists typically at depths of 200 m or more. In the same time, entire world arctic ecosystems only store about 61 Gt of carbon near the surface (Oeschel, 1989).

As already mentioned, gas hydrate in onshore arctic environment is typically closely associated with permafrost. It is generally believed that thermal conditions conducive to the formation of permafrost and gas hydrate have persisted in the Arctic since the end of the Pliocene (about 1.88 Ma) (Collett and Dallimore, 2000). Geologic studies by MacKay (1972) and Molochushkin (1978) and thermal modeling of subsea permafrost (Osterkamp and Fei, 1993) also indicate that permafrost and gas hydrates may exist within the continental shelf of the Arctic Ocean. Also, the potential presence of gas hydrates in the sediments of the Alaskan Arctic shelf can be supported by the analysis of mud-log gas-chromotographic data from 320 wells carried out by Collett (Collett, 1993). These studies show that methane is the dominant hydrocarbon gas in the near-surface sedimentary rocks of the North Slope. Analysis of gas evolved from recovered gas hydrate samples in the Prudhoe Bay area suggests that the in-situ gas hydrates are composed mostly of methane (87 to 99%) (Collett and Dallimore, 2000). Therefore methane gas chemistry is generally assumed for most assessments of gas hydrate stability conditions in northern Alaska (Collett and Dallimore, 2000).

Subsea permafrost and gas hydrates derive their economic importance from the current interest in the development of offshore petroleum resources in the

continental shelves of Alaska. Being part of a very sensitive arctic ecosystem, subsea permafrost and potential volumes of gas hydrate play a very important role in global climate. Current climate models of greenhouse warming predict that climatic change will be amplified in the Arctic and most likely occur there first (NAS, 1986). Permafrost temperatures reported by Osterkamp et. al., (1987a), Osterkamp and Romanovsky (1999) in Alaska indicate that some areas of the Arctic have already warmed 2 – 4 °C during last century, either as a result of greenhouse effect, or due to other causes. Since most subsea permafrost is degrading, any addition of heat will cause additional thawing, that will shrink the Gas Hydrate Stability Zone (GHSZ). As a result, emission of methane can occur. The potential amount of gas in Gas Hydrate Stability Zone is huge, so possible emission of gas from GHSZ due to change in climate poses a real hazard to ecosystems. Therefore, methane hydrates are not only of interest as a potential resource of natural gas but also as a possible source of atmospheric methane that could be released by climate warming. On the other hand, from an engineering point of view, the thawing makes subsea permafrost a difficult and serious problem for development. The design, construction, and operation of coastal facilities and structures founded on the seabed, subsea pipelines, and wells drilled for exploration and production must take into account the presence and characteristics of subsea permafrost. Thus, the study of subsea permafrost is important from both engineering and scientific points of view (Osterkamp, 2001). Scientific problems related to subsea permafrost include developing an understanding of the subsea permafrost properties and thermal regime, heat and salt movement in it, and the release of methane due to permafrost degradation.

1.2 Purpose

A mathematical model was developed by Gennady Tipenko based on previous works (Romanovskii and Tipenko 1998, Tipenko et. al., 1999, Romanovskii et. al., 1999) to determine the onshore and offshore temperature regime dynamics and temperature and pressure conditions within the gas hydrate stability zone. This thesis applies the model to four sites: Prudhoe Bay, Lonely, Barrow and Cape Thompson within the Alaskan Arctic shelf due to climate and sea level changes. Also the possible effect on global climate of the potential gas emission from destabilized gas hydrate was studied in this work. To achieve this goal, the estimation of gas volumes that could be released from the GHSZ due to its dynamics will be made in several key onshore-offshore profiles within Alaskan Arctic shelf. Also, an analysis of the relationship between subsea permafrost dynamics and GHSZ dynamics will be made. The major purpose of this thesis is to analyze the formation and evolution of both onshore/offshore permafrost and the gas hydrate stability zone under the influence of long-term climate fluctuations on the earth surface and sea regression and transgression within the Alaskan Arctic shelf.

1.3 Review of previous work

Due to warming of sediments in the continental shelves during periods of high sea level, destabilization of gas hydrates may be a periodic source of atmospheric methane over geological time (MacDonald, 1990). Warming of the permafrost and sediments and permafrost thawing eventually causes gas hydrates to become unstable resulting in the liberation of large volumes of gas. However, permafrost may act as a seal (because of ice in the pores) preventing the gases from escaping until sufficient ice has been thawed to generate escape routes for the gas (Osterkamp and Fei, 1993).

MacDonald (1990) has investigated the time scales for the response of the permafrost to submergence using one-dimensional analytical model. Since the model did not include latent heat effects, the predicted time scales are expected to be much too short. This means that his prediction regarding the time scales for production of atmospheric methane gas by destabilization of gas hydrates in continental shelves affected by permafrost are not correct.

The first idealized theoretical model to estimate the subsea temperatures was developed by Lachenbruch (1957) . In that analytical model, the solution was based on the assumptions of a constant position for the shoreline after submergence, constant soil properties, zero ice content and thus no phase change in subsea permafrost. According to that model, subsea permafrost at Prudhoe Bay could exist only within a thousand meters offshore with the depth not exceeding 30 meters (Fei, 1992). This model can also be applied to consider the case of a moving shoreline by superposition of solutions.

MacKay (1972) discussed the distribution and origin of subsea permafrost for the southern Beaufort Sea. Some relict permafrost with ground ice is present beneath the southern Beaufort Sea. The amount of permafrost aggradation was roughly estimated by using Neumann's solution modified for soils. The solution used was based upon a 0 °C temperature for the unfrozen soil below permafrost, a freezing temperature of 0°C, and fresh pore water. The aggradation and degradation rates of permafrost were calculated from the solution.

A simple conduction model with constant thermal conductivities to estimate the depth of subsea permafrost at Prudhoe Bay was developed by Lachenbruch et. al. (1982). In this model, the combined effect of the rise in sea level and erosion along

the shore was taken into account, which gives the time that the area has been submerged by seawater. The model suggests that the recently submerged region is underlain by near-melting permafrost to depths of 300 to 500 meters.

A relatively simple model based on Neumann's solution has been used by Osterkamp et. al. (1987a), Calculations were carried out for Norton Sound, based on data on sea level history and paleoclimate. The results suggest that under emergent conditions all of the ice-bearing permafrost formed under Norton Sound prior to and during the last glacial period should have thawed from the bottom by geothermal heat flow and from top by salt penetration into the seabed (Harrison and Osterkamp, 1978; Swift et. al., 1983; Osterkamp and Harrison, 1982, 1985; Osterkamp et. al., 1989).

Nixon (1986) carried out the first thermal simulation of subsea saline permafrost by using a one-dimensional finite element model for a simulation period of 10,000 years since submergence of permafrost. The initial temperature profile was assumed to be linear, varying between -9.0 °C at the ground surface and -1.8 °C at the base of ice-bearing permafrost. The surface temperature was assumed to have changed to -0.8 °C following submergence. In his model, constant values of thermal conductivity for frozen and unfrozen soil and a temperature-dependent heat capacity were assumed. Results from his model suggest that for any given period since submergence, a cooler temperature profile would be predicted for saline soil than that for a soil with a discrete freezing point. Outcalt (1985) performed a similar simulation with comparable results.

Calculations using one-dimensional analytical models (e.g. MacKay, 1972; Lachenruch et. al., 1982) and numerical models (Outcalt, 1985; Nixon, 1986) for the transient response of permafrost to submergence generally suggest the presence of

relatively thick subsea permafrost even in areas of deeper water. The occurrence of subsea permafrost implies the potential presence of a stability zone for gas hydrates. However, one-dimensional models are not completely satisfactory because of possible lateral heat flow in the subsea permafrost particularly near shore.

Fei (1992) and Osterkamp and Fei (1993) applied a two-dimensional finite element computational technique to simulate the history of subsea permafrost near Prudhoe Bay and Lonely due to changes in sea level and paleoclimate. As input parameters in their model they used changes in sea level, that provide the shoreline position, and changes in paleoclimate that provide the boundary condition on the land surface. Both of these factors, as well as the complicated geometry of the seabed, have been taken into account in the simulation. Also, the effect of saline pore fluids on latent heat and thermal parameters were taken into account (Osterkamp and Fei, 1993). The model predicts the temperature distribution in the continental shelf, the ice-bearing permafrost base and the ice-bearing permafrost table, as well as the ice-bearing permafrost thickness changes over the last interglacial period. Combined with this model, the phase diagram of methane gas hydrates was used to evaluate the stability of gas hydrates in the continental shelf.

The most important difference with the current model is that the effect of latent heat in all phase transitions was taken into account, and that the GHSZ was calculated simultaneously with the temperature distribution and not as an ad hoc application of the phase diagram to the modeling results as in Fei (1992) and Osterkamp and Fei (1993). This allows us to see the dynamics not only of temperature distribution but also the GHSZ. Using such an approach, we can trace the history of subsea permafrost formation, the behavior of the GHSZ in time and

understand the relationship of climate change and GHSZ in both: how climate effects the formation of GHSZ and vise versa how GHSZ can trigger the climate change due to its degrading.

CHAPTER 2

Regional information and input parameters for modeling

2.1. Regional Information on Studied Areas

Using a mathematical modeling approach to investigate the dynamics of subsea permafrost and the GHSZ assumes that some necessary parameters are defined, such as geometry of the studied region, initial and boundary conditions, and thermal properties of the soil. Boundary conditions on the surface are determined by the paleoclimatic temperature and sea level history.

To apply the model we choose four areas within Alaskan Arctic Shelf: Prudhoe Bay, Lonely, Point Barrow, and Cape Thompson.

The study site near Prudhoe Bay was chosen because of availability of data on thermal observations and drilling for over the last 40 years. Prudhoe Bay is a small embayment of the Alaskan Arctic Coast in the portion of the Arctic Ocean known as the Beaufort Sea. Since the discovery of large petroleum reserves there in the 1960's, it has been the site of intense geophysical exploration and production drilling. It lies at the northern edge of a treeless lake-strewn coastal plain in which the geomorphic characteristics of the surface and the thermal regime at depth are interrelated by the presence of permafrost which typically extends to depths of hundreds of meters. Permafrost blocks the downward percolation of the surface water, thereby contributing to the generally wet condition of the surface sediments and the abundance of standing bodies of water. Most of the processes that mold the natural landscape result from annual thawing and refreezing associated with the accumulation of solar heat by the wet surface, ponds and rills, and the resulting collapse or flowage of the ice-rich materials (Lachenbruch et. al., 1982). Generally, the seabed in this area

is sandy gravel or gravelly sand with some silt overlain by a thin layer of silt or sandy silt which increases in thickness seaward. Quartz was the major mineral present in all samples analyzed with calcite, feldspar, dolomite and chlorite occurring in minor (<10%) or trace quantities (Osterkamp and Harrison, 1976).

The study site offshore from Lonely which is about 135 km southeast of Barrow, Alaska, was chosen because of availability of data from other research and from onshore and offshore petroleum exploration wells. Available data consist of geophysical logs and samples from the J.W. Dalton-1 (JWD) well onshore and the Antares well offshore (Collett et. al., 1989), results of thermal studies in five shallow drill holes along an offshore line to the northwest from Lonely (Osterkamp and Harrison, 1980, Harrison and Osterkamp, 1981). The onshore surficial deposits were mapped as interglacial nearshore and lagoon sand, silty fine sand, and pebbly sand. Shallow offshore drilling data (Osterkamp and Harrison, 1980, Harrison and Osterkamp, 1981) indicate that the seabed sediments are fine-grained to about 30 m depth. At the JWD well, the deeper well logs indicate relatively coarse material (conglomerate and sandstone) down to the 270 to 300 m depth or so overlying finer material (siltstone) (Collett et. al., 1989). The nearest offshore well (Antares) is about 24 km distant, on a line bearing N55°E from Lonely, in about 15 m of water. Well logs indicate that relatively fine-grained material exists in the upper section (above 190 m) where permafrost might be expected, with some coarser material from 190 to 312 m. The use of geophysical logs to determine the presence or absence of ice-bearing permafrost is very difficult because of the lack of contrast in physical properties between the thawed material and any warm and marginally ice-bearing permafrost which would be thawing from both the top and bottom (Osterkamp and

Fei, 1993).

The study site near Barrow is very close in terms of properties and shelf geometry to Lonely site. The only major difference in the input conditions for the modeling in these two sites is a colder temperature at Barrow.

Cape Thompson site, according to Kachadoorian et. al. (1960), is underlain chiefly by mudstone, siltstone, and sandstone. These rocks are overlain by as much as 10 m of unconsolidated deposits consisting of flood plain deposits, colluvium, silt and sand, and terrace deposits. The particular feature of the sea shelf near Cape Thompson is extremely wide belt of shallow sea water (65 km offshore the depth of sea water is only 55 m). Hence, during Pleistocene lowstands of sea level, the entire shelf was emergent with a pretty severe climatic condition, and therefore exposed to deep freezing. Another particularity of the Cape Thompson shelf, when compared with Prudhoe Bay and Lonely, is the rapid increase of sea depth near shore. The depth is 5 m at a distance of 100 m from the shore. As a result, the shoreline has been located near its present position for a long time period (for example, 5 Ka B.P. the distance between former shoreline and its present position was 250 m. 3 Ka B.P. this distance was only 100 m) (Kachadoorian et. al., 1960). During all this time, the permafrost degradation appeared within the entire previously dry shelf.

At the peak of the last glaciation, sea level was assumed to be 118 m lower than the present sea level on the continental shelves at Prudhoe Bay and Lonely. The sea level history curve obtained by Bard et. al. in 1990 was used. Local tectonic and isostatic effects on sea level history in the Beaufort Sea have been neglected. Our two-dimensional model was applied to the region that extends 20 km onshore and 180 km offshore. Such a long profile offshore is needed to prevent any possible effect of

lateral heat flow. In the vertical direction, the lower boundary of the region was set to 3000 m in order to define a level where surface temperature variations have a negligible effect.

The geometry of the shelf zones near Prudhoe Bay and Lonely was obtained from bathymetric contour map (USGS, 1976, U.S.NOAA, 1985).

The spacing of the element grid was chosen to be slightly uneven. The vertical spacing was set to be 10 meters up to the depth of 1820 m, and then it gradually increases to 100 m. The horizontal spacing was set to be constant and equal to 2 km.

2.2. Soils Properties

One of the most significant factors when solving any kind of heat transfer related problem is defining the thermal parameters of the media. Another is porosity – this parameter causes some changes in the thermal properties as well. In the modeling, thermal parameters to be considered are: thermal conductivity, apparent volumetric heat capacity, and latent heat of phase transitions. These parameters for soils can be calculated from the component values (Osterkamp, 1987). The presence of unfrozen water makes the component values strongly temperature dependent. In our case, we omit the fact that density and salt distribution vary with temperature changes, and assume that the effect of unfrozen water content plays more significant role in determining of temperature-dependant thermal properties of soil. Another assumption that we make is that the entire pore space of the soils is filled by free gas (in this particular case by methane dissolved in water), so that any void volume or volume expansion caused by melting or freezing of the ice can be neglected.

2.2.1. Thermal Conductivity

Thermal conductivity of the permafrost is a more complicated parameter than

it is for other media. The reason is that permafrost usually contains water in its different phase states. As is well known, the thermal conductivity of water varies by more than 4 times (0.56 W/mK for water and 2.4 W/mK for ice) from liquid to solid phase. At the same time, as already mentioned, permafrost contains some amount of unfrozen water especially within the temperature range that lies close to the freezing point. If permafrost does not contain unfrozen water, then thermal conductivity can be considered to be about constant and depends on soil type and ice content. In our modeling we considered two types of soil for Prudhoe Bay site – coarse-grained and fine-grained, one case was taken into account for calculations near Lonely and Barrow, and another case was taken for calculations near Cape Thompson.

In general the values of thermal conductivity of soils can be calculated by using methods suggested by Osterkamp (1987). The thermal conductivity of permafrost containing unfrozen water was calculated by using simplified weighted geometric mean equation (Lachenbruch, 1982):

$$\boldsymbol{K} = \boldsymbol{K}_s^{1-\theta_f} \boldsymbol{K}_i^{\theta_i} \boldsymbol{K}_u^{\theta_u}$$

where K_s, K_i, and K_u are the thermal conductivities of the soil, ice, and brine components respectively.

Since we didn't take into account the presence of the brine in the soil, this equation was simplified and can be presented as following:

$$K = K_s^{1-\theta_f} K_i^{\theta_i}$$

The porosity in the frozen state is given by

$$\theta_f = \theta_i + \theta_u \approx \theta_t$$

where θ_t is thawed porosity and θ_i and θ_u are the volume fractions of ice and

unfrozen water.

Then, θ_i and θ_u can be presented as following:

$$\theta_i = \left(\frac{\rho_b}{\rho_i}\right) w_i \quad \text{and}$$

$$\theta_u = \left(\frac{\rho_b}{\rho_u}\right) w_u$$

where w_i and w_u are the mass fractions of the ice and unfrozen water and ρ_b is a dry bulk density of the frozen soil which is different for different soil types. Even in spite of the density of ice ρ_i and density of unfrozen water ρ_u are the functions of salinity, since we assume no salt presence in our soils, ρ_i and ρ_u have the values of density of clear ice and pure water respectively.

Unfrozen water content can be represented by an equation with two empirical coefficients (Lovell, 1957):

$$w_u = \alpha V^{\beta}$$

where α and β are empirical constants and V is absolute value of the temperature (°C) below freezing point.

Unfrozen water content curves are presented on figures 2.1.

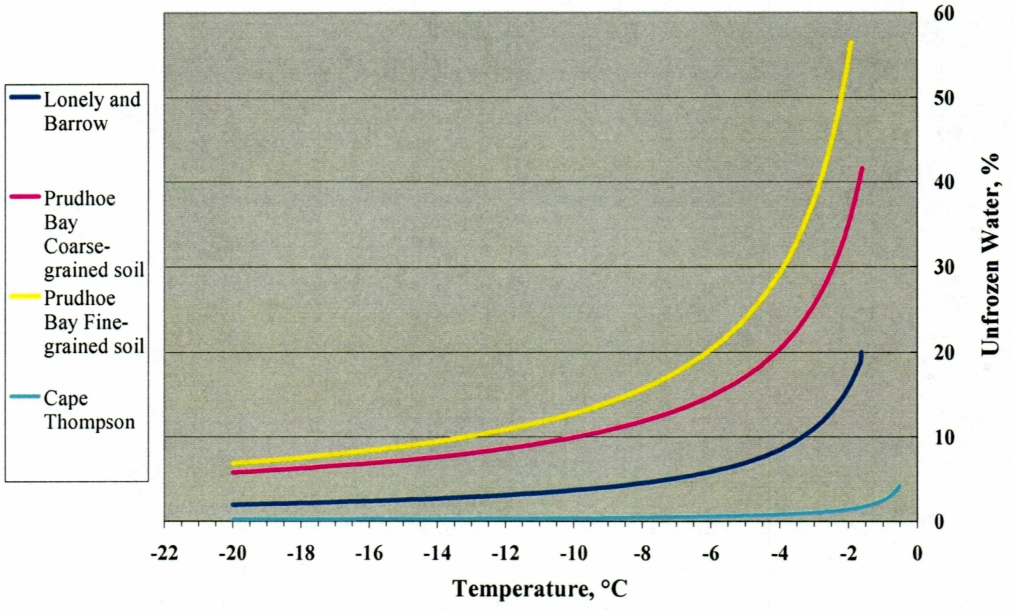

Figure 2.1 Unfrozen water content at studied sites.

2.2.2 Volumetric Heat Capacity

When permafrost does not contain unfrozen water, the volumetric heat capacity depends only on soil type and ice content. As known, heat capacity is an additive parameter, so it can be presented as a sum of several values which includes the heat capacity of every part of the media:

$$C = \sum_{1}^{n} C_i$$

where C_i is a heat capacity of each constituent.

In case of frozen state, heat capacity of permafrost is

$$C_t = C_b + \theta_i C_i + \theta_u C_u$$

where C_b, C_i, and C_u are the heat capacities of dry bulk soil, ice, and unfrozen water respectively.

In thawed state it is even simpler:

$$C_t = C_b + \theta_t C_w$$

where C_w is a heat capacity of water.

Since, in our modeling, we deal with media containing gases and gas hydrates, when temperature – pressure conditions are suitable for the formation of gas hydrates, calculating of thermal properties of soils are being modified such as parts of equations that depends on ice properties are substituted by the equations with the gas hydrates properties respectively. It plays a really significant role in determining heat properties of permafrost for each time step because the difference in the properties of ice and gas hydrate are quite large.

The following algorithm of choosing thermal properties of soil was applied:

To get values of thermal properties of soil containing gas hydrate, three major

parameters (thermal conductivity of soil in frozen and thawed state and thawed heat capacity of soil) were set arbitrarily (see Table 2.1), then using the dependencies described above and knowing porosity and α and β coefficient for unfrozen water content, all other thermal parameters were calculated (see Table 2.1).

2.2.3 Thermal Diffusivity

The thermal diffusivity is defined as

$$D = K / C$$

and can be calculated from the thermal conductivity and heat capacity. For constant thermal conductivity and heat capacity, thermal diffusivity is also constant, and for temperature-dependent parameters, it can be derived from equations described in 2.2.1 and 2.2.2

Table 2.1 Thermal Properties of soils

Parameter	*index*	Soil Type				Dimension
		Type I Prudhoe Bay, coarse-grained	Type II Prudhoe Bay, fine-grained	Type III Lonely and Barrow	Type IV Cape Thompson	
Porosity	θ	0.416	0.565	0.2	0.042	n/a
Density of ice	ρ_i	0.917				g/cm^3
Density of water and unfrozen water	ρ_u	1.0				g/cm^3
Dry bulk density of soil[1]	ρ_b	1.62	1.19	2.12		g/cm^3
Coefficient α[1]	α	0.3795	0.8775	0.1435	0.02506	n/a
Coefficient β[1]	β	-0.779	-0.8977	-0.902	-0.7987	n/a
Freezing point temperature[1]	T_e	-1.6	-1.92	-1.63	-0.524	°C
Thermal conductivity of water	K_w	0.56				W/mK
Thermal conductivity of ice	K_i	2.4				W/mK
Thermal conductivity of gas hydrate[2]	K_h	0.45				W/mK
Dry bulk thermal conductivity of soil	K_b	4.16	1.9145	2.537	2.9489	W/mK
Thermal conductivity of frozen soil	K_f	3.39	2.05	2.5	2.93	W/mK
Thermal conductivity of thawed soil	K_t	1.97	1.32	1.7	2.8	W/mK
Thermal conductivity of soil containing gas hydrate	K_m	1.8157	1.2355	1.604	2.781	W/mK
Heat capacity of water	C_w	4.22				MJ/m^{3}K
Heat capacity of ice	C_i	1.96				MJ/m^{3}K
Heat capacity of gas hydrate[2]	C_h	1.8967				MJ/m^{3}K
Dry bulk heat capacity of soil	C_b	2.115	2.494	1.342	2.331	MJ/m^{3}K
Heat capacity of frozen soil	C_f	2.057	2.332	1.506	2.32	MJ/m^{3}K
Heat capacity of thawed soil	C_t	2.9	3.016	2.105	2.39	MJ/m^{3}K
Heat capacity of soil containing gas hydrate	C_m	2.033	2.313	1.489	2.3175	MJ/m^{3}K
Latent heat of water↔ice	333					MJ/m^{3}K
Latent heat of gas hydrate	477.48					MJ/m^{3}K

[1] Fei, T., 1992
[2] Sloan, 1990

2.3. Sea Level Change as One of the Upper Boundary Condition

Changes in sea level as well as temperatures on the surface are those two major factors that determine the process of formation of subsea permafrost and the gas hydrate stability zone. They are closely related since one of the most important contributing factors in seal level change is melt of land ice; another is thermal expansion of the oceans. Of course, there are a lot of other direct and indirect factors that can cause a change in sea level, such as vertical land movement (isostatic and tectonic), differences in atmospheric pressure, winds, ocean currents, etc., but in time scale of tens of thousands of years, the most important climate-related factors are likely to be thermal expansion of the oceans and melting of land ice (Fei, 1992).

For the calculations, the sea level curve of Bard et. al. (1990) was used. It represents a long term sea level estimation which was obtained by U-Th dating. This curve covers the last interglacial period and is considered to be one of the best long term sea level curves (Fig. 2.3). Of course this curve shows very approximate sea level history and doesn't take into account any specific events for the particular area, but for the purpose of this modeling it gives reasonably enough accuracy in such a large time scale model.

On fig. 2.3 we can see that regression of the sea began approximately 120,000 years ago, that caused the shelf to be exposed to cold air temperatures and hence, permafrost to form. During 120,000 – 95,000 years ago, regression of sea was not very fast and reached not more than 15-20 m in magnitude. Then after minor transgression, sea level began to drop faster and during the following 20,000 years reached almost 70 m below present day sea level. This means that almost 80 km of shelf near Prudhoe Bay, approximately 55 km of shelf near Lonely and Barrow, and

the entire shelf near Cape Thompson were exposed. The transgression that followed this abrupt sea level drop was approximately 45,000 – 50,000 years ago when the sea level rose to -50 m mark. After this transgression there was another significant regression when during 25,000 years sea level dropped to its lowest level (≈ -120 m). The average rate of sea level drop was 2.5 mm/year. The lowest sea level, 20,000 – 18,000 years ago, also corresponds to the coldest period (Bard et. al., 1990) (Fig. 2.4). We can assume that during that time permafrost reached its maximum thickness. During the 18,000 – 20,000 years sea level has been rising constantly, but we can split this period into two main parts: 1) 18,000 – 20,000 till 8,000 years ago when sea level rose very fast (with average rate about 7 mm/year) and reached -20 m; 2) the last 8,000 years when sea level transgression slowed and reached present position.

2.4 Boundary Conditions

Two types of boundary conditions were considered for this problem: boundary with given temperature and boundary with geothermal gradient. On the surface, temperature distribution in time was set for exposed parts of shelf during sea regressions, and sea water temperature (that was assumed to be constant in time) was set for covered parts of shelf. Sea water temperature was assumed to be -1°C for Prudhoe Bay, Lonely and Barrow and 0.2°C for Cape Thompson. Surface distribution of temperature was chosen according to a paleoclimatic scenario. The original paleotemperature curve was developed by Maximova and Romanovsky (1988) (Romanovsky et. al., 1989) for southeast Siberia. In this case the curve was modified for different sites in Alaska to produce a present mean temperature; T = -11°C in Prudhoe Bay and Lonely sites, -12.5°C in Barrow, and -7.1°C in Cape Thompson (fig. 2.4). This approach was successfully used by Osterkamp and Gosink (1991), Fei

(1992), and Osterkamp and Fei (1993) and was found to give pretty good agreement with current permafrost thickness.

The lower boundary condition was taken to be controlled by the geothermal gradient and was set on the depth of 3000 m. In perfect case of physical model lower boundary conditions should be set on an infinite depth, but after several test calculations the depth of 3000 m was chosen because it did not disturb the temperature regime on the surface and had no influence on the final results of the calculations. For Prudhoe Bay, geothermal gradient was chosen to be 0.0349 °/m based on data obtained by Lachenbruch et. al. (1982) where they measured a geothermal heat flux of 0.0565 W/m^2. For the Lonely and Barrow sites a value of 0.0262°/m for geothermal gradient was chosen (corresponding heat flux is a bit higher than in Prudhoe Bay and equal to 0.065 W/m^2, and for Cape Thompson site we used value of 0.02071°/m for the gradient (approximate heat flux of 0.058 W/m^2). The two side boundaries were assigned a zero horizontal heat flux. For that purpose such a long offshore profile (180 km offshore for Prudhoe Bay, Lonely and Barrow, and 65 km for Cape Thompson; 20 km onshore for all four sites) were chosen.

2.5 Initial Conditions

Defining the initial conditions for this study complicates setting a start time for the simulations. Because the initial shoreline position (sea level) would affect the temperature distribution in the ground, and the exact temperature distribution is unknown, only a reasonably logical assumption can be given, the steady state solution. In order to get rid of this transient caused by the inexact assumption for initial conditions, the model must be run over a period of longer than the transient time scale (Osterkamp and Gosink, 1991). To improve this approach of defining the

initial temperature distribution we did the following: 120 ka cycle was chosen (because of similar air temperatures and sea level) to look at how the temperature regime can form during this period of time using simplified version of the program (which doesn't take into account either unfrozen water content or latent heat of gas hydrate formation), then temperature distribution that was acquired at the end of this cycle was used as an initial condition once again and so on. After 5 – 6 consecutive runs of the program we mentioned that the temperature regime became stable all over the simulated area which means that a periodically-stable regime has formed. This temperature distribution now can be used as an initial condition for the simulations. Such an approach was used to define the initial conditions for all sites. Figure 2.5 illustrates the number of cycles needed to form periodically-stable conditions for each studied site. Initial temperature distributions for all sites are presented on figures 3.1.3a,b, 3.1.6,b, 3.2.3,b.

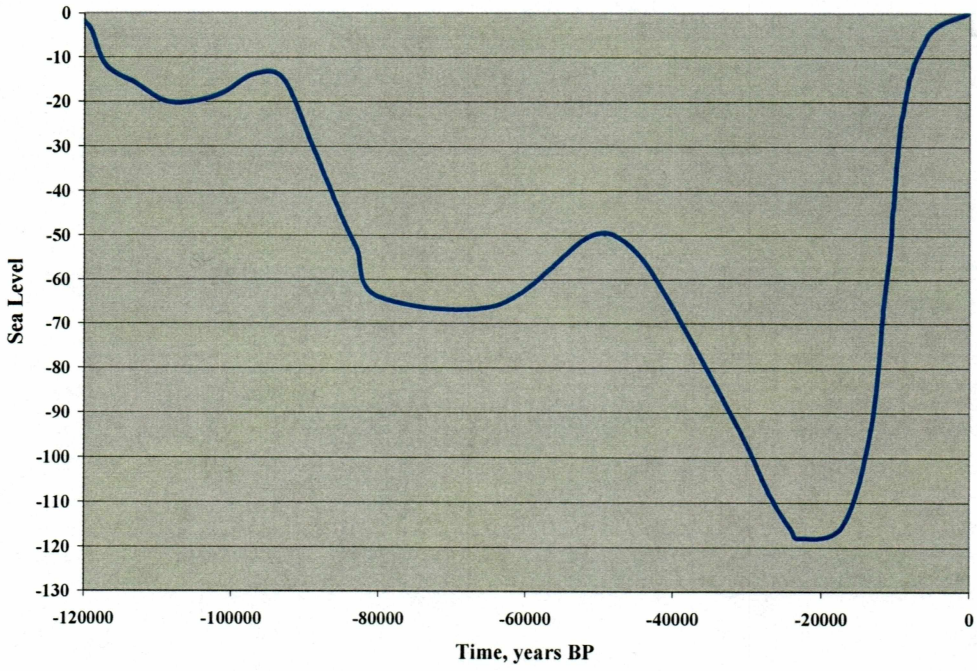

Figure 2.3 Sea level curve obtained by U-Th dating (Bard et. al., 1990).

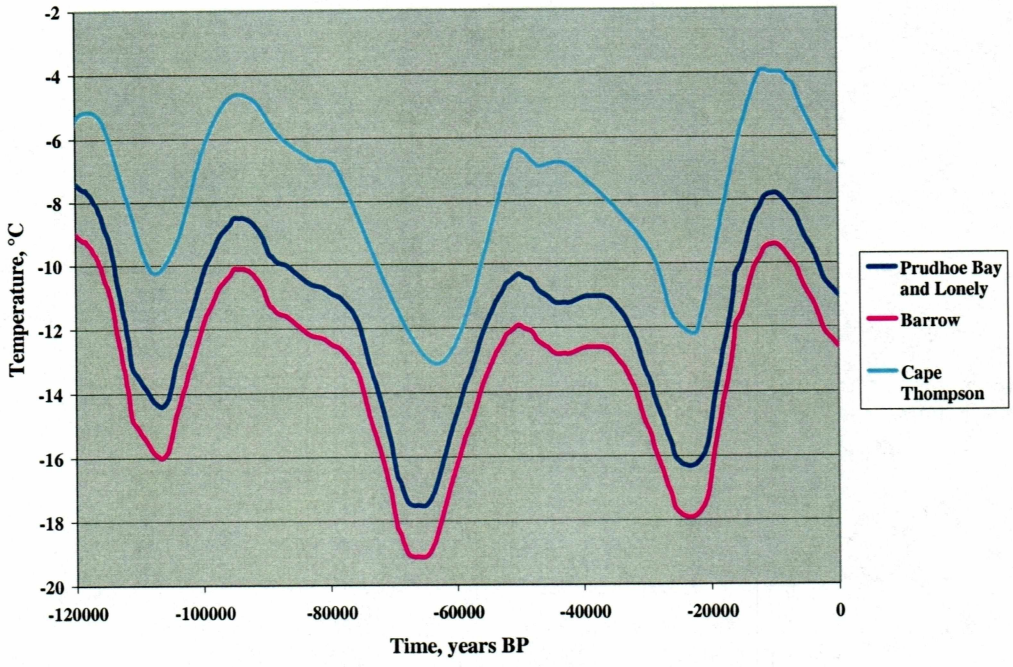

Figure 2.4 Paleotemperature model for the surface temperature of permafrost based on a model for East Siberia (Maximova and Romanovsky, 1988) modified for Alaska.

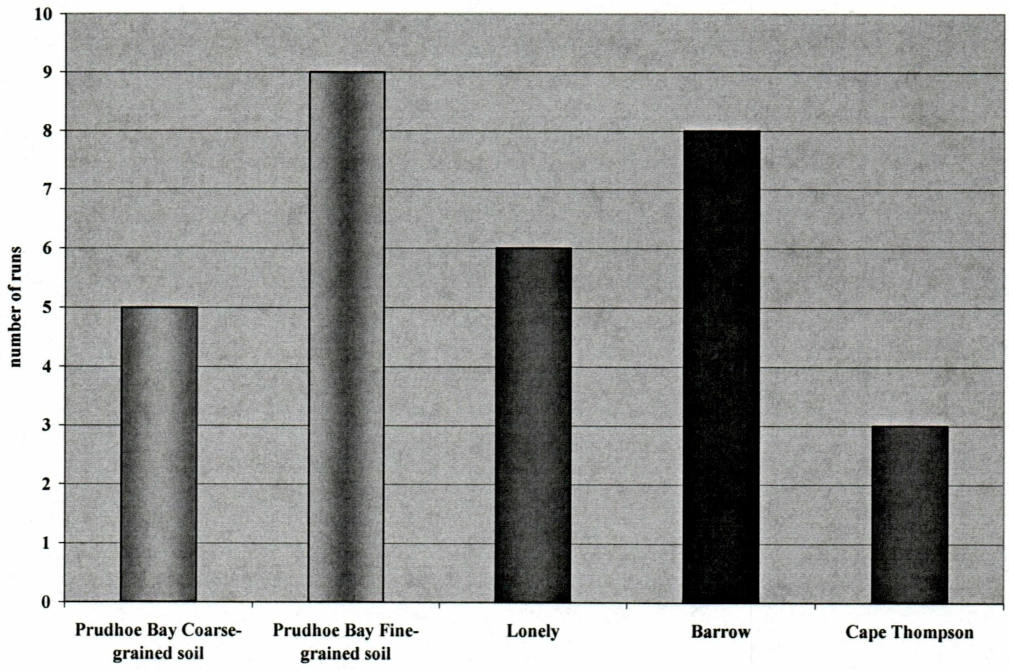

Figure 2.5 Number of runs needed to get periodically steady-state regime for the initial conditions.

CHAPTER 3

Results of Modeling and Discussion: Permafrost

As stated in previous chapters, mathematical modeling was carried out for four sites in the Alaskan Arctic. In Prudhoe Bay, calculations were made for two different soil types. Two versions of the program were used in all studied sites: one that takes into account the latent heat of gas hydrate formation (Type II) and the other one that does not (Type I). Both, Type I and Type II programs take into account unfrozen water content and hence changing thermal properties of soils with temperature. Also, numerical calculations were made using solutions of the Stefan Problem (step-like change in liquid water content when all water changes its state [liquid or solid] at a fixed temperature), Type III. In this chapter the results of the modeling are presented and discussed for all four sites: Cape Thompson, Barrow, Lonely, and Prudhoe Bay. The prediction for the permafrost table and base positions and its thickness are for the ice-bearing permafrost, not for the 0°C isotherm.

3.1. Simulations at Prudhoe Bay

For comparison, two types of material, coarse-grained and fine-grained, have been used in the simulations. Results of calculations of permafrost and Gas Hydrate Stability Zone in the continental shelf are presented and discussed. All properties of soils that have been used in the modeling are presented in Table 2.1. The positions of the permafrost base and table were determined for a specific freezing point depression: for coarse-grained material it was -1.6°C and for fine-grained material it was -1.92°C (Fei, 1992).

3.1.1. Coarse-grained material, results of modeling using the Type I program

Figures 3.1.1a and 3.1.1b show the predicted current temperature distribution

in the continental shelf along the profile at Prudhoe Bay. The thickness of ice-bearing permafrost onshore is 521 m and it gradually decreases from both top and bottom offshore. The subsea permafrost has a wedge-like shape and extends up to 82 km offshore. At 14 km offshore, which corresponds to approximately the 9 m isobath, the subsea permafrost table is at 36 m depth and the base of the permafrost is at 483 m that gives a 476 m of thickness. At 40 km offshore, which corresponds to approximately 28 m isobath, the subsea permafrost table is at 42 m depth and the base of the permafrost is at 380 m, giving a 338 m thickness. The unfrozen water content curve that has been used for this calculation gives a -1.6°C freezing point depression with a porosity of 0.416. The use of this curve might under-estimate the depth of the ice-bearing permafrost table in the offshore continental shelf. In the near shore region, sea ice freezes to the bottom annually, hence the salinity of the brine at the permafrost table is higher than normal sea water which lowers the phase equilibrium temperature to -2.41°C (Osterkamp et. al., 1989). At the North Prudhoe State #1 well, which is just onshore along the simulation profile, the depth of the ice bearing permafrost is about 560 m with a phase equilibrium temperature of -1.3°C (Lachenbruch et. al., 1982). This value is in a good agreement with the onshore permafrost thickness obtained using this type of program. The error for predicted thickness is only about 7% (Table 3.1.). However, the values of subsea permafrost thickness offshore are high in comparison with the data from Reindeer Island (Fei, 1992). Therefore, using -1.6°C as an equilibrium temperature for the offshore permafrost underestimates the subsea ice-bearing permafrost table.

Lateral heat flow is large within the first several kilometers offshore, but from 50 to 80 km offshore permafrost is almost isothermal. At 82 km offshore – the

maximum extent of permafrost, the -1.6°C isotherm is nearly vertical, which indicates horizontal heat flow. At the depth 520 m and below, the calculations shows a nearly uniform vertical temperature gradient except beyond 82 km from the present shoreline.

Fig. 3.1.1c illustrates the predicted temperature distribution for 18 Ka B.P. – the time period when the sea level dropped to its lowest position and the shelf was exposed to the atmosphere. During that time, permafrost reached its maximum thickness (590 m) and extent (more than 90 km offshore). From 18 Ka B.P., sea level started to rise; hence due to this sea transgression, permafrost started to degrade. The degradation of permafrost for the last 18 Ka is 16.5% in thickness onshore and the tip of subsea permafrost moved back towards the shore by 10 km. Also the permafrost table deepened by approximately 40 m near the shoreline and about 80 m at the subsea permafrost tip during the last 18 Kyr.

3.1.2. Coarse-grained material, results of modeling using the Type II program

Figures 3.1.2a and 3.1.2b demonstrate the predicted current temperature distribution in the continental shelf along the profile at Prudhoe Bay. The thickness of ice-bearing permafrost onshore is 425 m and permafrost has a tubular shape within 22 km of the calculation domain (20 km onshore and 2 km offshore) with a nearly horizontal lower boundary. Then, there is an abrupt decrease of the permafrost base boundary from 425 m to 312 m within a 4 km interval. From 6 km offshore up to 66 km offshore the base of permafrost moves upwards gradually and, at 66 km offshore, reaches 172 m below the sea bed. The subsea permafrost table deepens offshore, but not linearly: in the first 6 km from the modern shore line it goes down by 25 m, over the next 6 km it moves down very little (almost parallel to the sea bed), in the next 2

km the depth of permafrost table increases by 8 m and remains almost constant for the next 14 km (parallel to the sea bed). From 28 to 40 km offshore the subsea permafrost table position varies slightly when abrupt deepenings alternate with relatively horizontal intervals. In general, the depth to the permafrost table increases almost linearly with the distance offshore. Subsea permafrost has a wedge-like shape with the maximum predicted extent of about 66 km. The maximum thickness of the subsea permafrost is 418 m near the shore line; the minimum thickness is about 90 m at the farthest offshore (65 km). At 14 km offshore, which corresponds to approximately 9 m isobath, the subsea permafrost table is at 38.5 m depth and the base of the permafrost is at 292 m, that gives a 284.5 m thickness. Even though the permafrost table depth is not in good agreement with the data from Reindeer Island (90 m), the predicted depth of the permafrost base is (292 m predicted vs. 320 m observed, relative error 9%). Because of prescribed unfrozen water and freezing point that have been used for this calculation some under-estimation of the depth to the ice-bearing permafrost table in the offshore continental shelf may occur.

Lateral heat flow is very high within the first several km offshore, but from 16 to 66 km offshore permafrost is almost isothermal. At 66 km offshore (the maximum extent of permafrost), the -1.6°C isotherm is nearly vertical, which indicates horizontal heat flow. Below the permafrost layer, calculations show a nearly uniform vertical temperature gradient except for the part of the shelf where subsea permafrost is absent (about 66 km and farther from the present shoreline).

Fig. 3.1.2c reveals the predicted temperature distribution for 18 Ka B.P. During that time, permafrost reached its maximum thickness (545 m) and extent (more than 90 km offshore) over the last glacial cycle of 120 Kyrs. From 18 Kyrs BP

with the sea level rising, the shelf started to submerge, hence permafrost started to degrade. The degradation of permafrost for the last 18 Ka is 23% in thickness onshore and the permafrost tip moved back towards the shore by more than 25 km. Permafrost has been thawing not only from the bottom but from the top as well. As mentioned above, the permafrost table deepened by 35 – 90 m in the offshore zone during last 18 Kyr.

If we compare the results of modeling using Type I and Type II programs, it can be clearly seen that there is a significant difference in permafrost thickness both onshore and offshore. Using the same soil properties as well as initial and boundary conditions, the only thing that could have affected the temperature distribution is the latent heat of the gas hydrate formation. It turned out that taking into account this effect influences the temperature field dynamics dramatically. The differences in predicted permafrost thickness using these two different types of programs reach almost 20% for onshore and even more for the offshore region. Also, it has some effect on the permafrost table far offshore. It can be explained that the latent heat of gas hydrate formation combines with latent heat of water – ice transition and the system becomes more inertial.

3.1.3. Coarse-grained material, results of modeling using the Type III program

This type of program, which doesn't take into account unfrozen water content in soils, assuming the step-like transition from thawed to frozen state of the media, or the latent heat effect of gas hydrate. The program has two major purposes: 1) to define initial temperature distribution for Type II and Type III programs; 2) to determine the effect of temperature-dependant soil properties on the present permafrost distribution and its dynamics over the last 120 Kyrs. The program was run 6 consecutive times

(see chapter 2.6) in order to get the "periodically steady state regime". For every new run, the result of the previous calculation was used as an initial condition. Figures 3.1.3a and 3.1.3b show the temperature distribution along the profile near Prudhoe Bay after 6 runs. In the onshore zone the thickness of permafrost is 592 m and it remains constant up to 2 km offshore. Further offshore the base of the permafrost moves upwards by 10 m on the 4 km interval, stays constant for the next 8 km then again moves upwards slowly (90 m on the 22 km interval). From 36 to 68 km offshore the base of the subsea permafrost is horizontal (430 m below the sea level) and from 68 to 88 km it moves up again. The subsea permafrost table oscillates with a smaller range and in general goes almost parallel to the sea bottom at the depth of 70 – 80, m slightly deepening towards offshore.

Lateral heat flow is very high within the first several km offshore, but the rest of the offshore permafrost is almost isothermal. At 88 km offshore, the maximum extent of permafrost, the -1.6°C isotherm is close to vertical, which indicates horizontal heat flow. Below the permafrost layer, the calculations show nearly uniform vertical temperature gradient except near 88 km from the present shoreline.

Using this type of program overestimates the thickness of offshore permafrost but gives relatively good values of the permafrost thickness onshore (Table 4.1) with a relative error about 6%.

Analysis of the results of all three type of programs used for the simulations near Prudhoe Bay suggests that for onshore permafrost the best prediction of thickness can be obtained using either Type I or Type III programs (each of them has the small relative error towards underestimation or overestimation), but for the offshore permafrost neither of them show satisfactory results. In case of offshore

permafrost thickness, the best prediction can be made using Type II program, but still some corrections should be made for the subsea permafrost table due to excess of brine in the upper layer of the bottom sediments that lowers the freezing point dramatically.

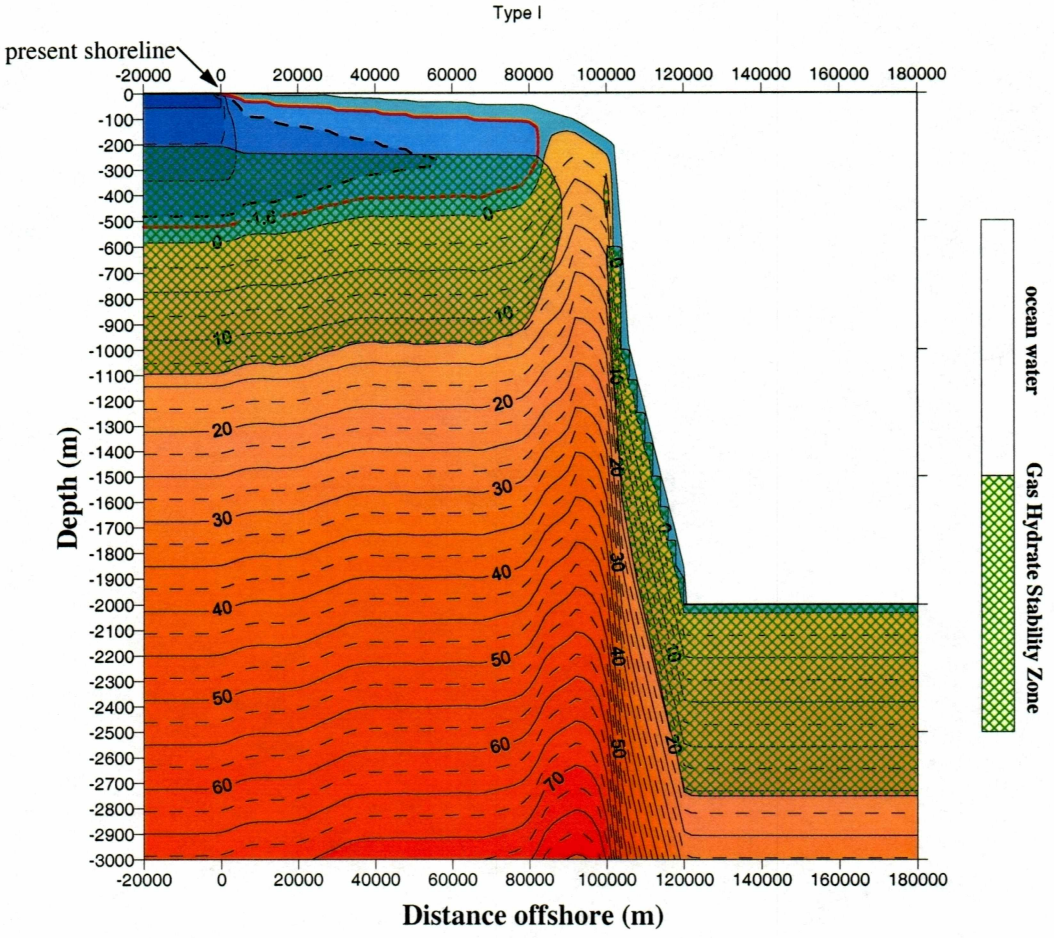

Figure 3.1.1a Results of modeling using Type I program. Temperature distribution and Gas Hydrate Stability Zone at present time for coarse-grained material at Prudhoe Bay.

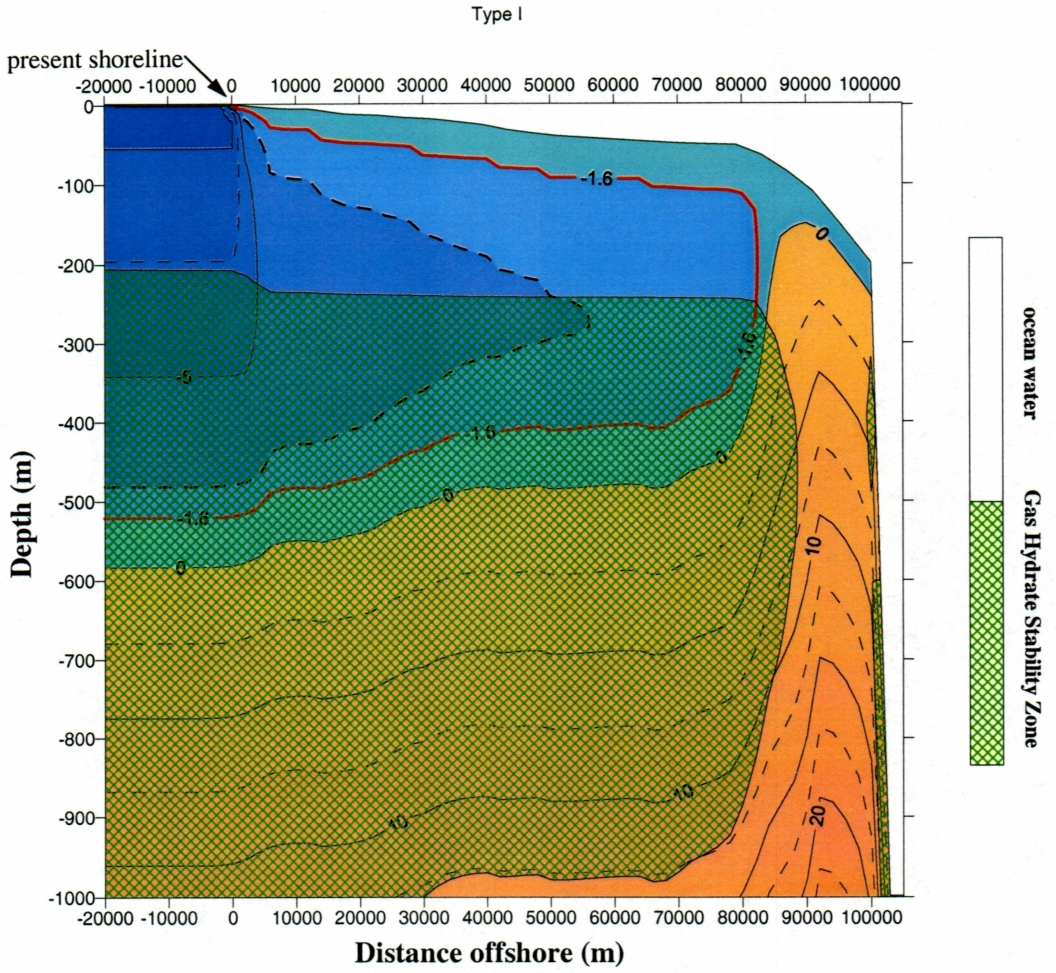

Figure 3.1.1b Results of modeling using Type I program. Temperature distribution and Gas Hydrate Stability Zone at present time for coarse-grained material at Prudhoe Bay. Larger scale.

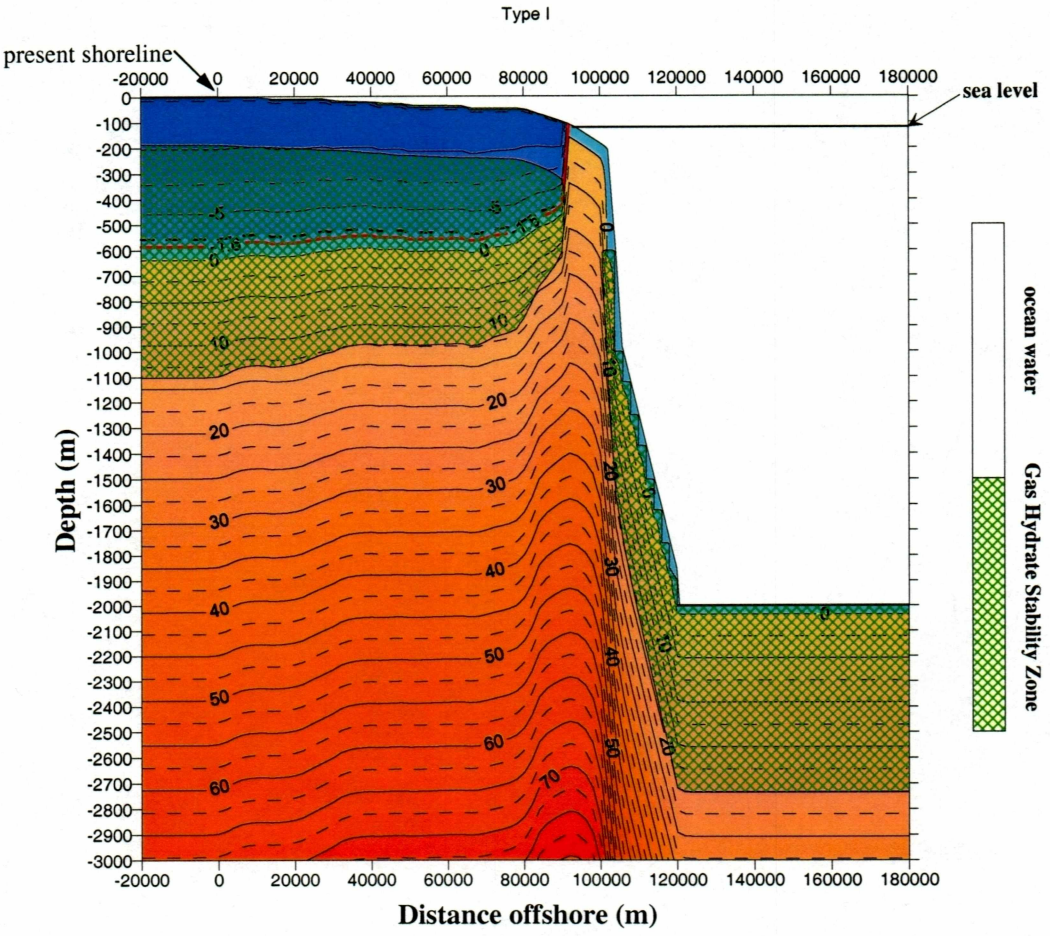

Figure 3.1.1c Results of modeling using Type I program. Temperature distribution and Gas Hydrate Stability Zone at 18 Kyrs BP for coarse-grained material at Prudhoe Bay.

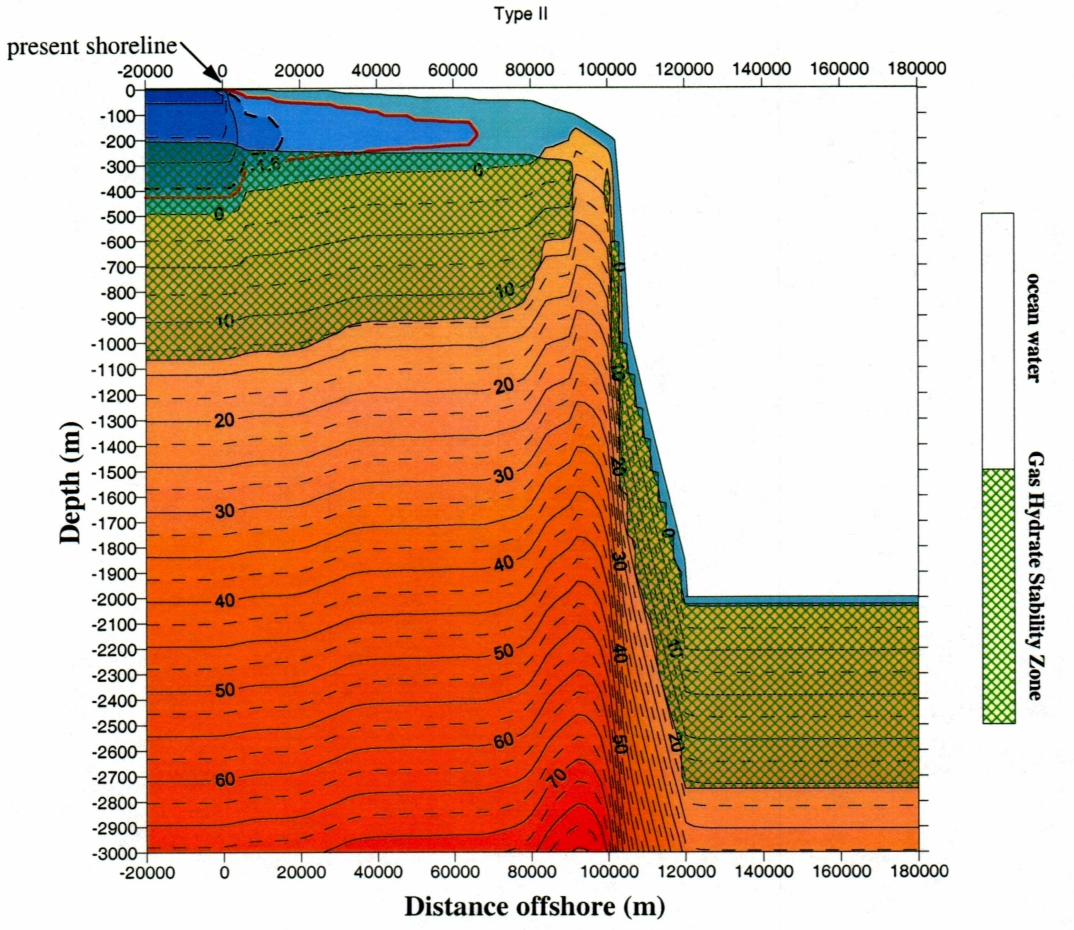

Figure 3.1.2a Results of modeling using Type II program. Temperature distribution and Gas Hydrate Stability Zone at present time for coarse-grained material at Prudhoe Bay.

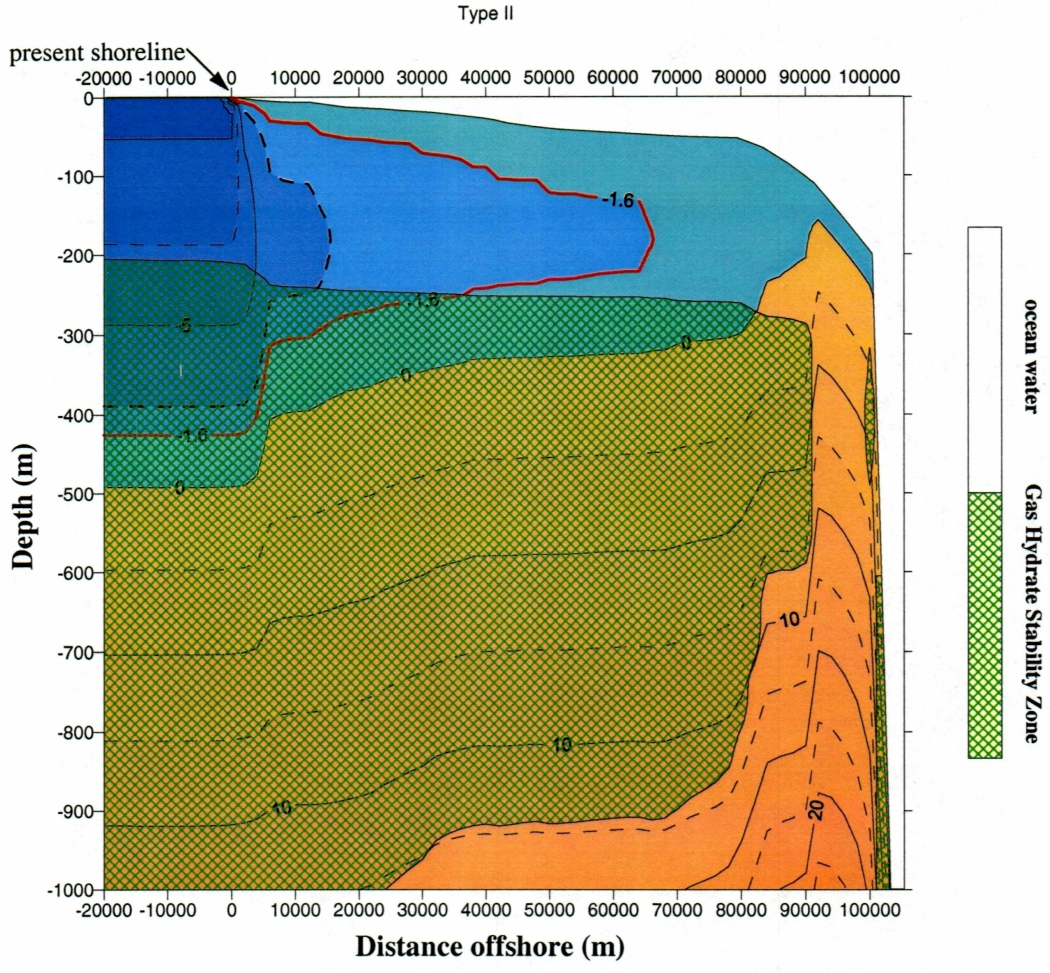

Figure 3.1.2b Results of modeling using Type II program. Temperature distribution and Gas Hydrate Stability Zone at present time for coarse-grained material at Prudhoe Bay. Larger scale.

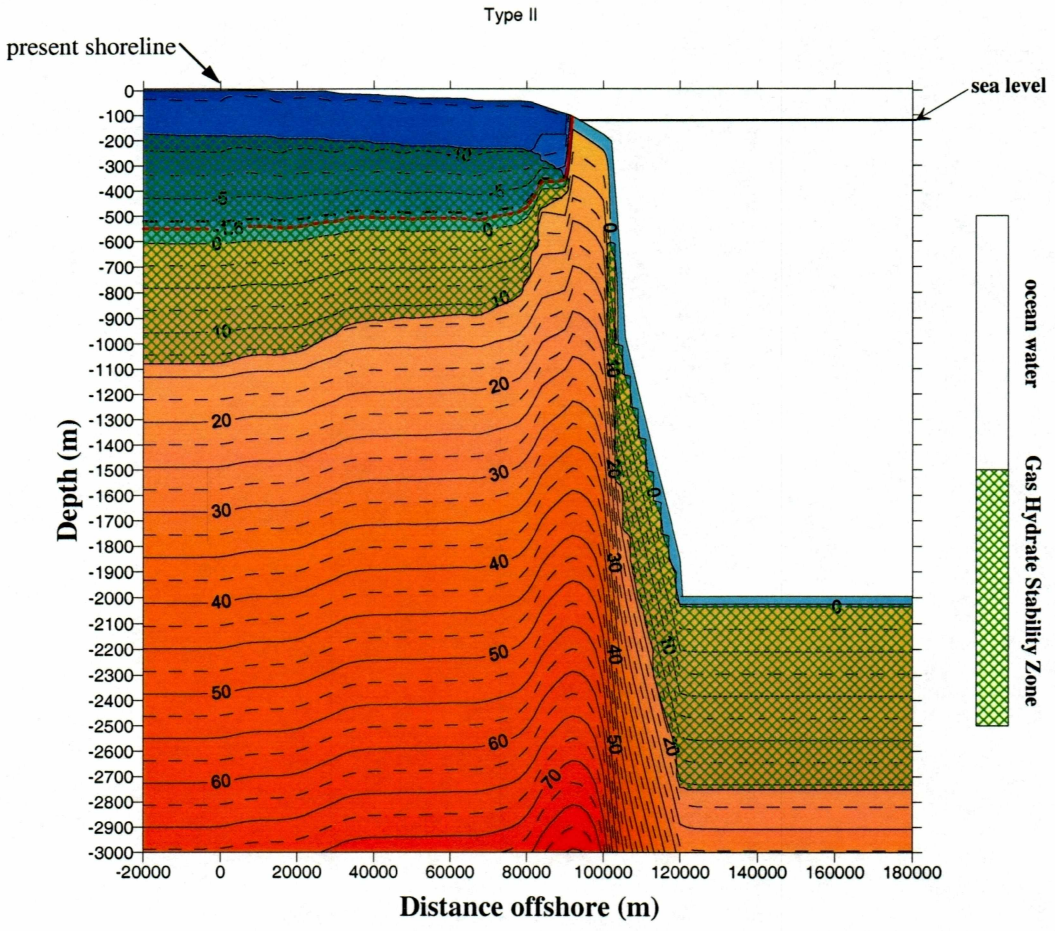

Figure 3.1.2c Results of modeling using Type II program. Temperature distribution and Gas Hydrate Stability Zone at 18 Kyrs BP for coarse-grained material at Prudhoe Bay.

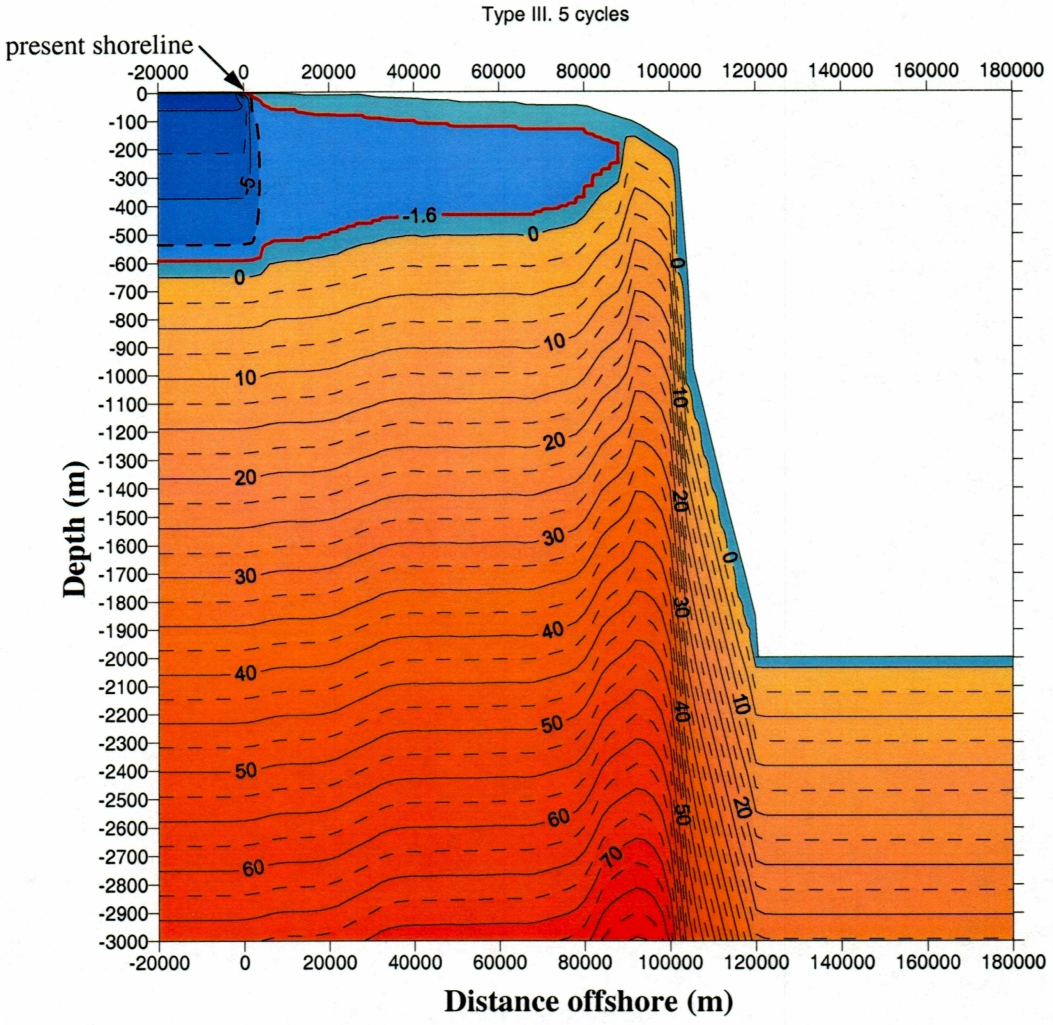

Figure 3.1.3a Results of modeling using Type III program (initial conditions for Type I and Type II). Temperature distribution at present time for coarse-grained material at Prudhoe Bay.

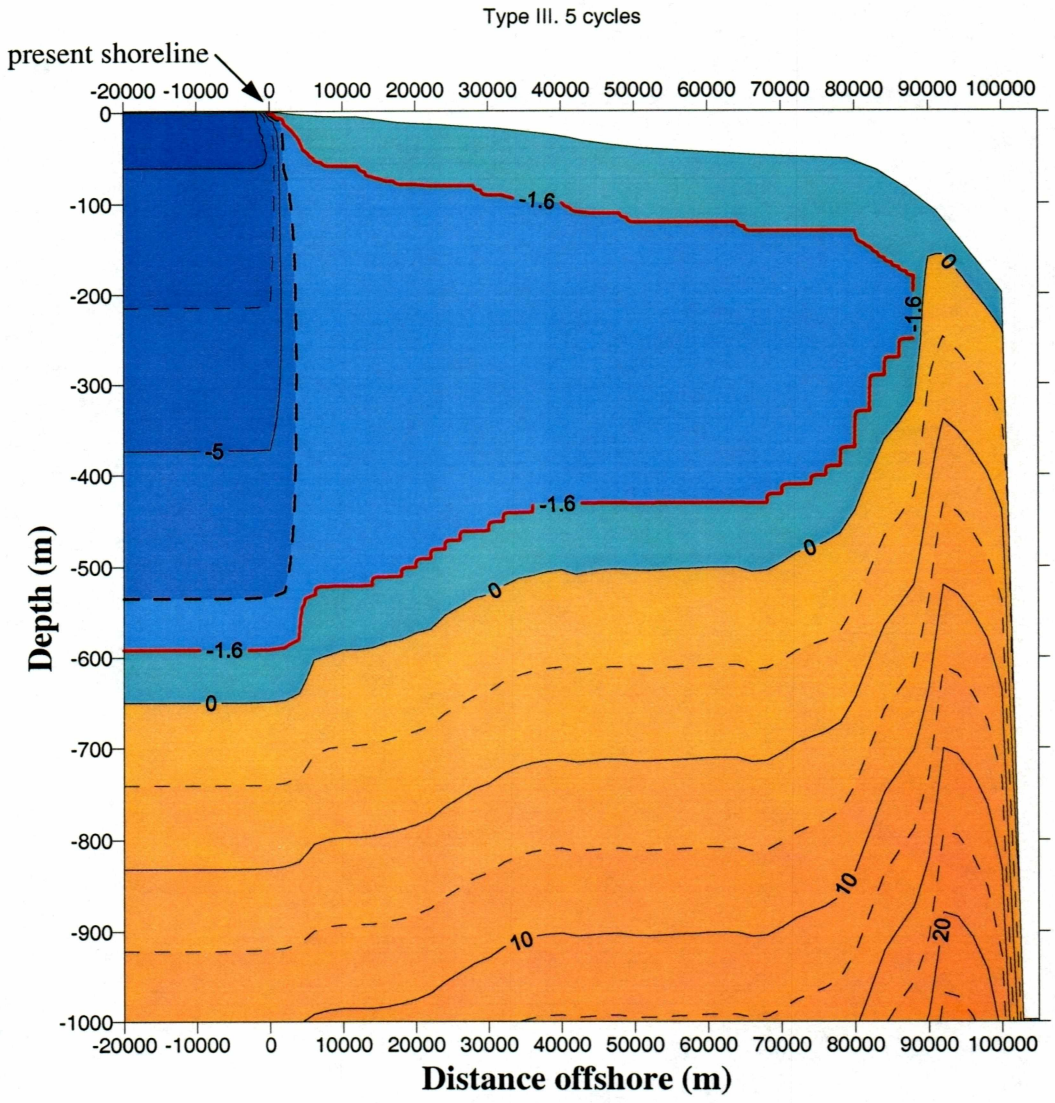

Figure 3.1.3b Results of modeling using Type III program (initial conditions for Type I and Type II). Temperature distribution at present time for coarse-grained material at Prudhoe Bay. Larger scale.

Table 3.1 Depth of predicted and measured permafrost base and table at Prudhoe

		Predicted						
		Prudhoe Bay, Coarse-grained soil			Prudhoe Bay, Fine-grained soil			Observed
		I	II	III	I	II	III	
Onshore	Permafrost thickness, m	521	425	592	301	288	344	560
	Error	-7%	-24%	6%	-46%	-49%	-39%	
14 km offshore	Permafrost table, m	36	39	62	40	40	57	90
	Error	-60%	-57%	-31%	-56%	-56%	-37%	
	Permafrost base, m	483	292	520	273	262	290	320
	Error	51%	-9%	62%	-15%	-18%	-9%	
	Permafrost thickness, m	447	254	457	233	223	233	230
	Error	94%	10%	99%	1%	-3%	1%	
Offshore extension of subsea permafrost, km		82	66.5	88	78	82	86	

3.1.4. Fine-grained material, results of modeling using the Type I program

Figure 3.1.4a shows the predicted current temperature distribution in the continental shelf along the profile at Prudhoe Bay. The thickness of ice-bearing permafrost onshore is 301 m and it gradually decreases from top and bottom offshore. The subsea permafrost has a wedge-like shape and extends up to 78 km offshore. At 14 km offshore, which corresponds to approximately 9 m isobath, the subsea permafrost table is at 40 m depth and the base of the permafrost is at 273 m, that gives 233 m of permafrost thickness. At 40 km offshore, which corresponds to approximately 28 m isobath, the subsea permafrost table is at 47 m depth and the base of the permafrost is at 195 m, that gives a 148 m of thickness. The unfrozen water content curve that has been used for this calculation gives a -1.92°C freezing point depression with a porosity of 0.565. The use of this curve might under-estimate the depth of the ice-bearing permafrost table in the offshore continental shelf. As already mentioned in 3.1.1., at the North Prudhoe State #1 well the depth of the ice bearing permafrost is about 560 m with a phase equilibrium temperature of -1.3°C (Lachenbruch et. al., 1982). This value is much larger than the onshore permafrost thickness obtained using this type of program and the soil properties in comparison with the coarse-grained case. The error for predicted thickness is about 46% (Table 4.1.). On the other hand, the values of subsea permafrost thickness offshore seem to be relatively close to the data from Reindeer Island (Fei, 1992). At 14 km offshore the error in predicted permafrost base is 15% and the error of total subsea permafrost thickness is 15% even though the results of predicted position of the subsea permafrost table are not really good (the error is more than 50%). Poor prediction of the permafrost table position might be, once again, caused by underestimation of the

phase equilibrium temperature in the upper layers of the sea bottom sediments due to seasonal freezing and thawing, hence higher salinity of the brine. Therefore, using -1.92°C for this temperature underestimates subsea ice-bearing's permafrost table, and for better prediction, equilibrium temperature in the upper layer of bottom sediments should be adjusted in accordance with this fact.

Lateral heat flow is high within first tens of kilometers offshore. From 42 to 78 km offshore permafrost is almost isothermal. At 78 km offshore (the maximum extent of permafrost) the -1.92°C isotherm is nearly vertical, which indicates horizontal heat flow. At the depth 300 m and below, the calculations show nearly uniform vertical temperature gradient except beyond 78 km offshore from the present shoreline.

Fig. 3.1.4b illustrates the predicted temperature distribution for 18 Ka B.P. During that time, permafrost reached its maximum thickness (353 m) and extent (more than 90 km offshore) after the glacial temperature minimum (22 – 23 Kyrs BP, t = -16.3°C) and the lowest sea level (22 Kyrs BP, sea level = -118 m) (fig 2.3). From 18 Ka B.P. sea level started to rise, hence due to this sea transgression, permafrost started to degrade. The degradation of permafrost for the last 18 Ka is 16.5% in thickness onshore, and the tip of subsea permafrost stepped back towards the shore by 10 km. Also, the permafrost table deepened by 40 m (closer to the present shoreline) to 80 (farther offshore) below the sea bottom during last 18 Kyr.

3.1.5. Fine-grained material, results of modeling using the Type II program

Figure 3.1.5a demonstrates the predicted current temperature distribution in the continental shelf along the profile at Prudhoe Bay. The thickness of ice-bearing permafrost onshore is 288 m and permafrost has a tubular shape within 22 km of the domain for calculations (20 km onshore and 2 km offshore), with a nearly horizontal

lower boundary. Then there is a step of the permafrost base from 288 m to 264 m within only a 4 km interval. From 6 km offshore up to 32 km offshore the base of permafrost moves upwards gradually and at 32 km offshore reaches 215 m below the sea bed. The subsea permafrost table deepens towards the offshore stepwise. Major steps are: 6 – 12 km, where the permafrost table is almost parallel to the sea bottom at 23 m depth; 14 – 28 km, where the depth of the permafrost table is about 40 m and still parallel to the bottom; at 30 – 40 km interval the table deepens to 50 – 52 m, 42 – 48 km offshore shows a horizontal permafrost table when the depth decrease from 60 to almost 50 m, at the 50 – 64 km offshore interval the table is again nearly horizontal with a depth of 65 – 67 m, and finally at the 66 – 80 km interval the permafrost table gets deeper to its maximum (78 m from the sea bottom). Between all these steps the permafrost table shows abrupt increases of its depth (usually about 10 m in depth on 2 km intervals). This step-like shape of the permafrost table could probably be explained by the coarse grid of the domain of calculation, because other factors like rate of transgression cannot give a reasonable explanation (sea transgression over last 18 Kyrs was very fast with mostly constant speed, it slowed down only during the last several thousand years). Subsea permafrost has a wedge-like shape with the maximum predicted extent of about 82 km. The maximum thickness of the subsea permafrost is 282 m right near the shore line; the minimum thickness is about 90 m at the farthest offshore (80 km). At 14 km offshore, which corresponds to approximately 9 m isobath, the subsea permafrost table is at 40 m depth and the base of the permafrost is at 262 m that gives a 222 m of thickness. Predicted permafrost table depth is not in good agreement with the data from Reindeer Island (90 m). The predicted depth of the permafrost base indicates relative error of 9% (262 m predicted

vs. 320 m observed). Once again, the depth to the ice-bearing permafrost table is under-estimated because of assumption of uniform equilibrium temperature within the domain of calculation (Table 3.1).

Lateral heat flow is very high within first several km offshore, it gets smaller toward the sea, and from 34 to 82 km offshore permafrost is almost isothermal. At 82 km offshore, the maximum extent of permafrost, the -1.92°C isotherm is nearly vertical, which indicates horizontal heat flow. Below the permafrost layer, the calculations show nearly uniform vertical temperature gradients except near 82 km and farther from the present shoreline.

Fig. 3.1.5b reveals the predicted temperature distribution for 18 Ka B.P. Permafrost onshore and offshore reached its maximum thickness (350 m) and extent (more than 90 km offshore), due to cold air temperature (5°C lower than present) and maximum shelf exposure (more than 90 km of shelf was exposed). From 18 Ka B.P. sea level started to rise (fig. 2.3), hence due to this sea transgression, permafrost started to degrade. The degradation of permafrost for the last 18 Ka is 17.7% in thickness onshore and permafrost moved towards the shore by more than 10 km. The permafrost has been thawing not only from the bottom but from the top as well. As mentioned above, the permafrost table deepened by 25 – 80 m in offshore zone during last 18 Kyr.

As in the coarse-grained material case, comparison of the results of modeling using Type I and Type II programs shows that there are differences in permafrost thicknesses and shape both onshore and offshore. The difference in predicted permafrost thickness using these two types of program reaches 4 to 6% for onshore and offshore region. But the difference is smaller in fine-grained material than in

coarse-grained because the larger values of porosity and moisture content in fine-grained soils make this media more inertial. The most visible differences occur at the lower boundary of permafrost: the base of permafrost looks smoother in case of Type II program. It is clearly understandable because of the auxiliary latent heat effect involved in the Type II program makes boundaries smoother and the whole system more inertial.

3.1.6. Fine-grained material, results of modeling using the Type III program

This version of the program assumed several very significant simplifications in comparison with the Type I and Type II versions: all phase transitions take place in an infinitely small temperature range (equilibrium temperature). In other words, it is assumed that there is no unfrozen water in the soils at temperatures below equilibrium; and the latent heat effect of gas hydrate phase transitions is not taken into account. This type of program was used to define initial temperature distributions for Type II and Type III programs and to determine the effect of temperature-dependant soil properties on the present permafrost distribution and its dynamics over the last 120 Kyrs. The program was run 9 consecutive times in order to get the "periodically steady state regime". For every new run the result of the previous calculation was used as an initial condition. Figure 3.1.6 shows the temperature distribution along the profile near Prudhoe Bay after 9 consecutive runs. In the onshore zone the thickness of permafrost is 344 m and it remains constant up to 2 km offshore. Farther offshore the base of the permafrost moves upwards by 10 m over a 2 km interval. At 4 km offshore there is an abrupt step in the base of permafrost, the boundary jumps almost by 40 m, stays nearly horizontal for the next 12 km then starts to gradually move upwards (40 m on the 14 km interval). From 30 to 78 km offshore the base of the

subsea permafrost remains almost horizontal and from 78 to 86 km it moves up again. The depth of the subsea permafrost table oscillates with a smaller range and, in general, increases almost linearly offshore reaching its maximum of 70 m below the sea bed at the farthest offshore zone.

Lateral heat flow is very large within first several kilometers offshore, but the rest of the offshore permafrost is almost isothermal. Below the permafrost layer, the calculations show a nearly uniform vertical temperature gradient except near 86 km and farther offshore.

Using this type of program with this set of soil properties underestimates the thickness of onshore permafrost but gives reasonable values of the permafrost base position offshore (relative error 9%, Table 3.1).

Comparing the results for coarse-grained and fine-grained material (figures 3.1.1a, 3.1.1c, 3.1.2a, 3.1.2c, and 3.1.4a, 3.1.4a, 3.1.5a, 3.1.5b), it can be seen that during last 18 Kyrs the degradation of permafrost for the fine-grained material is relatively slower. The reason for this is probably higher porosity and moisture content that were assumed for fine-grained soil case. Thawing from the bottom of permafrost requires more heat because of the larger amount of water changes its phase, thereby the thawing rate lowers.

Analysis of the results of all tree type of programs and two types of material used for the simulations near Prudhoe Bay suggests that for onshore permafrost the best prediction of thickness can be obtained using either Type I or Type III programs with coarse-grained soil properties (each of them has the smallest relative errors towards underestimation or overestimation). For the prediction of offshore permafrost thickness the best results can be obtained from Type II program with coarse-grained

soil parameters or any type of programs with fine-grained soil properties. The depth of subsea permafrost table is underestimated using both coarse-grained and fine-grained soil cases and all three types of calculation methods, because of not taking into account layer salinity of the near-bottom sediments (which occur on the shelf due to annual freezing-thawing processes when the sea ice freezes to the bottom). The fact that Type III programs do not seem to work well in offshore permafrost prediction implies that it is not possible to adequately simulate the thermal regime of subsea permafrost by using constant thermal parameters, and that constant thermal parameters can only be used on land. Even more accurate results for subsea permafrost thickness and position of the base and table of permafrost can be obtained if the latent heat effect of gas hydrate formation along with temperature-dependant (as a function of unfrozen water content) soil properties are used for the modeling.

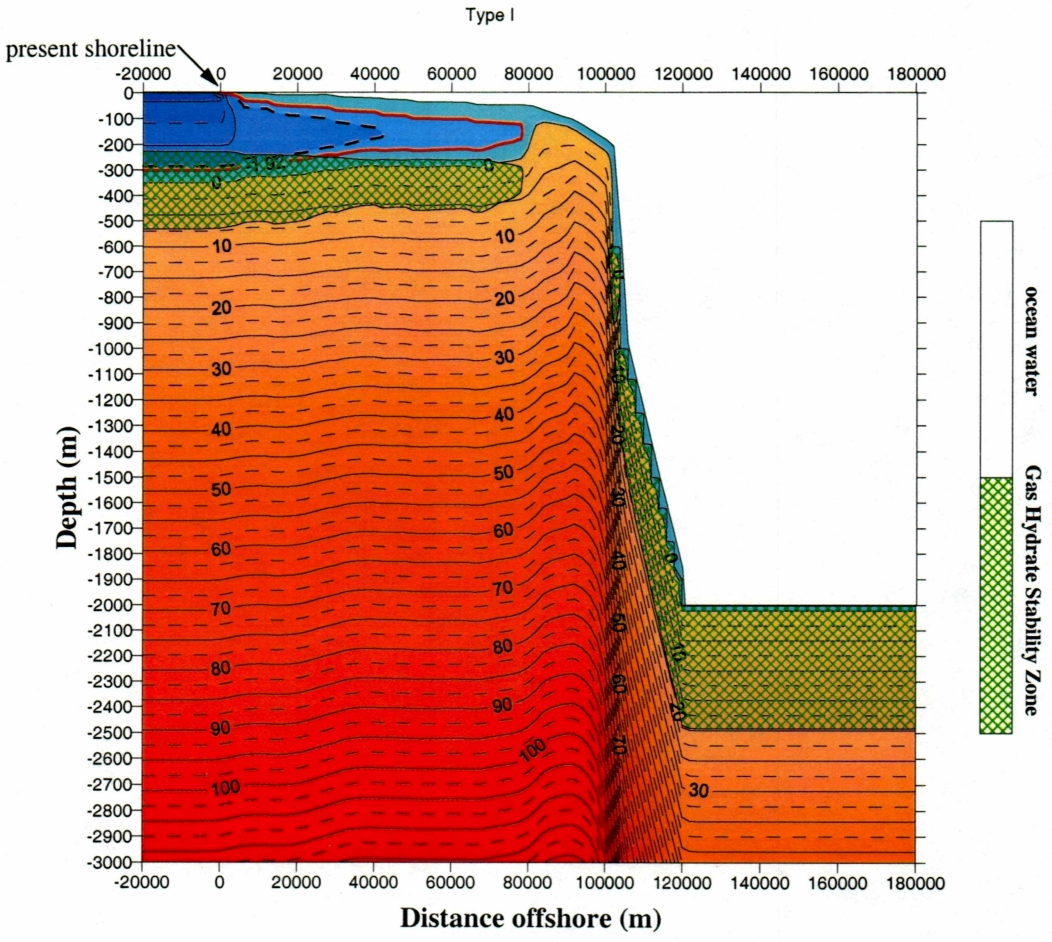

Figure 3.1.4a Results of modeling using Type I program. Temperature distribution and Gas Hydrate Stability Zone at present time for fine-grained material at Prudhoe Bay.

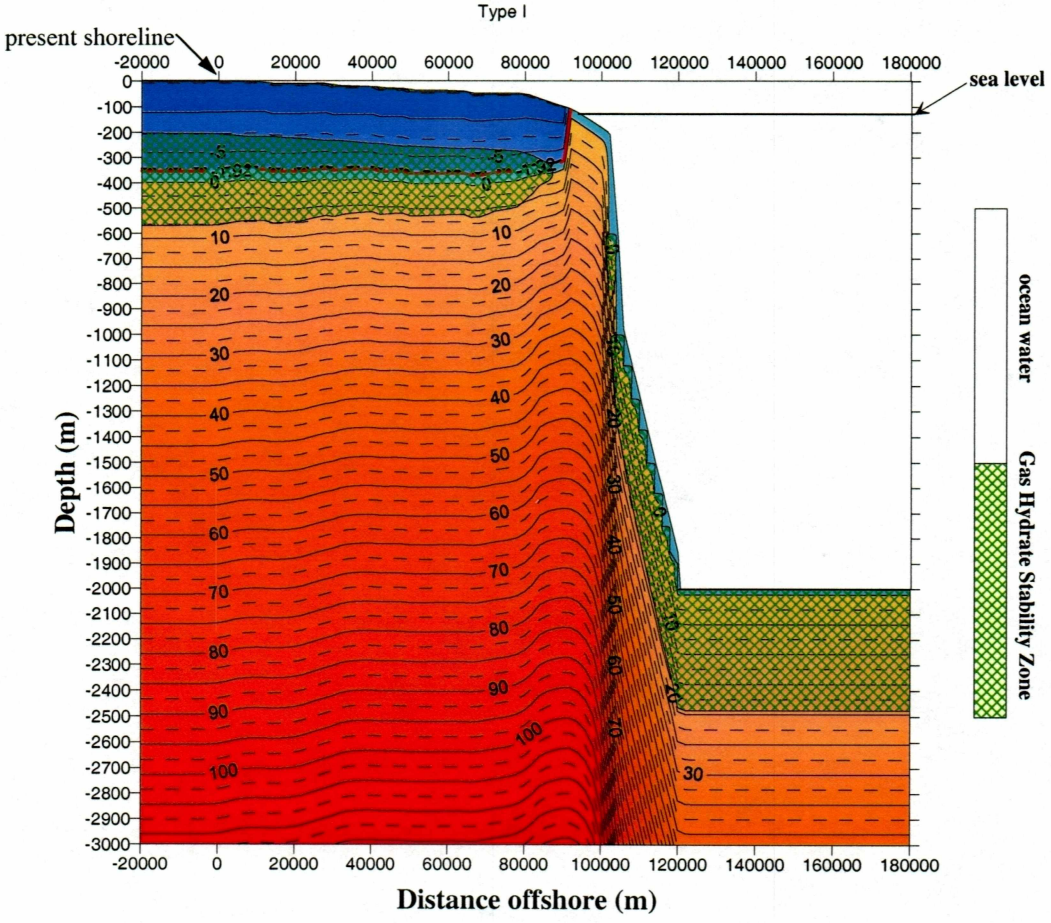

Figure 3.1.4b Results of modeling using Type I program. Temperature distribution and Gas Hydrate Stability Zone at 18 Kyrs BP for fine-grained material at Prudhoe Bay.

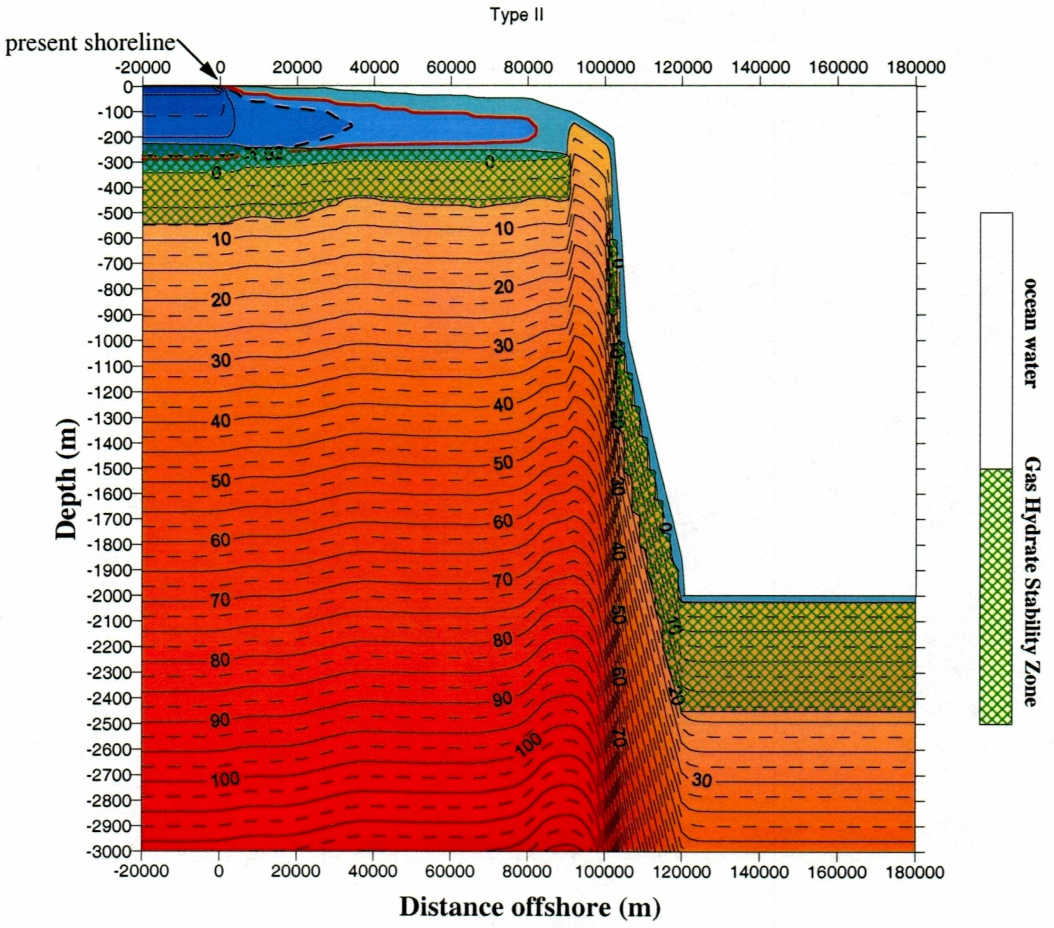

Figure 3.1.5a Results of modeling using Type II program. Temperature distribution and Gas Hydrate Stability Zone at present time for fine-grained material at Prudhoe Bay.

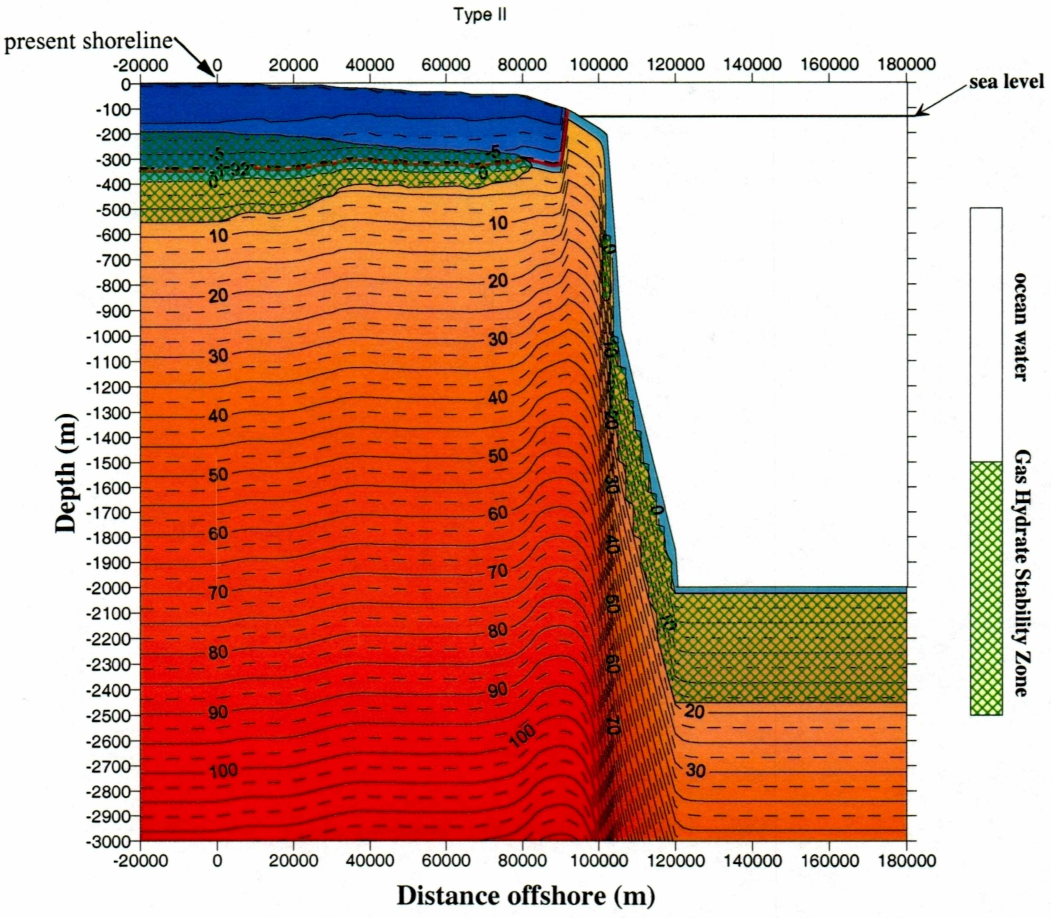

Figure 3.1.5b Results of modeling using Type II program. Temperature distribution and Gas Hydrate Stability Zone at 18 Kyrs BP for fine-grained material at Prudhoe Bay.

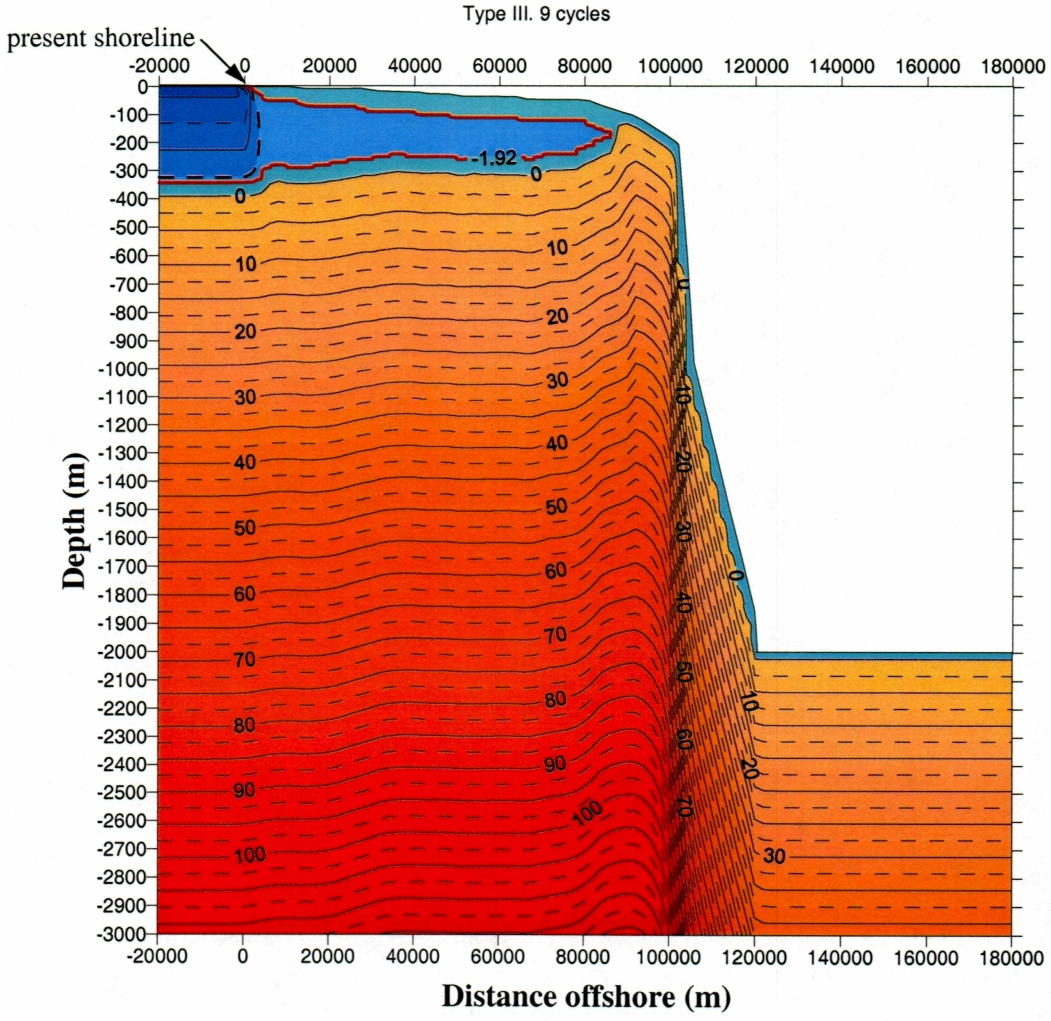

Figure 3.1.6 Results of modeling using Type III program (initial conditions for Type I and Type II). Temperature distribution at present time for fine-grained material at Prudhoe Bay.

3.2. Simulations at Lonely

This site, offshore from Lonely, was chosen because of availability of data from other research (Osterkamp and Fei., 1993), from onshore and offshore petroleum exploration wells, such as Antares and J.W. Dalton-1 (Collett et. al., 1989, Deming et. al., 1992), and from results of thermal studies in shallow drill holes (Harrison and Osterkamp, 1981).

Simulations were carried out for fine-grained material using three types of programs (described in 3.1). Properties of sediments that have been used for the simulations are presented in Chapter 2. The lower boundary condition was assumed to be the temperature gradient at 3000 meters depth and has been calculated to correspond to the 0.065 W/m^2 value of geothermal heat flow, which is typical for that region. According to soil properties, the position of the base and the table of permafrost were determined for the specific freezing point depression – 1.63°C.

3.2.1. Results of modeling using the Type I program

Figure 3.2.1a shows the current temperature distribution for the calculation domain. Permafrost extends offshore only to 22 km and has a tabular shape, slightly deformed towards the sea. The predicted thickness of permafrost onshore is 312 m, which in comparison to the interpretation of Osterkamp and Fei (1993), gives an error of 13.3% (360 vs. 312 m) (Table 3.2.). Permafrost base is horizontal up to 12 km offshore, and then the depth of the permafrost base starts to decrease and at the distance of 22 km closes up with permafrost table with a small tip. The depth of subsea permafrost table increases with distance offshore slow by within the first 12 km interval (at 8 km offshore, the depth of permafrost table is 7 m which is in a good agreement with data obtained during drilling (Harrison and Osterkamp, 1981)).

Farther offshore it starts to increase very fast and at 22 km offshore closes up with the permafrost base. The tip of subsea permafrost is at a depth of about 82 meters and it is the remains of wide-spread shelf permafrost, which has been degrading during last 18 Kyrs because of the sea transgression.

Figure 3.2.1b illustrates the temperature and permafrost distribution at 18 Kyrs BP. By that time the shelf was almost completely exposed (up to 118 m isobath) and permafrost occupied the shelf up to 86 km from the present shore line. The thickness reached 420 m. Since 18 Kyrs BP, the sea transgression began and permafrost started to degrade from 3 directions: from the top, bottom and laterally. Degradation from the bottom reached almost 100 m or 24.3% and laterally permafrost retreated by more than 60 km.

Lateral heat flow is relatively high within the entire cross-section, especially at 22 km offshore, where isotherms are almost vertical and indicate horizontal heat flow. Vertical temperature gradients become nearly uniform with depth below 360 m, but still, there are some distortions in the area close to the continental slope.

3.2.2. Results of modeling using the Type II program

Figure 3.2.2a demonstrates the temperature profile at the present time at Lonely. Predicted thickness of permafrost onshore is 312 m which is the same as the solution for the Type I program. In general, permafrost has an almost identical shape as in 3.2.1., but there are some insignificant differences, such as: maximum extent of permafrost is 2 km farther offshore as a result of a more elongated tip. The permafrost table is at the same depth as in chapter 3.2.1. Even though the difference in -1.63°C position is insignificant, hence the shape of permafrost in both these cases looks much alike, some other isotherms positions differ in 3.2.1.and 3.2.2. The reason is that the

Gas Hydrate Stability Zone strongly influences the temperature regime. This topic will be covered in Chapter 4.

The temperature distribution at 18 Kyrs BP is shown on Figure 3.2.2b. In comparison with Type I results, the thickness of permafrost at its maximum is slightly thinner (380 m vs. 420m). The degradation of permafrost from the bottom over the last 18 Kyrs is 16.3%. Since all input parameters were assumed to be the same for Type I and Type II programs, the slower rate of permafrost thawing can be explained only by auxiliary latent heat effect of the gas hydrate formation.

3.2.3. Results of modeling using the Type III program

Results of modeling using the Type III program are presented in Figure 3.2.3. This type of program represents the solution for temperature-independent soil properties, where all phase changes take place at the equilibrium temperature (assumed to be -1.63°C) and there is no unfrozen water in the pore space below this temperature. Hence, thermal conductivity and heat capacity of the material remain constant at temperatures below equilibrium. The predicted thickness of onshore permafrost is 355 m, which is in a good agreement with J.W. Dalton-1 well data. The results also show that a relatively thin layer of subsea permafrost exists in the continental shelf up to 36 km offshore. Large values of lateral heat flow are indicated in the near shore area (about 3 km offshore). Farther offshore the heat flow decreases and in the permafrost layer from 10 to 36 km offshore, nearly uniform temperature can be observed. In the offshore region, the predicted base of permafrost remains constant at first 4 km offshore, slightly rises over the next 6 km (by 5 m), then rises rapidly at the 10 to 20 km offshore interval. At 20 to 36 km interval the base of permafrost continues to rise but with a slower rate, where it reaches its minimum

depth of 117 m below the sea bed.

In comparison with Prudhoe Bay, distribution of permafrost near Lonely is quite different. The difference is mainly caused by soil properties and higher geothermal heat flow, which increases the thawing rate from the bottom. At Lonely the porosity of the material is only 0.2 (in comparison to 0.416 and 0.565 for Prudhoe Bay) and the permafrost contains much less ice and hence, much less heat is needed to thaw the permafrost. Also, less porosity makes the difference between thermal conductivity in the thawed and frozen state smaller, which in its turn makes the whole system less inertial.

Results of modeling show that the model Type III gives the best prediction for on-land permafrost thickness. Similar results were obtained for on-land permafrost thickness prediction at Prudhoe Bay as well. However because of lack of data for the offshore permafrost table and base position, it cannot be unambiguously concluded what type of program works better for offshore permafrost prediction. At the same time, the better prediction for the permafrost table offshore can be obtained using either Type I or Type II programs. Still some underestimation of the depth of permafrost table might occur due to not taking into account increased salinity of the upper layer of the bottom sediments in the near shore area.

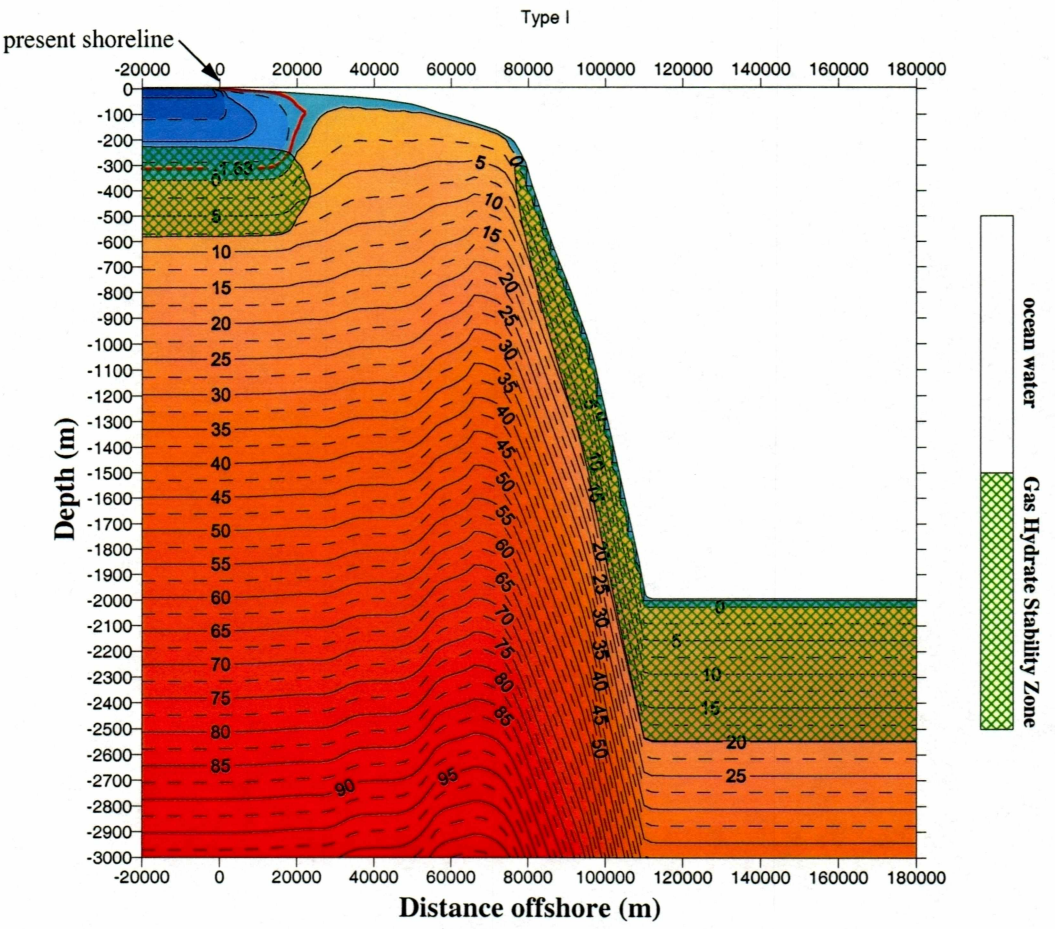

Figure 3.2.1a Results of modeling using Type I program. Temperature distribution and Gas Hydrate Stability Zone at present time at Lonely.

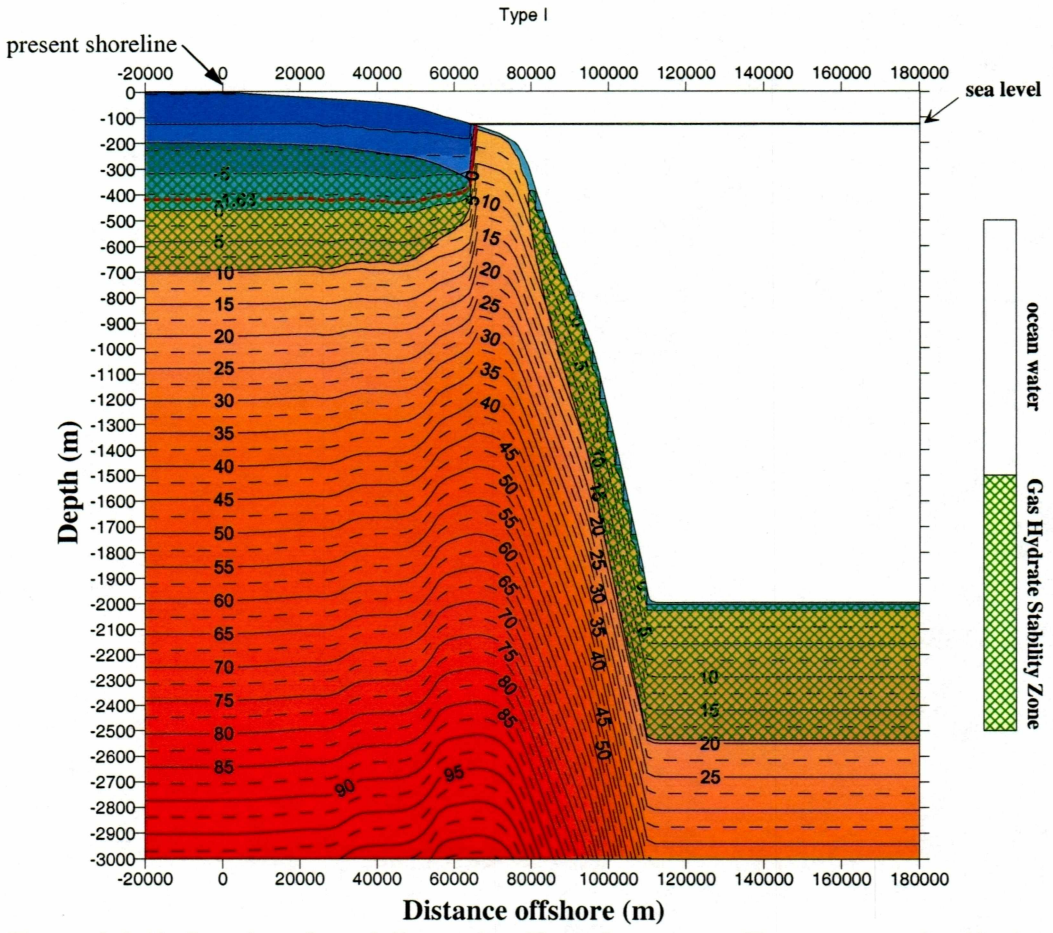

Figure 3.2.1b Results of modeling using Type I program. Temperature distribution and Gas Hydrate Stability Zone at 18 Kyrs BP at Lonely.

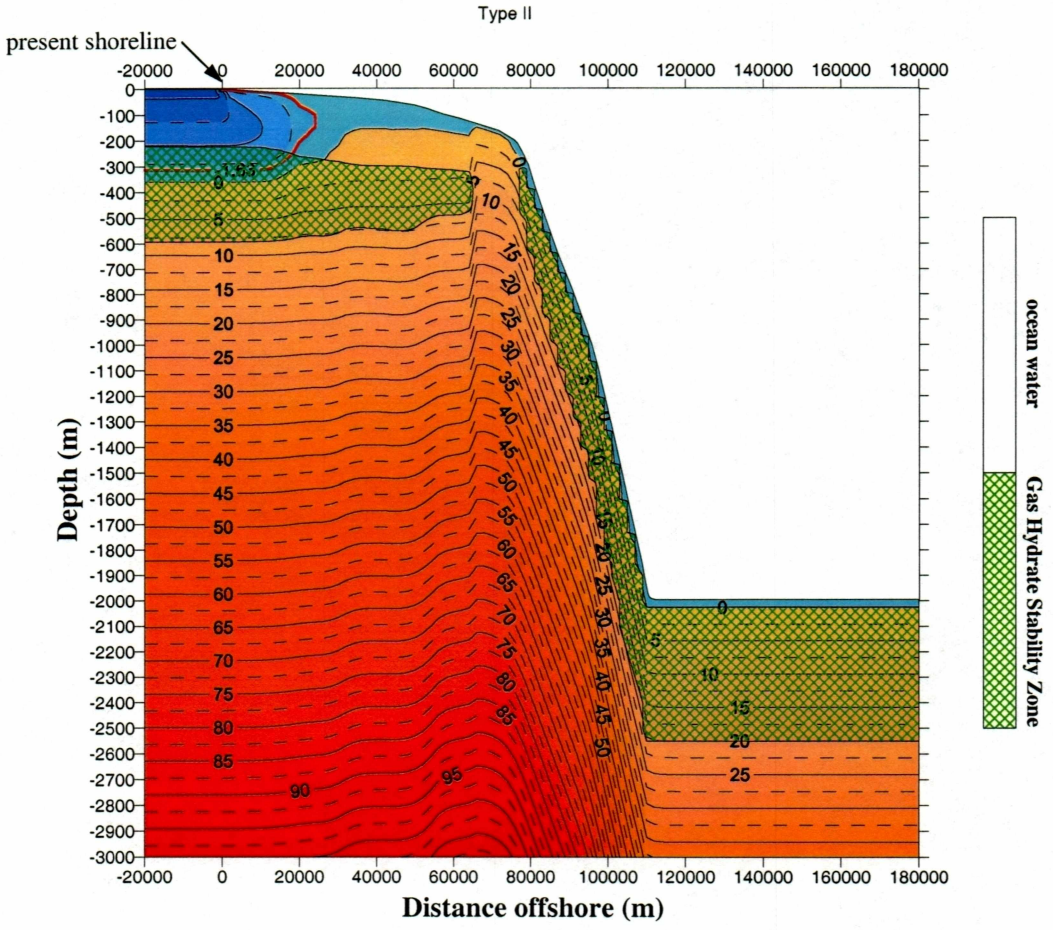

Figure 3.2.2a Results of modeling using Type II program. Temperature distribution and Gas Hydrate Stability Zone at present time at Lonely.

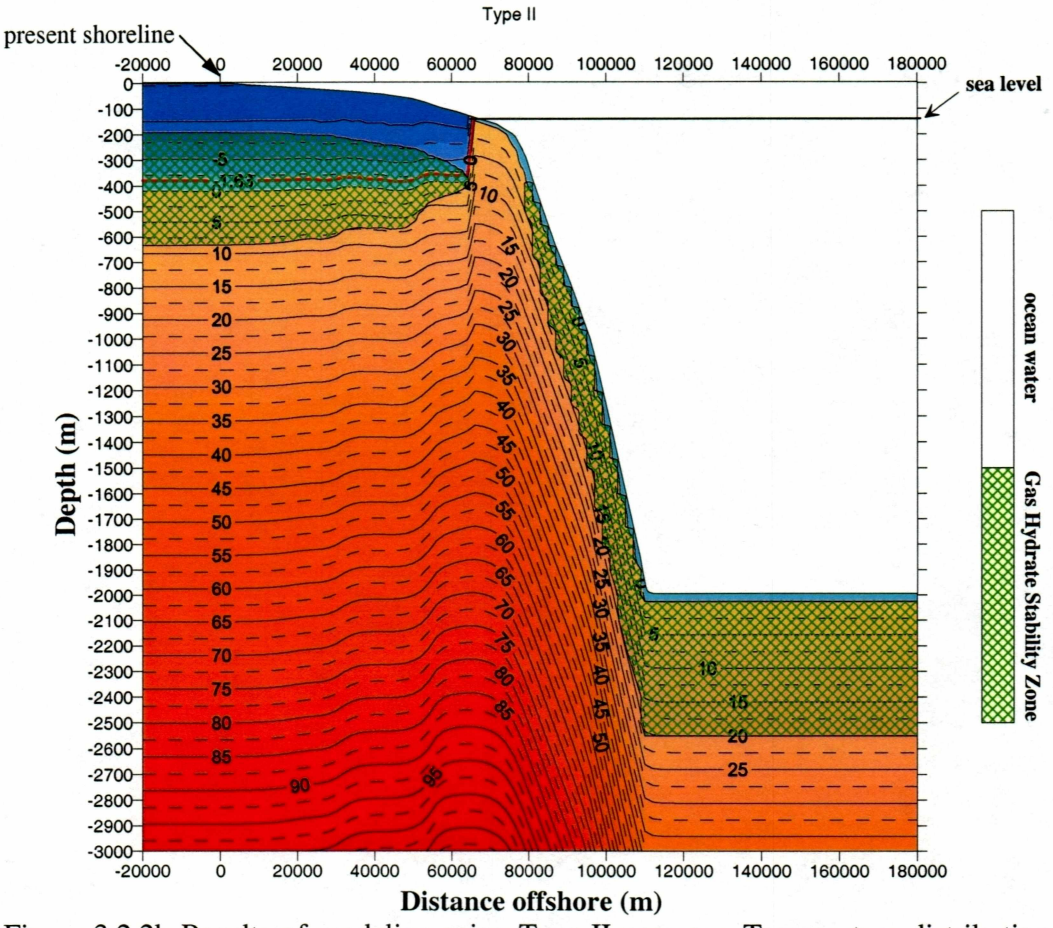

Figure 3.2.2b Results of modeling using Type II program. Temperature distribution and Gas Hydrate Stability Zone at 18 Kyrs BP at Lonely.

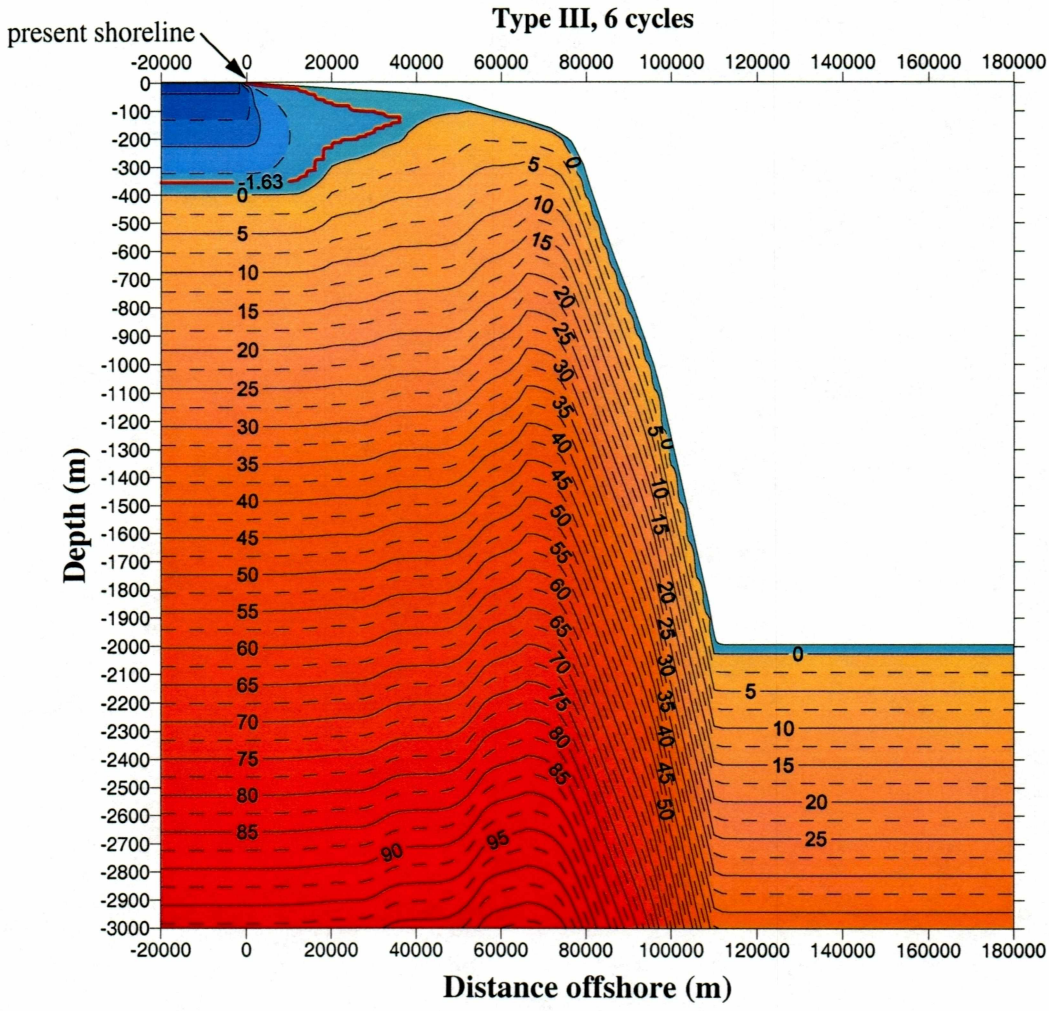

Figure 3.2.3 Results of modeling using Type III program (initial conditions for Type I and Type II). Temperature distribution at present time at Lonely.

Table 3.2 Depth of predicted permafrost base and table at Lonely.

		Type I	Type II	Type III	Observed[3]
Onshore	Permafrost thickness, m	312	312	355	360
	Error	13.3%	13.3%	1.4%	
≈ 8 km offshore	Permafrost table, m	7	7.5	13	7 – 15
	Error	-	-	-	
	Permafrost base, m	311	310	350	-
	Error	-	-	-	
	Permafrost thickness, m	304	302.5	337	-
	Error	-	-	-	
≈ 20 km offshore	Permafrost table, m	60	60	65	-
	Error	-	-	-	
	Permafrost base, m	160	200	230	272
	Error	41%	26.5%	15.4%	
	Permafrost thickness, m	100	140	165	-
	Error	-	-	-	
Offshore extent of subsea permafrost, km		22	24	36	-

[3] Osterkamp and Fei, 1992

3.3. Simulations at Barrow

Modeling of permafrost conditions at Barrow was done using the same scenario as at Lonely (see 3.2). Barrow is located 135 km northwest from Lonely. The bathymetry at the shelf near Barrow is very similar to that at Lonely. Soil properties were assumed to be the same as in 3.2. The main difference was in upper boundary conditions, where the paleotemperature curve was modified to provide current mean annual temperature (fig. 2.5).

3.3.1. Results of modeling using the Type I program

In figure 3.3.1a, the predicted current temperature distribution is presented. Thickness of on-land permafrost is 371 m, and permafrost extends out to 28.5 km offshore. The depth to the subsea permafrost table is between several meters near the coast and up to 80 m at the subsea permafrost tip (at 28 km offshore). The base of permafrost is 371 m deep onshore and it remains constant up to 12 km offshore, then it starts to decrease very fast. Table 3.3 shows predicted positions of the permafrost table and base.

The temperature distribution for the period of coldest temperature and maximum shelf exposure (18 Kyrs BP) is shown in fig. 3.3.1b. The thickness of permafrost reached 470 m and permafrost covered the entire shelf (about 65 km from present shoreline). From 18 Kyrs to the present sea level has been rising and permafrost has been degrading from the top and the bottom and also in a lateral direction towards the shore. Vertical degradation for the last 18 Kyrs is 21%; permafrost retreated by 36.5 km towards the shore during the period.

Lateral heat flow in permafrost is relatively large within the entire cross-section. From 20 to 28 km offshore, isotherms are almost vertical, which indicates

horizontal heat flow.

3.3.2. Results of modeling using the Type II program

Figure 3.3.2a shows the current temperature profile at Barrow. Permafrost onshore is almost 20 meters thinner than that shown in the Type I results (351 vs. 370 m). The shape of subsea permafrost is very similar to that shown in 3.3.1. The offshore extent of permafrost is 26 km, which is 2.5 km less than for the Type I program. The table of subsea permafrost is 6.5 m deep at 10 km offshore and it gets deeper toward the sea. The main difference in the results of calculations using the Type I and Type II program occurs at the 25 – 65 km distance offshore at depths up to 700 meters because of the presence of Gas Hydrate Stability Zone within this area in Type II results.

Temperature distribution at 18 Kyrs BP is revealed in fig. 3.3.2b. The thickness of permafrost is 50 meters less than results obtained using Type I program (420 vs. 470 m). Because the latent heat of gas hydrate formation is taken into account in this type of program, more energy is expended for the phase transition processes, and, hence, the thickness of permafrost at 18 Kyrs BP is smaller for the Type II program. The degradation of permafrost from the bottom over the last 18 Kyrs for the Type II program is also smaller (16.7%).

3.3.3. Results of modeling using the Type III program

Results are presented in fig. 3.3.3. The temperature distribution profile shows distinctive differences when compared to Type I and Type II. The permafrost extends farther offshore (up to 48 km) and has a wedge-like shape from 10 km offshore to its tip. Also, from 10 km offshore, nearly uniform temperature in permafrost can be observed. Such a wedge-like shape of subsea permafrost can be explained by the

following: when sea level started to rise, covering the previously exposed and frozen shelf with relatively warm water, permafrost started to degrade from the top. Since this type of program does not take into account unfrozen water content in soils, all phase transitions happen at the equilibrium temperature, so the temperature regime reacts very fast on the changes in boundary conditions. With the sea level rising, the temperature field started to change to reach an equilibrium state. Because of constant geothermal heat flow, the vertical temperature gradient started to change as well. Both of these two factors, as a result, formed this wedge-like shape.

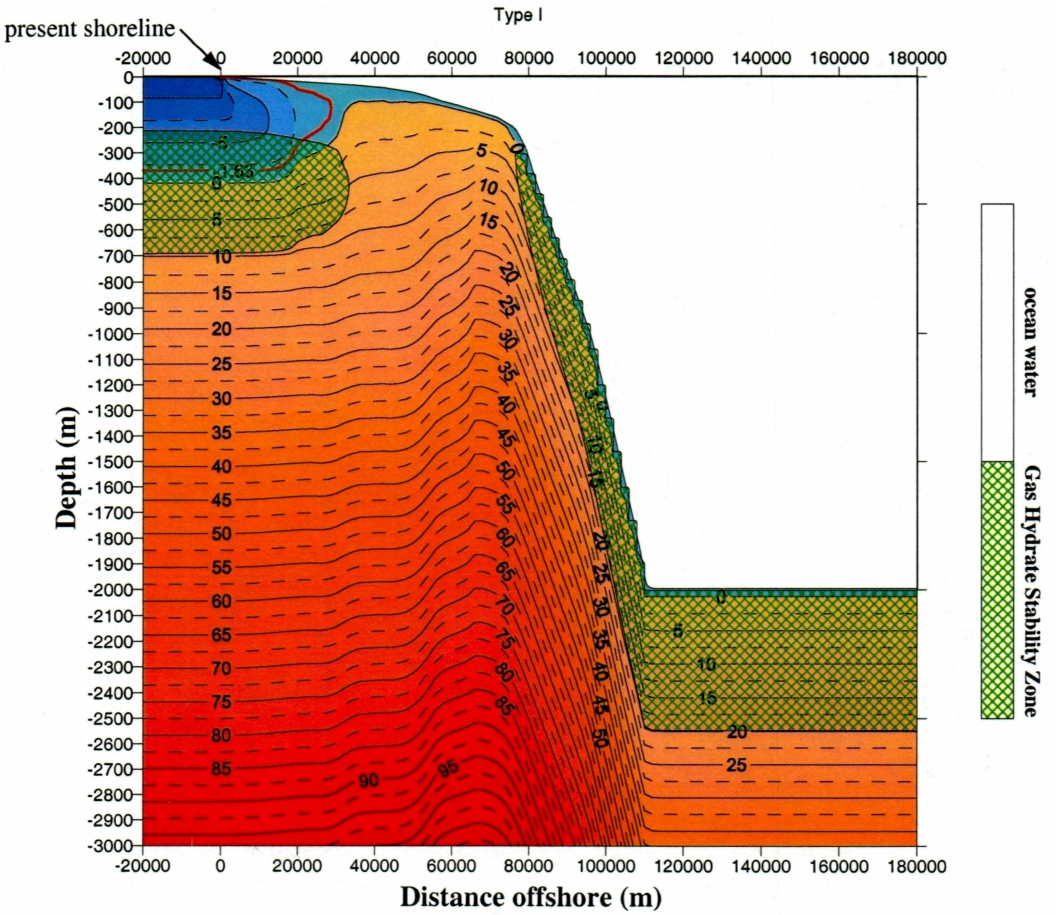

Figure 3.3.1a Results of modeling using Type I program. Temperature distribution and Gas Hydrate Stability Zone at present time at Barrow.

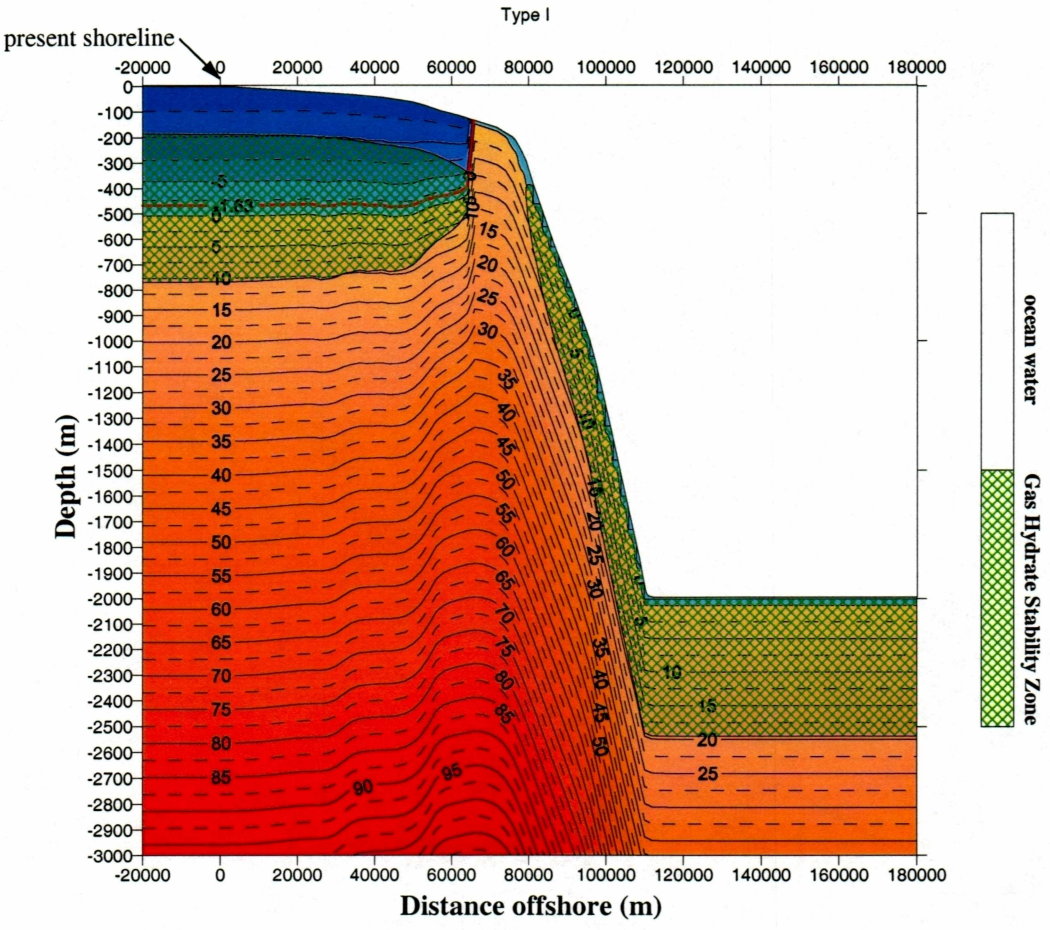

Figure 3.3.1b Results of modeling using Type I program. Temperature distribution and Gas Hydrate Stability Zone at 18 Kyrs BP at Barrow.

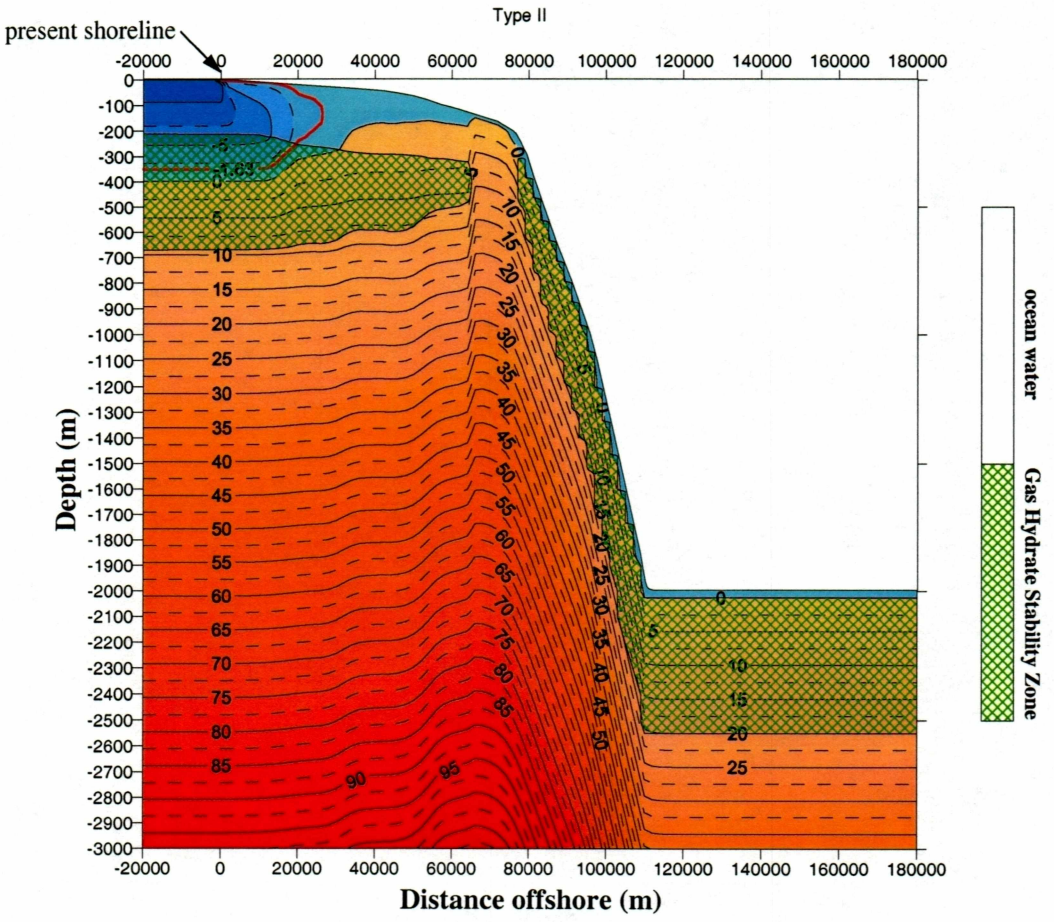

Figure 3.3.2a Results of modeling using Type II program. Temperature distribution and Gas Hydrate Stability Zone at present time at Barrow.

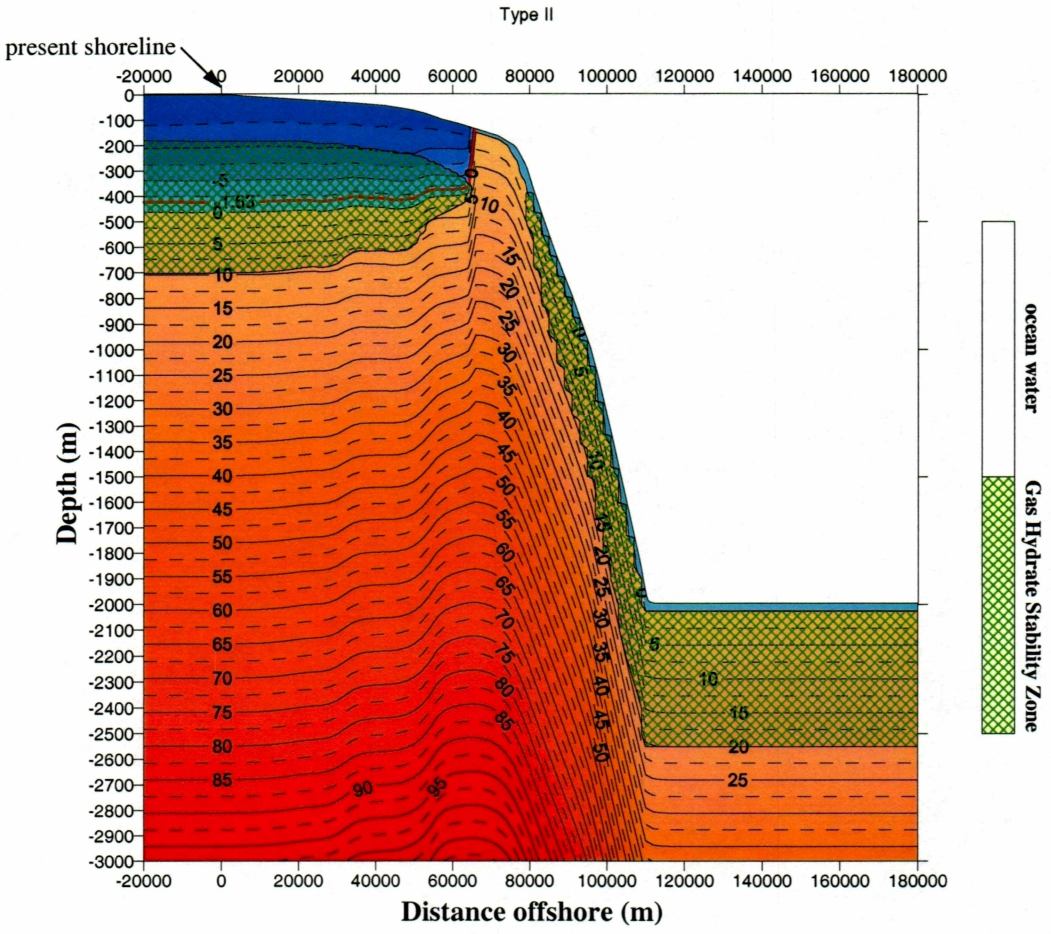

Figure 3.3.2b Results of modeling using Type II program. Temperature distribution and Gas Hydrate Stability Zone at 18 Kyrs BP at Barrow.

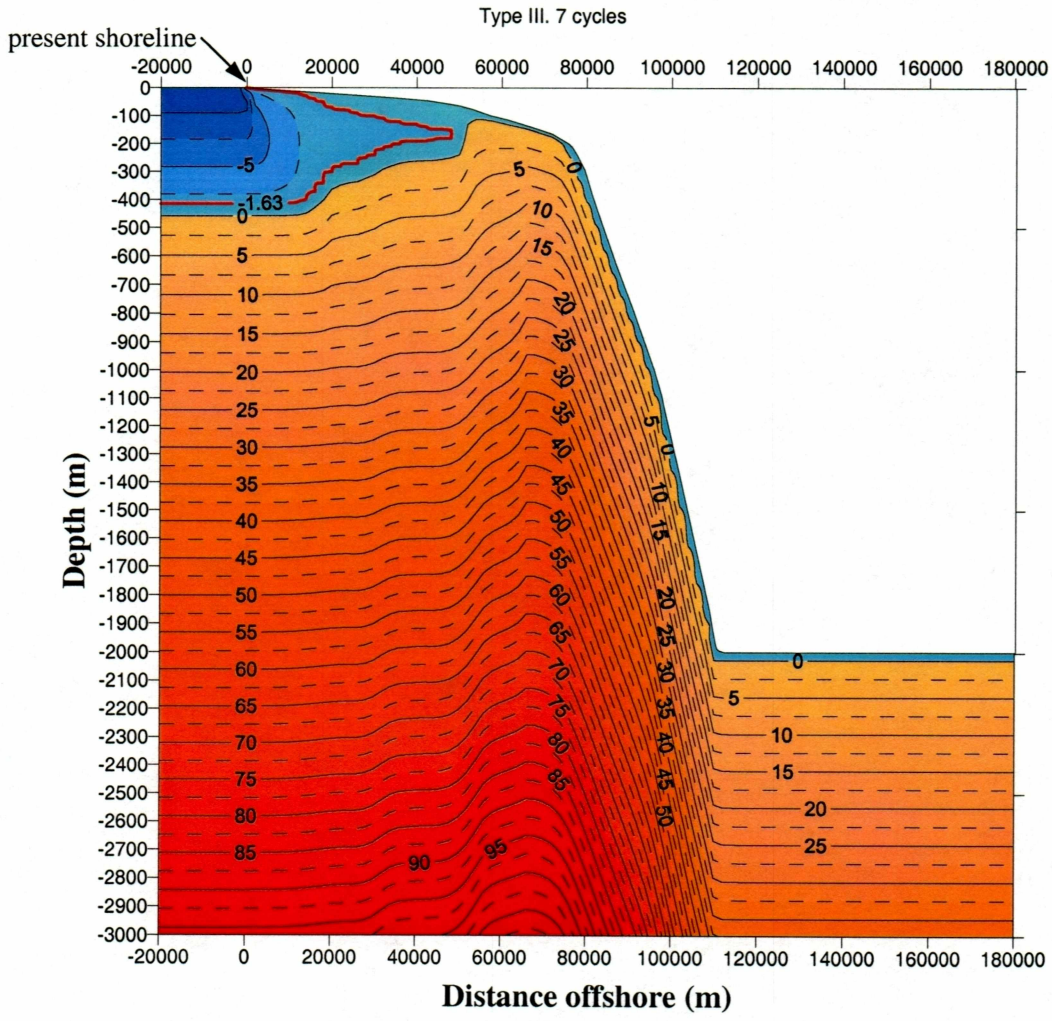

Figure 3.3.3 Results of modeling using Type III program (initial conditions for Type I and Type II). Temperature distribution at present time at Barrow.

Table 3.3 Depth of predicted permafrost base and table at Barrow.

		Type I	Type II	Type III
Onshore	Permafrost thickness, m	371	350	413
≈ 10 km offshore	Permafrost table, m	6.5	6.5	15
	Permafrost base, m	367	342	405
	Permafrost thickness, m	360.5	335.5	390
≈ 20 km offshore	Permafrost table, m	45	50	65
	Permafrost base, m	260	232	285
	Permafrost thickness, m	215	182	230
offshore extent of subsea permafrost		28.5	26	48

3.4. Simulations at Cape Thompson

Simulations for a site near Cape Thompson were carried out for very fine-grained material (mudstone) with extremely low porosity 0.042 (see Table 2.1). The freezing point depression for this type of material was set to -0.524°C. Geothermal heat flow from the lower boundary for this site was taken as 0.058 W/m^2 or, in terms of the geothermal temperature gradient, 0.02071°C/m. Other differences in boundary conditions for this site were the temperature of the sea water: at the Cape Thompson site it was assumed to be 0.2°C, also the paleotemperature curve were modified (see Fig. 2.4).

3.4.1. Results of modeling using the Type I program

Figure 3.4.1a illustrates predicted current temperature distribution for Cape Thompson. On-land permafrost reaches 302 m thickness, which is in good agreement with data obtained by Lachenbruch et. al. (1966). Subsea permafrost was almost completely thawed during the last sea transgression and is now only 0.8 km, possibly even less. Figure 3.4.1b shows the temperature and permafrost distribution at 18 Kyrs BP. Permafrost thickness at that time reached almost 458 m. Because of the limited size of the calculated domain, the maximum offshore extent of permafrost can not be predicted, but due to the fact that shelf of Chukchi Sea at that time was completely exposed, it suggests that permafrost occupied the entire shelf, from Cape Thompson up to the shore of Chukchi peninsula. Vertical degradation of permafrost during the last 18 Kyrs onshore is 34%, offshore permafrost, as mentioned above, has completely disappeared at least within 65 km offshore near Cape Thompson. Lachenbruch et. al. (1966) suggest that subsea permafrost near Cape Thompson cannot exist more than 300 m offshore, while our results of modeling show the

possible extent of subsea permafrost up to 800 m. Such a big difference can be explained by the lack of a fine enough-grid in our modeling (lateral step interval of 2 km was used), and, also, by inaccurate selection of sea water temperature. However, the main goal of the modeling was to look at the permafrost distribution in a larger scale, so these results are satisfactory.

Lateral heat flow is very high near shoreline, where the isotherms are almost vertical. Under the permafrost, the vertical temperature gradient is close to linear except in the near-shore region.

3.4.2. Results of modeling using the Type II program

Results of modeling using the Type II program are presented in fig. 3.4.2a and 3.4.2b. Fig.3.4.2a shows the predicted temperature distribution for the present. In comparison with the results of Type I program, permafrost thickness on-land is insignificantly larger (307 m vs. 302 m) at present, while the offshore extent of subsea permafrost is the same. As already mentioned, material at Cape Thompson is very fine-grained, the porosity is very low, making the difference in the results using Type I or Type II programs small. Even in these conditions, the effect of taking into account the latent heat of gas hydrate formation influences the temperature distribution and permafrost thickness. Figure 3.4.2b shows predicted temperature distribution at 18 Kyr BP, when permafrost was near its maximum thickness over the last 120 Kyrs. Results of modeling show a 446 m thickness of permafrost, which is 12 m less than in the Type I program. Also, the degradation of permafrost during last 18 Kyrs is 31%, which is 3% less than in 3.4.1. Slower degradation rate, thinner permafrost at 18 Kyrs BP, and thicker permafrost at the present are the result of auxiliary latent heat, that are accounted for the Type II calculations.

3.4.3. Results of modeling using the Type III program

The predicted temperature distribution at the present, which also has been used as initial conditions for Type I and Type II simulations, is shown in fig. 3.4.3. Permafrost thickness onshore is 305 m. The offshore extent of subsea permafrost is the same as in Type I and Type II simulations (800 m). In general, the temperature field looks very similar to the results of modeling using the Type I program. It is very predictable, because these programs (Type I and Type III) do not take into account the latent heat of gas hydrate formation and, due to very low porosity and unfrozen water content, the effect of the unfrozen water on the thermal properties of material becomes very small.

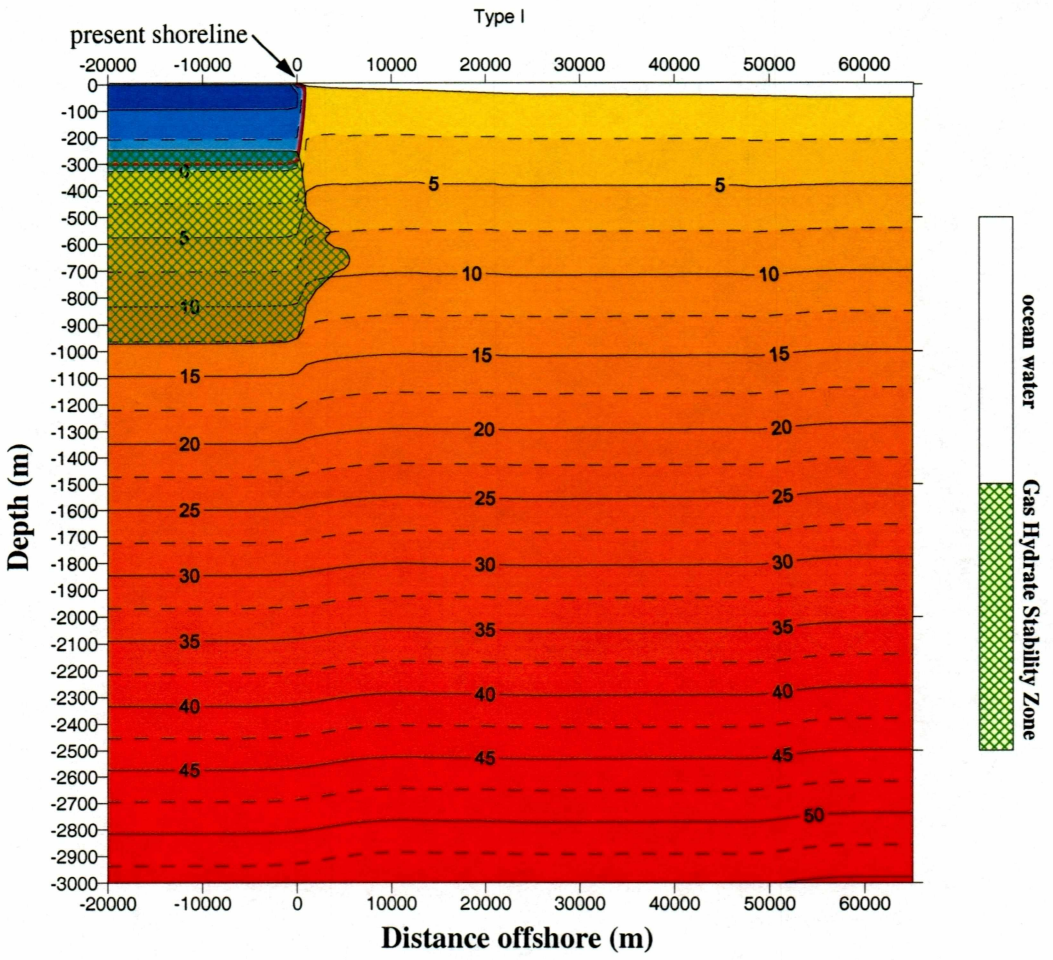

Figure 3.4.1a Results of modeling using Type I program. Temperature distribution and Gas Hydrate Stability Zone at present time at Cape Thompson.

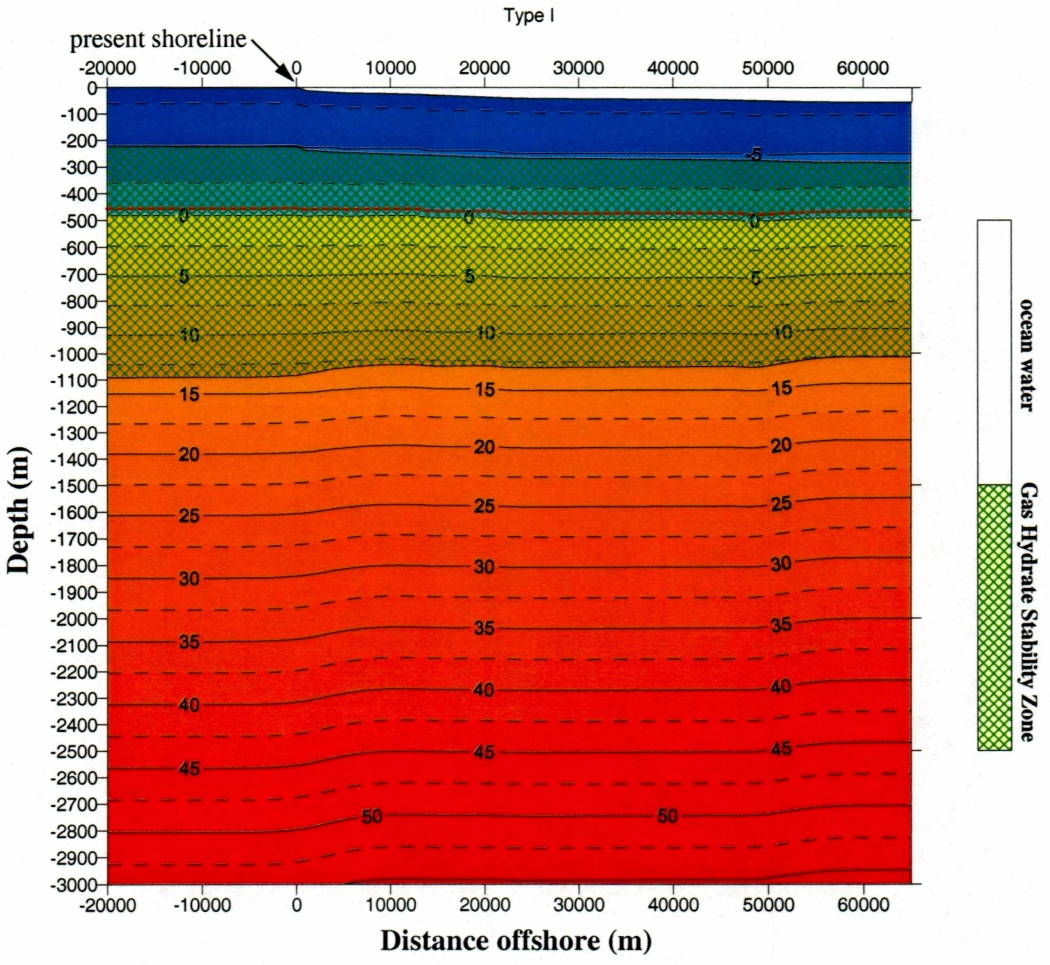

Figure 3.4.1b Results of modeling using Type I program. Temperature distribution and Gas Hydrate Stability Zone at 18 Kyrs BP at Cape Thompson.

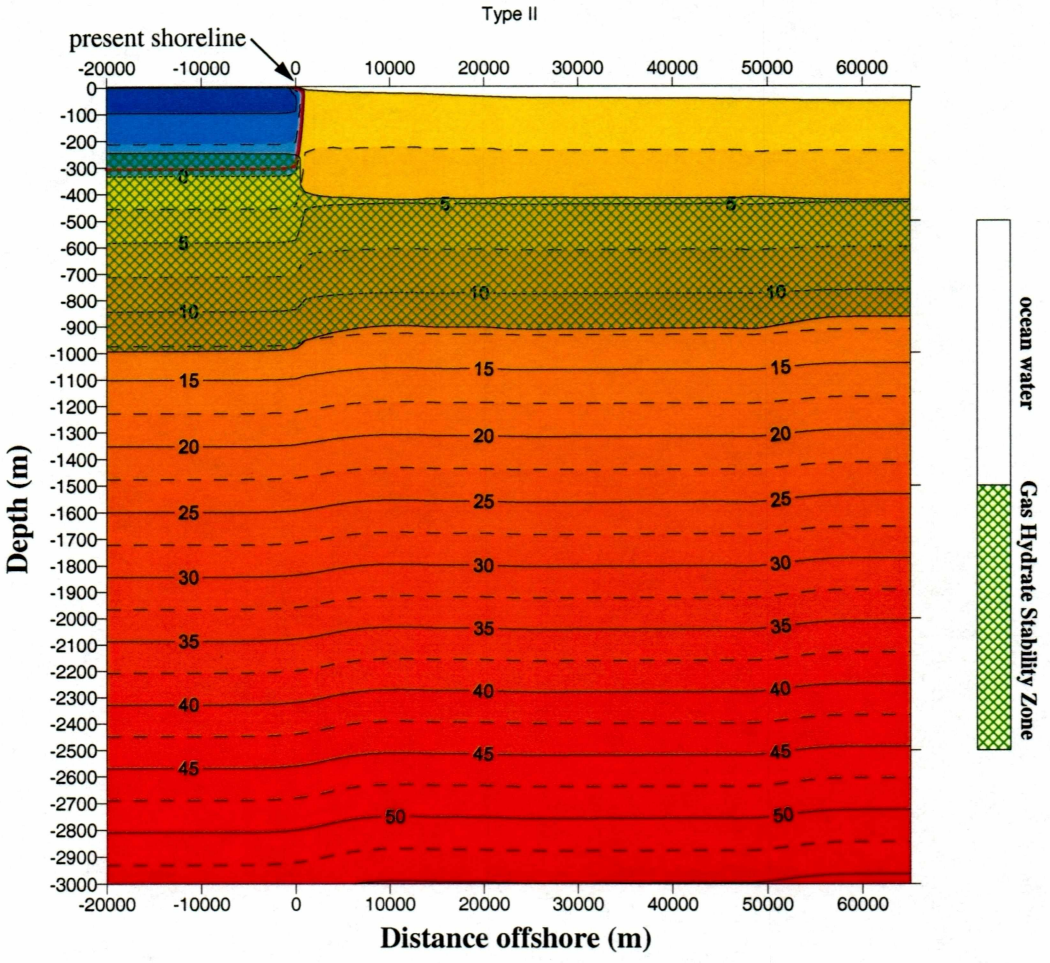

Figure 3.4.2a Results of modeling using Type II program. Temperature distribution and Gas Hydrate Stability Zone at present time at Cape Thompson.

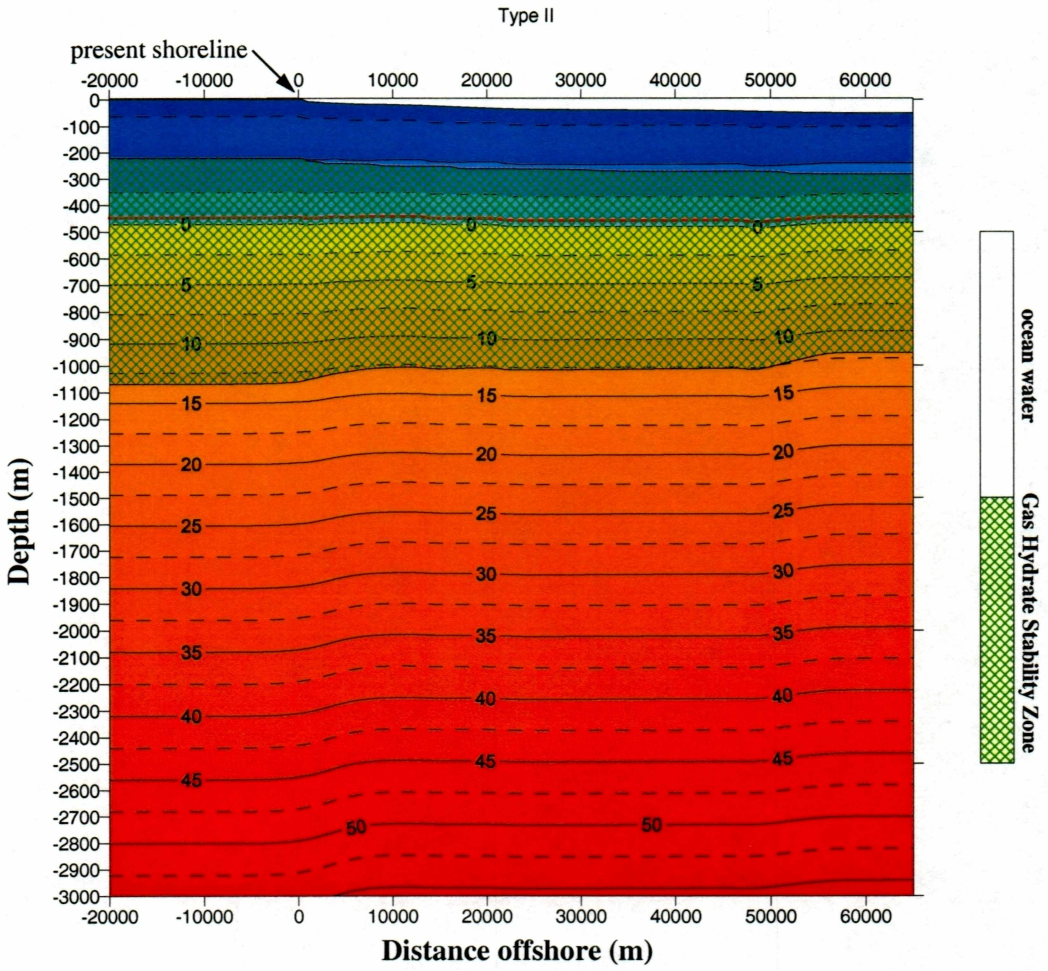

Figure 3.4.2b Results of modeling using Type II program. Temperature distribution and Gas Hydrate Stability Zone at 18 Kyrs BP at Cape Thompson.

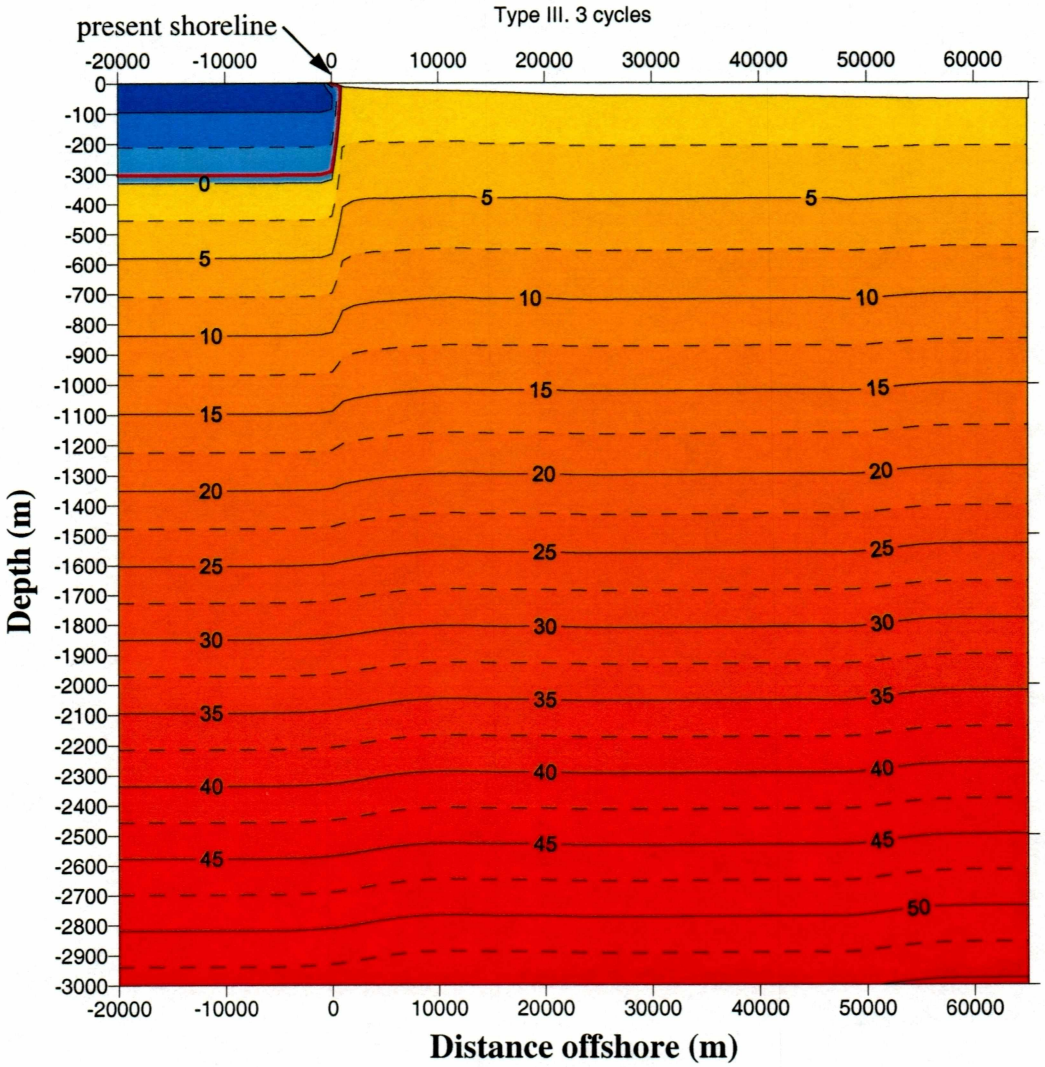

Figure 3.4.3 Results of modeling using Type III program (initial conditions for Type I and Type II). Temperature distribution at present time at Cape Thompson.

Table 3.4 Depth of predicted permafrost thickness at Cape Thompson.

		Type I	Type II	Type III
onshore	Permafrost thickness, m	302	307	304
Offshore extent of subsea permafrost, km		0.8	0.8	0.8

CHAPTER 4

Gas Hydrate Stability Zone

In the model it was assumed that the entire pore space of the soils was filled with water saturated with dissolved methane gas. Under specific temperature and pressure conditions, methane in combination with water can form a crystallized structure – gas hydrate. Since the range of temperature and pressure conditions that are suitable for stable gas hydrates is limited, gas hydrates can exist only in particular regions; one of them is shelf areas of the Arctic Ocean.

Analysis of the Gas Hydrate Stability Zone (GHSZ) thickness and its dynamics over the last 120 Kyrs was made on the basis of calculations described in Chapter 3. In the Type I program, the position of the gas hydrate stability zone was calculated in accordance with the phase diagram of gas hydrates (fig. 4.1) by applying these temperature–pressure conditions on the temperature distribution profile on each step of the calculation. The same method was used by Fei (1992) to evaluate the GHSZ. In the Type II program we modified the method of determination of the GHSZ by including the process of gas hydrate formation into the thermal simulations. The latent heat of gas hydrate formation was included into the calculation scheme, such that every component of the system – water (liquid and unfrozen), ice, gas, and gas hydrate – interacts with the other during freezing – thawing processes. So, GHSZ was determined not only by the superposition principle as in the Type I program, but concurrently the temperature regime.

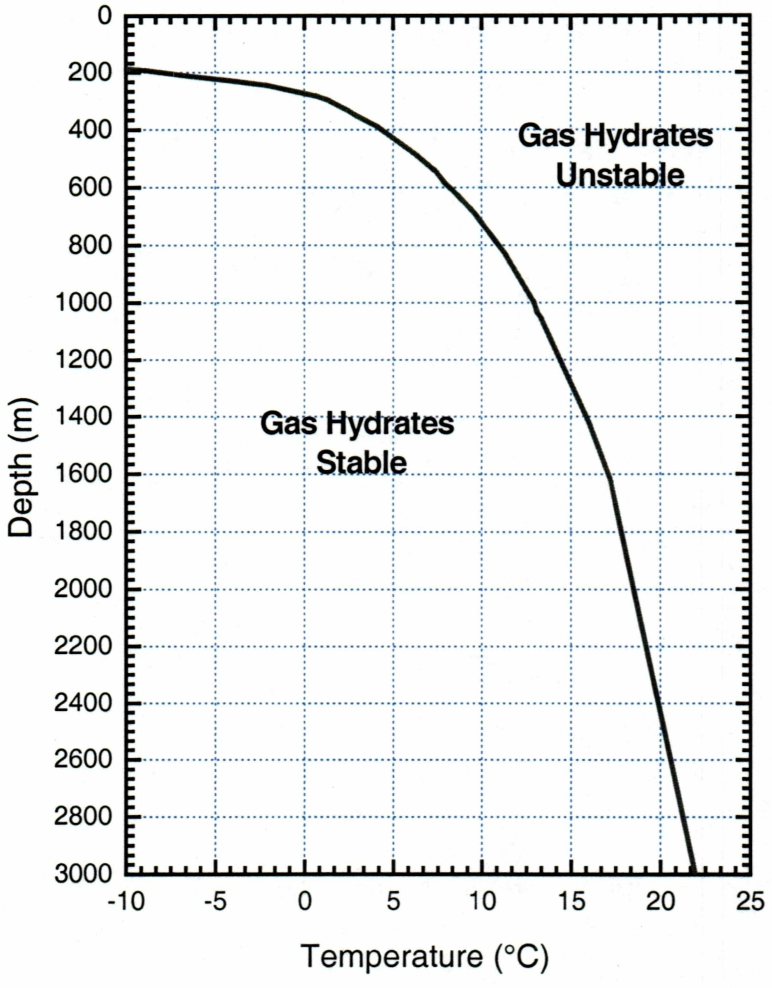

Figure 4.1 Phase diagram of gas hydrates (after MacDonald, 1990).

4.1. Gas Hydrate Stability Zone at Prudhoe Bay. Coarse-grained material

Results of modeling using the Type I program are presented in figure 3.1.1a, where the gas hydrate stability zone for current conditions is shown as a shaded area. Onshore the GHSZ is very thick, reaching about 900 m. The top of the stability zone is at approximately 200 m depth onshore and at 230 – 240 m offshore (225 – 200 m from the sea bottom). The depth of the GHSZ lower boundary is 1090 m onshore and it slightly decreases seaward to 980 m (938 m from the bottom). The predicted stability zone extends to 84 km offshore, which is only 2 km less than 18 Kyrs BP (fig. 3.1.1c). This suggests that the extent of the GHSZ offshore is related to the extent of subsea permafrost. Results of modeling using the Type II program shows a bit smaller thickness of the GHSZ either onshore and offshore (863 m onshore) (fig. 3.2.1a). The top of the stability zone looks similar to the Type I results with an exception that farther offshore the boundary goes slightly (about 20 m) deeper. There is a significant difference in the lower boundary of the GHSZ between the Type I and Type II cases. In general, up to 75-80 km offshore the shape of the lower boundaries looks similar (in Type II case 20-30 m shallower), but from 80 km to 84 km offshore the big difference occurs: on figure 3.1.1a, the GHSZ at its maximum extent has almost the same thickness as at 80 km offshore, but on figure 3.2.1a, the GHSZ is much thinner.

The dynamics of the GHSZ thickness over last 120 Kyrs are shown on figures 4.1.3a and 4.1.3b for Type I and Type II program's results respectively. The vertical axis shows the distance offshore, the horizontal axis is time, and the isolines represent the thickness of the GHSZ in a particular part of shelf at the given time. At each step of the calculation (10 years) the values of the GHSZ thickness along the profile of

calculation domain were stored in a separate file, making it possible to plot these charts. Thickness of the GHSZ in the case of the Type II program is a little bit smaller overall, but the biggest difference is that during period of 113 – 85 Kyrs BP, the GHSZ of the Type I program decreased dramatically and retreated up to 32 km offshore, while the Type II program the maximum reduction of the GHSZ occurred during the 85 – 75 Kyrs BP interval, with a much lower range (GHSZ retreated only by several km towards the shore).

Figures 4.1.1 and 4.1.2 illustrate the dynamics of the volume of gas hydrates calculated along the 1 km profile in comparison with paleotemperature and sea level history. To plot these graphs for every step of calculation, the area of the calculation domain filled by gas hydrates has been computed. Since the model is 2-dimensional, multiplying the area by 1km of the lateral shore section, the volume of the GHSZ on the shelf per 1 km of the shore can be obtained. Then, using the known value of porosity, the volume of the GHSZ can be recalculated into the volume of gas hydrates that fill the pore space. It is difficult to single out the effects of temperature and sea level changes on the change in the volume of gas hydrates quantitatively; still, some correlations can be seen. In general, the following tendencies occur: with rising temperature or/and sea level, the volume of gas hydrates decreases; with temperature decrease or/and sea level decrease, the volume of gas hydrates increases. Since sea level and temperature don't always go in the same direction, the combined effect of both of these factors can not be clearly determined. In addition, due to its inertia, the GHSZ reacts to climate change with a distinct lag. It makes the behavior of the GHSZ even more unpredictable. Still, some predictions on the change of volume of gas hydrates can be made according to the results of modeling: during the last several

thousand years the volume of stable gas hydrates decreases (indicated in both Type I and Type II results), most likely because of the rapid sea level rise that changed the temperature regime on the shelf and caused a significant portion of subsea permafrost to degrade. At the same, temperature has been decreasing during the last 10 Kyrs, meaning that soon enough (in geological terms) sea level is going to start dropping again, perhaps to the level of 120 Kyrs BP. That might lead the gas hydrates to destabilize significantly if the cycle is repeated.

If we compare the results of modeling the GHSZ dynamics using two types of programs, some very important differences can be clearly seen. By taking into account the latent heat of gas hydrate formation in the Type II program, the entire system becomes more inertial: the amplitude of GHSZ volume oscillation due to sea level and temperature changes decreases, the lag with which volume of GHSZ reacts on climate changes increases, and overall volume of GHSZ decreases in comparison with Type I simulations.

The thickness of the GHSZ is controlled not only by the upper boundary conditions (sea level, temperature), but lower boundary conditions as well as thermal properties of soils play a significant role. The higher thermal conductivity of material, for example, would give a lower temperature gradient, resulting in a thicker gas hydrate stability zone.

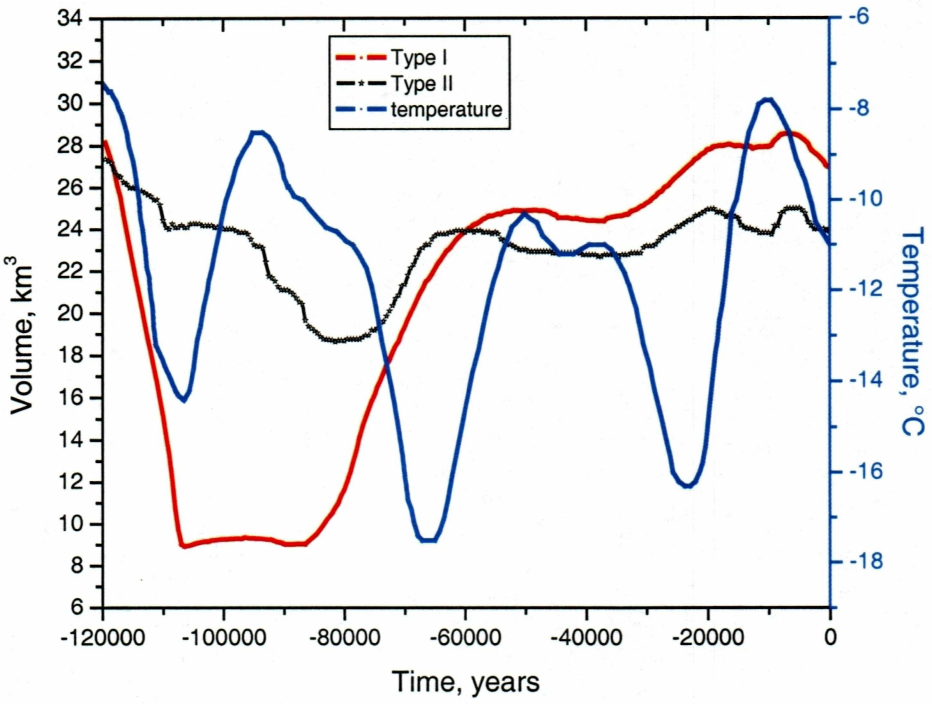

Figure 4.1.1 Dynamics of the volume of gas hydrates along the 1 km wide cross section of shelf zone in comparison with the surface paleotemperature curve, Prudhoe Bay, coarse-grained soil.

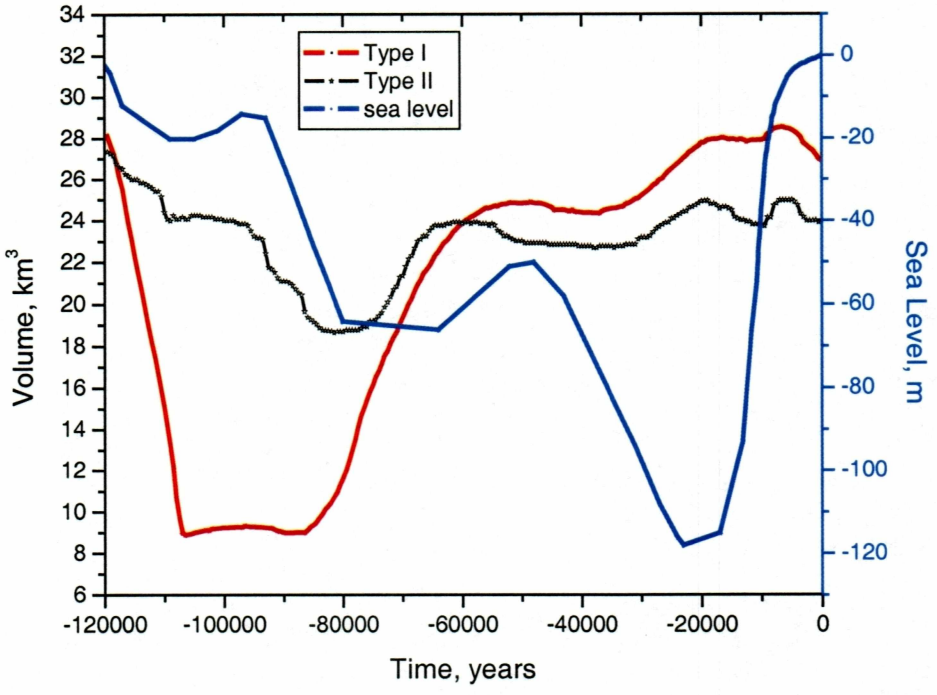

Figure 4.1.2 Dynamics of the volume of gas hydrates along the 1 km wide cross section of shelf zone in comparison with sea level curve, Prudhoe Bay, coarse-grained soil.

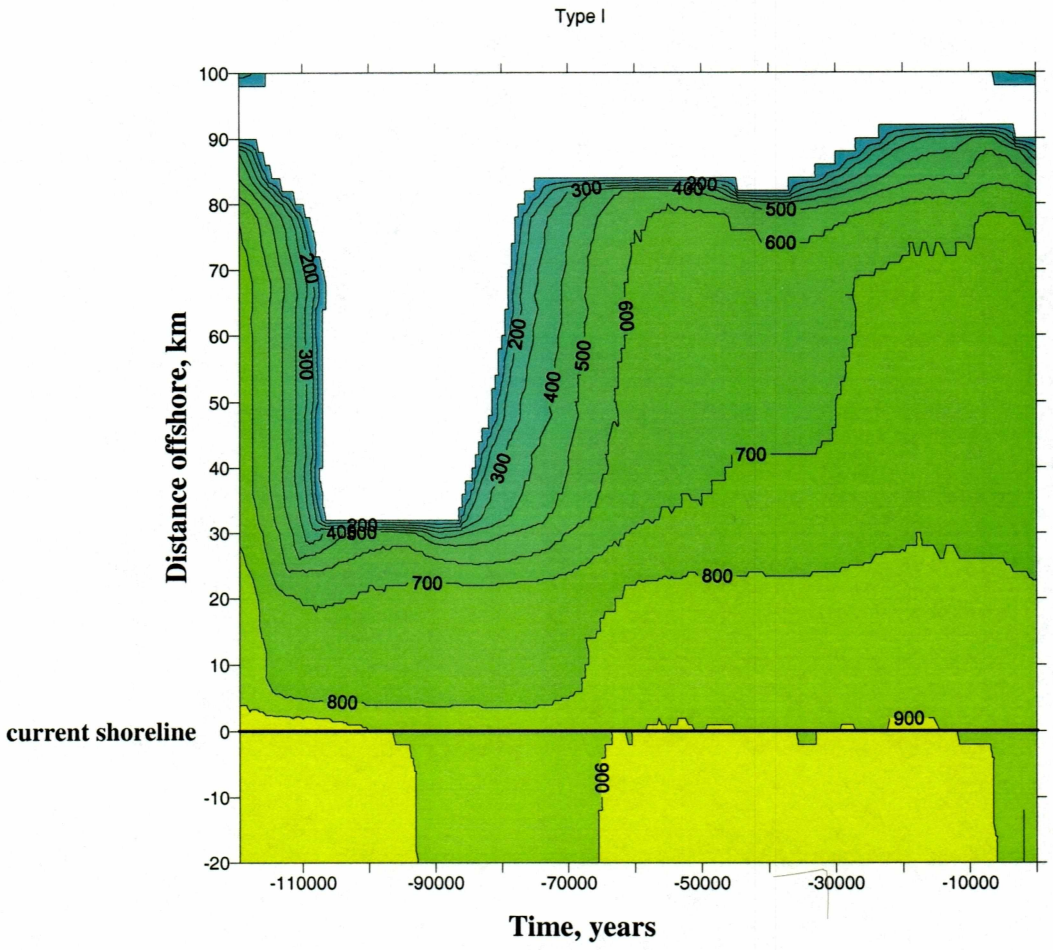

Figure 4.1.3a Dynamics of gas hydrate stability zone thickness over last 120 Kyrs at shelf of Prudhoe Bay, coarse-grained soils. Isolines show the GHSZ thickness. Results of modeling using Type I program.

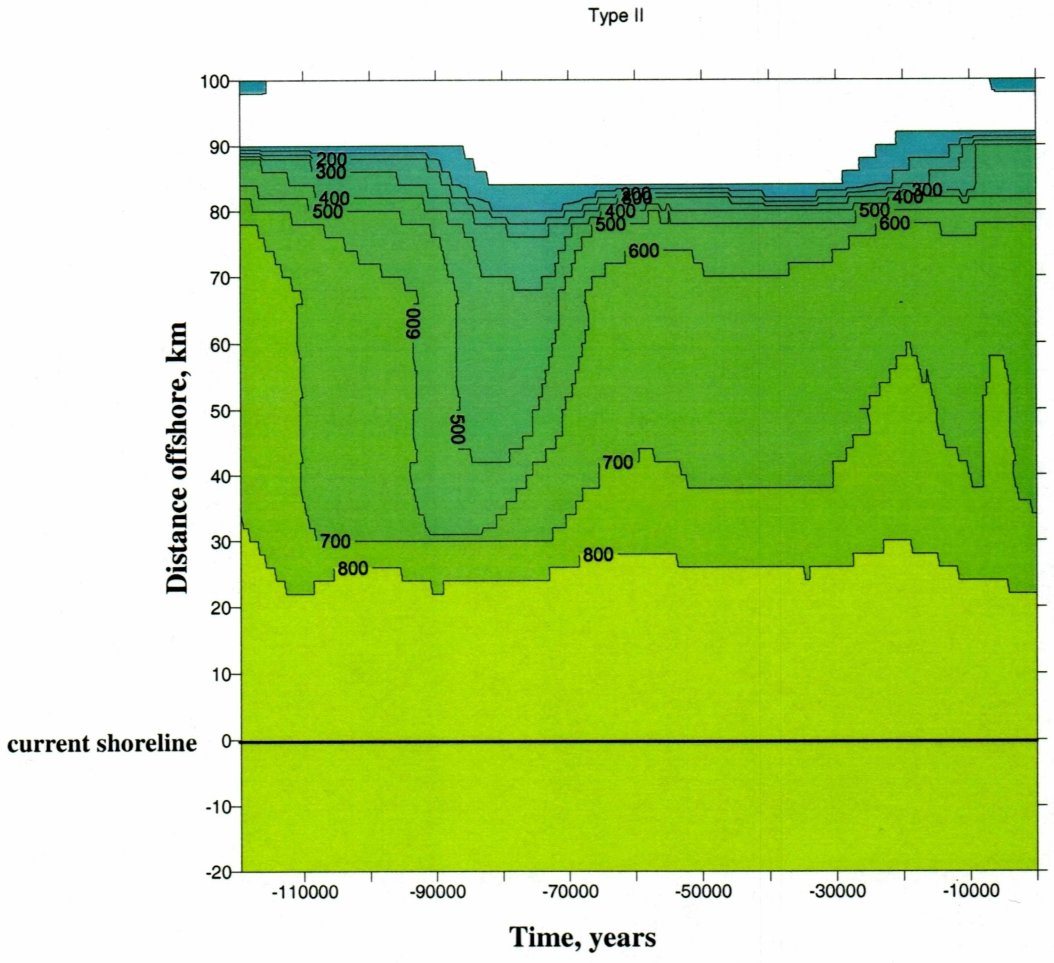

Figure 4.1.3b Dynamics of gas hydrate stability zone thickness over last 120 Kyrs at shelf of Prudhoe Bay, coarse-grained soils. Isolines show the GHSZ thickness. Results of modeling using Type II program.

4.2. Gas Hydrate Stability Zone at Prudhoe Bay. Fine-grained Material

Figure 3.1.4a demonstrates the predicted current stability zone of gas hydrates for fine-grained material at Prudhoe Bay using the Type I program. GHSZ thickness is much thinner than for the coarse-grained case, probably because of the lower thermal conductivity for fine-grained soil. Maximum thickness of the GHSZ is onshore, where it reaches 310 m. The depth of the upper boundary of the stable region is at 225 m onshore and it increases towards the sea to 260 m (220 m below sea bottom), and at the maximum extent (78 km offshore) it drops to 288 m (236 m below sea bottom). The lower boundary isn't as smooth as the upper one. The depth of the lower boundary onshore is at 535 m and it decreases towards the sea. The minimum thickness of GHSZ is at 35 km offshore (180 m). Using the Type II program, the following results were obtained: the upper boundary of the stable region looks very much like Type I results but in the offshore region the boundary is located 5 m higher than in Type I case (fig. 3.1.5a), and the lower boundary is 10 m deeper onshore, which makes the GHSZ thickness greater. Offshore, there is also a decrease of GHSZ thickness at about 35 km distance, but in the Type II case it is more substantial. The maximum extent of the GHSZ offshore in the Type II case is almost 92 km, which is 14 km more than for the Type I program. This can be explained by the slower process of subsea permafrost retreat towards the shore during last 18 Kyrs and by more overall inertial behavior of the system, in the case of the Type II program, because of latent heat of the gas hydrate.

If we take a look at fig. 4.2.1 and 4.2.2, where the dynamics of the volume of gas hydrates is plotted in comparison with paleotemperature and sea level curve, it can be seen that there is a significant difference in the results between two types of

programs we used. Results of the Type II program show a smoother curve of the volume of stable gas hydrates over 120 Kyrs period, with a smaller amplitude of oscillation in comparison with Type I. Figures 4.2.3a and 4.2.3b show the dynamics of the GHSZ at the shelf for the last 120 Kyrs. Again, like in coarse-grained material case, the biggest difference between two types of simulation (Type I and Type II) is in the periods of maximum retreat of the GHSZ (minimum extent on shelf).

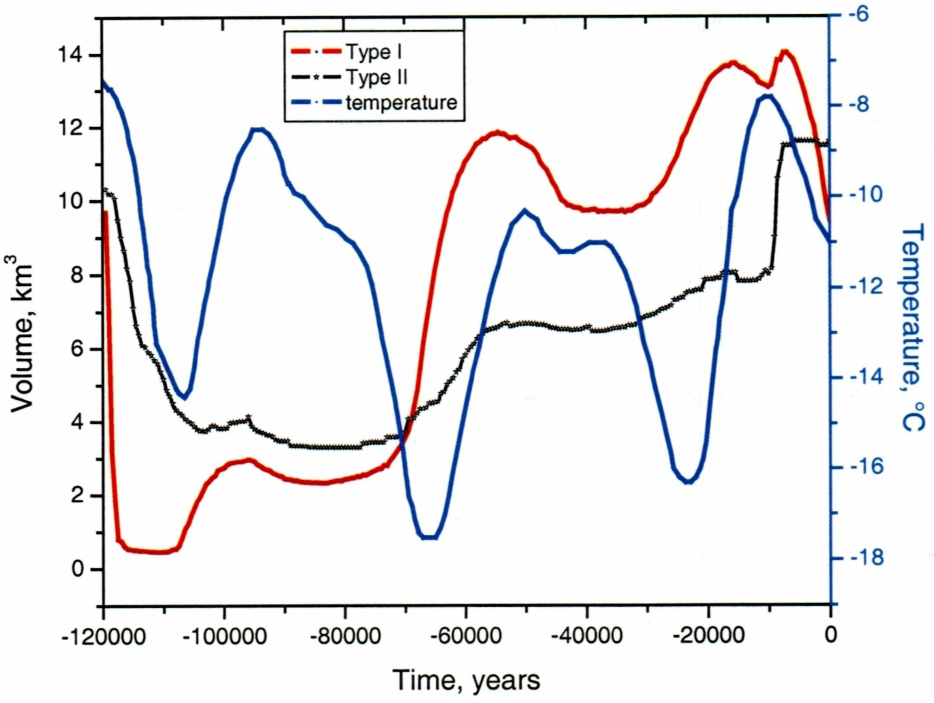

Figure 4.2.1 Dynamics of the volume of gas hydrates along the 1 km wide cross section of shelf zone in comparison with the surface paleotemperature curve, Prudhoe Bay, fine-grained soil.

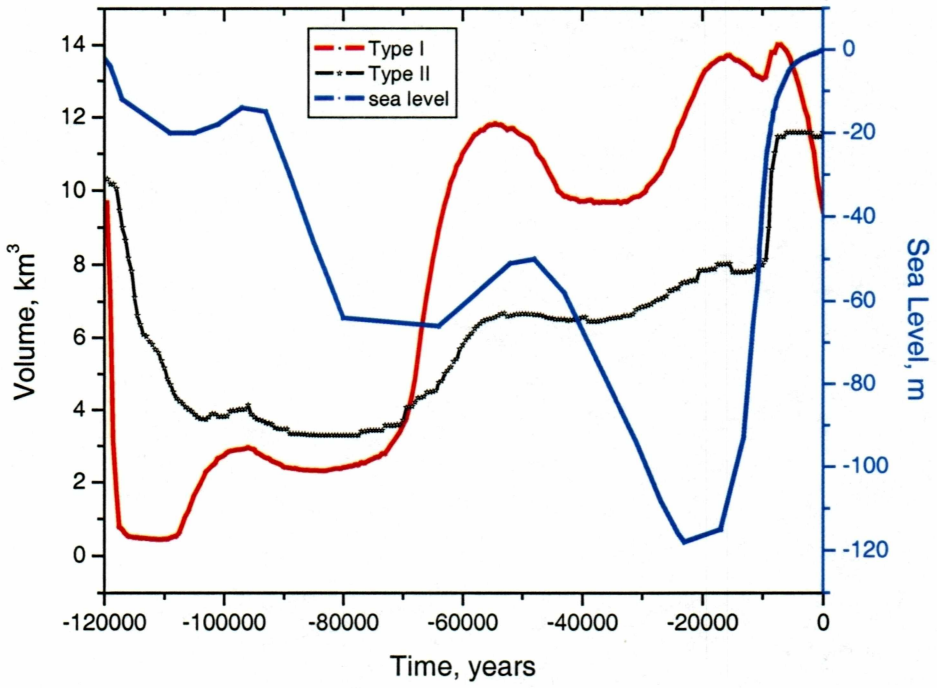

Figure 4.2.2 Dynamics of the volume of gas hydrates along the 1 km wide cross section of shelf zone in comparison with sea level curve, Prudhoe Bay, fine-grained soil.

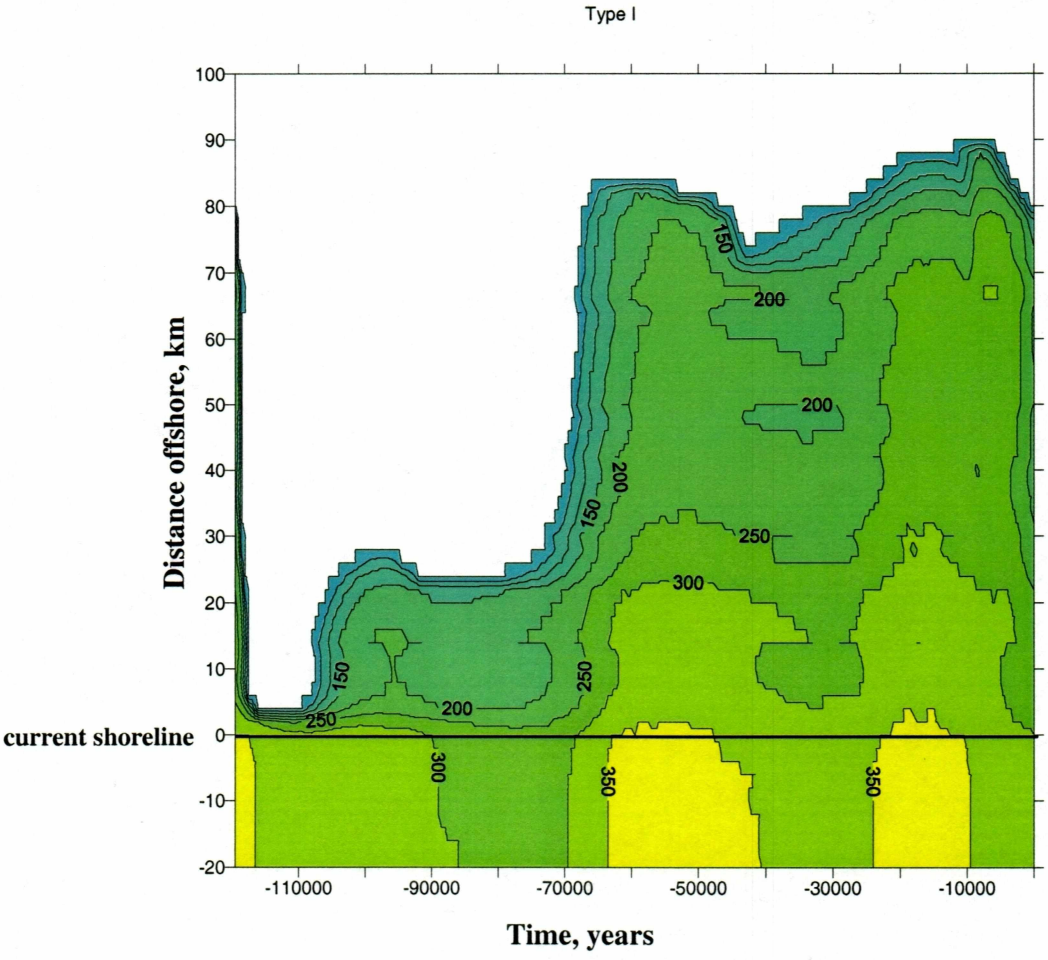

Figure 4.2.3a Dynamics of gas hydrate stability zone thickness over last 120 Kyrs at shelf of Prudhoe Bay, fine-grained soils. Isolines show the GHSZ thickness. Results of modeling using Type I program.

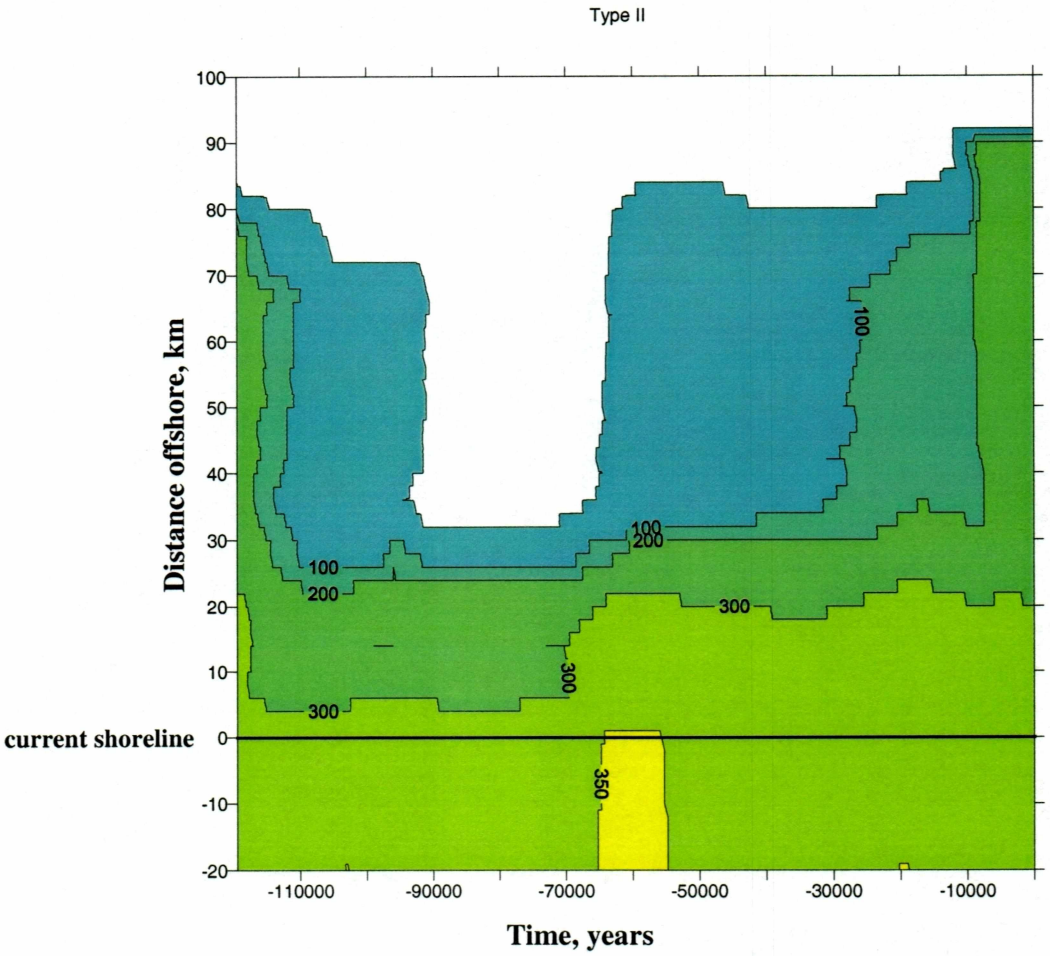

Figure 4.2.3b Dynamics of gas hydrate stability zone thickness over last 120 Kyrs at shelf of Prudhoe Bay, fine-grained soils. Isolines show the GHSZ thickness. Results of modeling using Type II program.

4.3. Gas Hydrate Stability Zone at Lonely

At Lonely, results of thermal simulations show that relatively thin permafrost exists in comparison with Prudhoe Bay, where coarse-grained material was assumed. Also, lateral extension of subsea permafrost on the shelf is much less at Lonely than in Prudhoe Bay. These two factors greatly restrict the stable region of gas hydrates. On fig. 3.2.1a the stable region for gas hydrates (Type I program) is shown as a shaded area. The results using the Type II program are shown on figure 3.2.2a. The upper boundary of the stable region onshore was located at 225 m and 222 m depth for Type I and Type II respectively. The lower boundary in the Type I case is located about 15 m higher than in the Type II case. The total thickness of the GHSZ onshore for Type I is 355 m, and for Type II is 373 m. The major difference in the results of modeling using Type I and Type II program is in the GHSZ extent offshore. While the stable zone in the Type I program is limited to 24 km offshore (the same extent as of subsea permafrost), results of Type II simulations show the stable zone can exist up to 65 km offshore. The upper boundary of the stable region offshore is located at 240 – 260 m below the sea bed. The depth of the lower boundary in the offshore region decreases towards the sea with some fluctuations (in accordance with the isotherms), and at the maximum extent, the GHSZ is 160 m thick, the upper boundary is at 220 m and the lower boundary is at 380 m below the sea bed.

The dynamics of the volume of gas hydrates are shown in figures 4.3.1 and 4.3.2. As in Prudhoe Bay, the Type II program predicted less volume of gas hydrates over the last 120 Kyrs than the Type I program, except for the last several thousands of years. The volume of gas hydrates using the Type II program is smaller over the whole period of calculation, but at the end of calculation, the volume of gas hydrates

is larger. The tendency of decreasing volume of gas hydrates over the last several thousand years can be seen for both type of calculations but in the Type I program it is much more significant than in the Type II program. The decrease of the volume of gas hydrates started 18 Kyrs BP for Type I simulations and only 10 Kyrs BP for Type II, suggesting a lag of 8 Kyrs. During last 1,000 years, simulations using the Type II program show slight increases of the volume of gas hydrates.

As in Prudhoe Bay, the volume of gas hydrates oscillates with smaller amplitude with the Type II program because of the greater inertia of the system when the latent heat of gas hydrate formation is taken into account.

The dynamics of the GHSZ thickness over the last 120 Kyrs are shown in figures 4.3.3a and 4.3.3b for Type I and Type II program respectively. The extent of the GHSZ offshore oscillates in time with a smaller range in Type II simulations. The minimum extent of the GHSZ offshore for both types of simulations was during 90 – 85 Kyrs BP. The Type I program shows a significant lateral retreat of the stability zone during the last several thousands of years.

The relatively thin GHSZ at Lonely in comparison with the Prudhoe Bay coarse-grained material is caused by the lower thermal conductivity and smaller porosity and also by higher values of geothermal heat flow. Higher geothermal heat flow makes subsea permafrost retreat faster, which in its turn reduces the size of the gas hydrate stability zone.

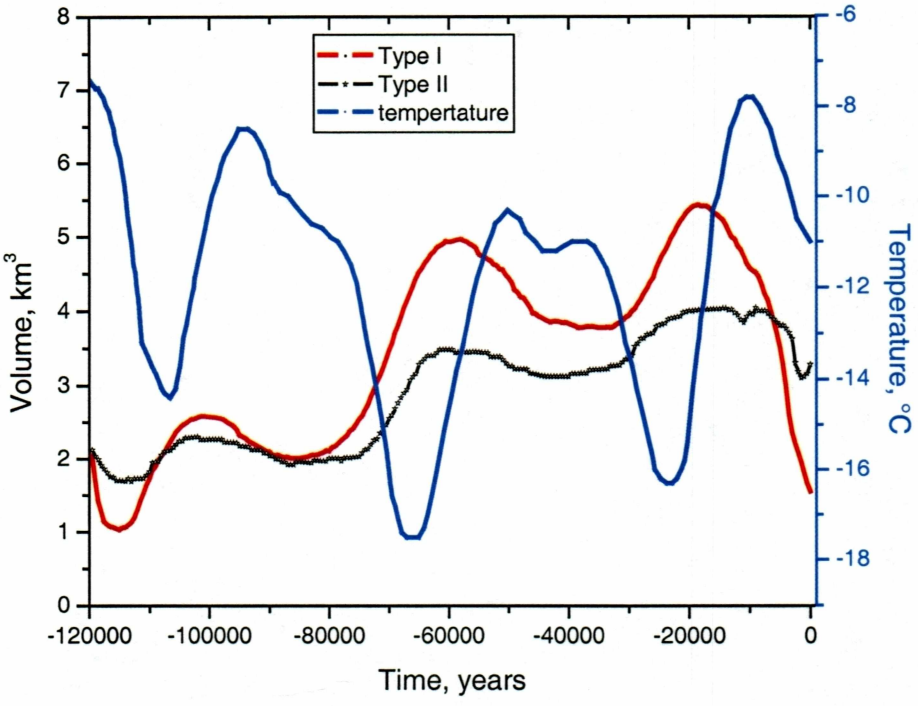

Figure 4.3.1 Dynamics of the volume of gas hydrates along the 1 km wide cross section of shelf zone in comparison with the surface paleotemperature curve, Lonely.

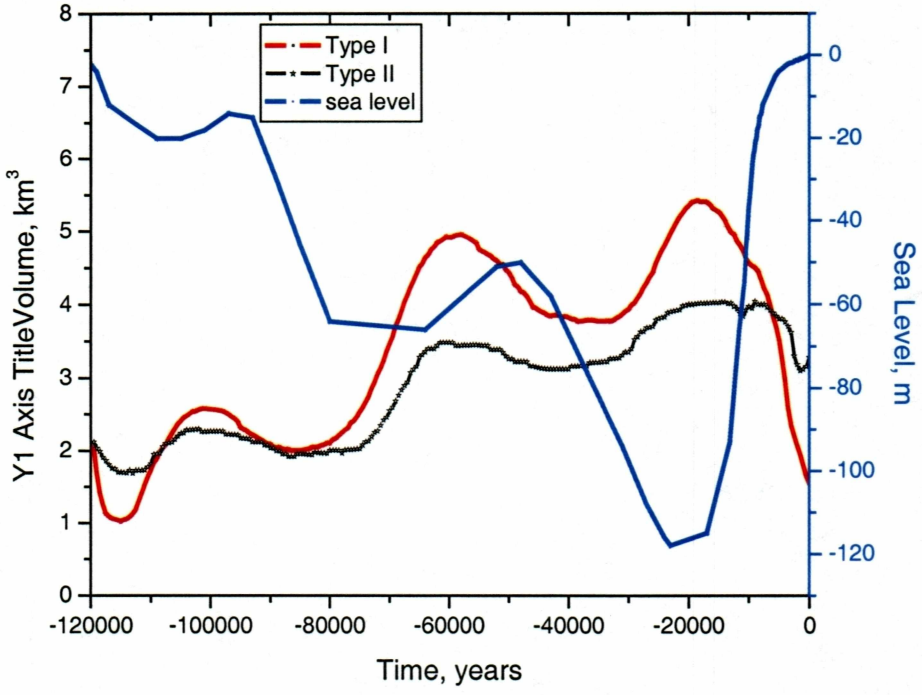

Figure 4.3.2 Dynamics of the volume of gas hydrates along the 1 km wide cross section of shelf zone in comparison with sea level curve, Lonely.

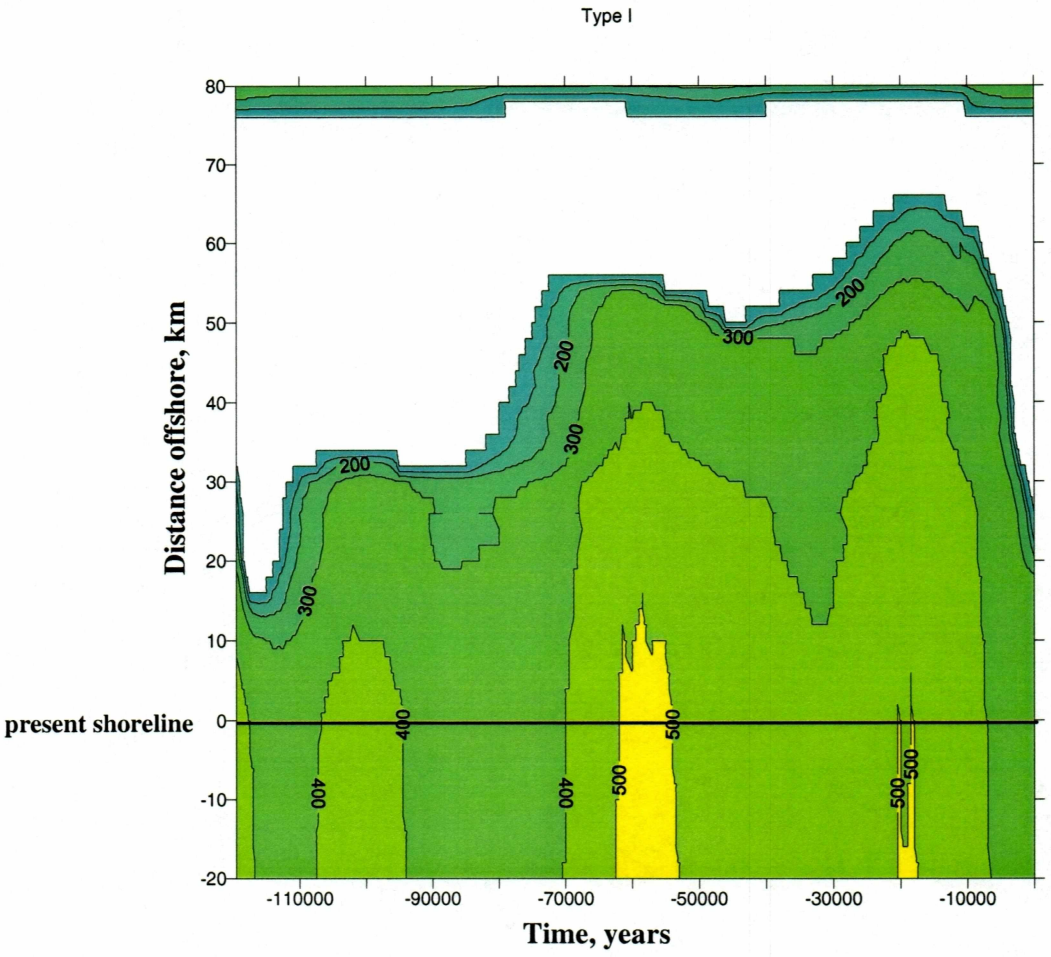

Figure 4.3.3a Dynamics of gas hydrate stability zone thickness over last 120 Kyrs at shelf of Lonely. Isolines show the GHSZ thickness. Results of modeling using Type I program.

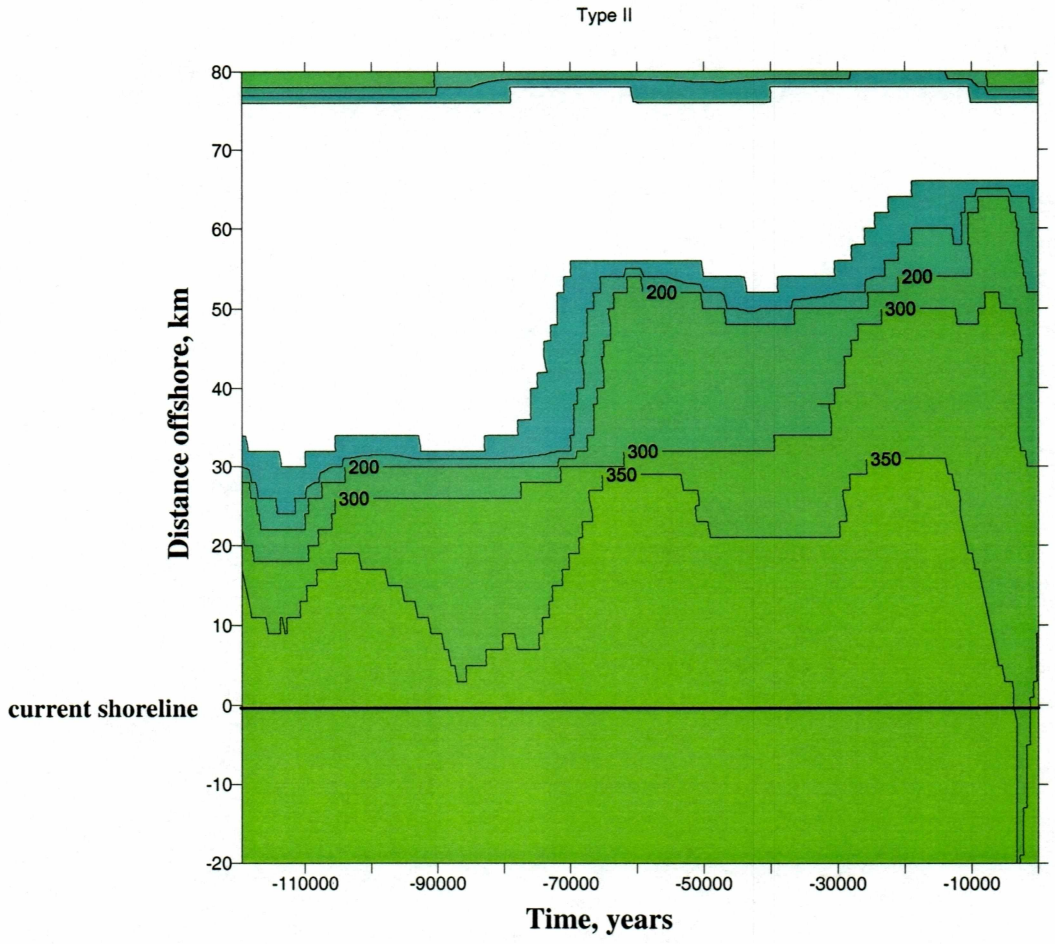

Figure 4.3.3b Dynamics of gas hydrate stability zone thickness over last 120 Kyrs at shelf of Lonely. Isolines show the GHSZ thickness. Results of modeling using Type II program.

4.4. Gas Hydrate Stability Zone at Barrow

At Barrow, in comparison with Lonely, results of thermal simulations illustrate that a thicker permafrost layer can exist. Also, the lateral extension of subsea permafrost on the shelf is greater by several kilometers. In fig. 3.3.1a, the stable region for gas hydrates, the Type I program is shown as a shaded area. The results of modeling using the Type II program are shown in figure 3.2.2a. The upper boundary of the stable region onshore is located at 212 m and 210 m depth for Type I and Type II respectively. The lower boundary in the Type I case is located at 692 m making onshore thickness of GHSZ 580 m. The thickness of the stable zone onshore obtained using the Type II program is 22 m less than in the Type I case (558 vs. 580 m). The major difference in the results of modeling using Type I and Type II programs is in the GHSZ extent offshore. While the stable zone in the Type I program is limited to 33 km offshore (which exceeds the extent of subsea permafrost by only 4.5 km), results of Type II simulations show the stable zone can exist up to 65 km offshore. The upper boundary of the stable region offshore is located at 212 – 265 m below the sea bed for the Type I case, and at 210 – 260 m for the Type II case. The depth of the lower boundary in the offshore region for the Type II case decreases towards the sea, and at the maximum extent, the GHSZ is 160 m thick, upper boundary is 210 m and the lower boundary is 370 m below the sea bed.

The dynamics of the volume of gas hydrates are shown of figures 4.4.1 and 4.4.2. As for Lonely simulations, the Type II program predicted less volume of gas hydrates over the last 120 Kyrs than the Type I program, except for the last several thousands of years. The volume of gas hydrates using the Type II program oscillates

with a smaller amplitude than the Type I program. From 18 Kyrs BP, the decrease of the volume of gas hydrate can be observed for both types of calculations, but in the case of the Type I program, the rate of the gas hydrate volume decrease is substantially higher. Because of the different rates of volume decrease, we can see that the Type I volume curve crosses the Type II volume curve approximately 3 Kyrs BP.

As in Prudhoe Bay and Lonely, the volume of gas hydrates oscillates with smaller amplitude if we use Type II program because of the greater thermal inertia of the system when the latent heat of the gas hydrate formation is taken into account.

The dynamics of GHSZ thickness over last 120 Kyrs are shown on figures 4.4.3a and 4.4.3b for Type I and Type II programs respectively. The extent of the GHSZ offshore oscillates in time with a smaller range in the Type II simulations. The minimum extent of the GHSZ offshore for both types of simulations was during 90 – 85 Kyrs BP and the Type I program shows significant lateral retreat of the stability zone during the last several thousands of years.

The relatively thicker GHSZ at Barrow in comparison with Lonely is caused by more severe upper boundary conditions (the paleotemperature is 1.5°C on average colder at Barrow over the last 120 Kyrs). Since all other input parameters were the same, the particular effect of temperature on the thickness and distribution of the GHSZ can be determined, and in this case it gives us about 33-38% increase of the GHSZ thickness onshore when we lower the temperature by 1.5°C.

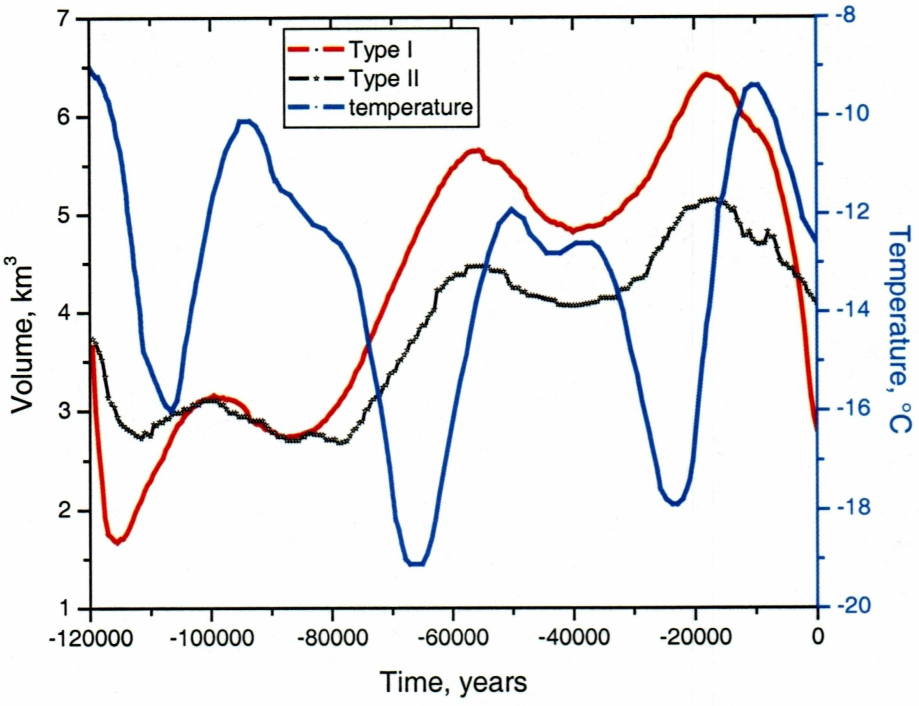

Figure 4.4.1 Dynamics of the volume of gas hydrates along the 1 km wide cross section of shelf zone in comparison with the surface paleotemperature curve, Barrow.

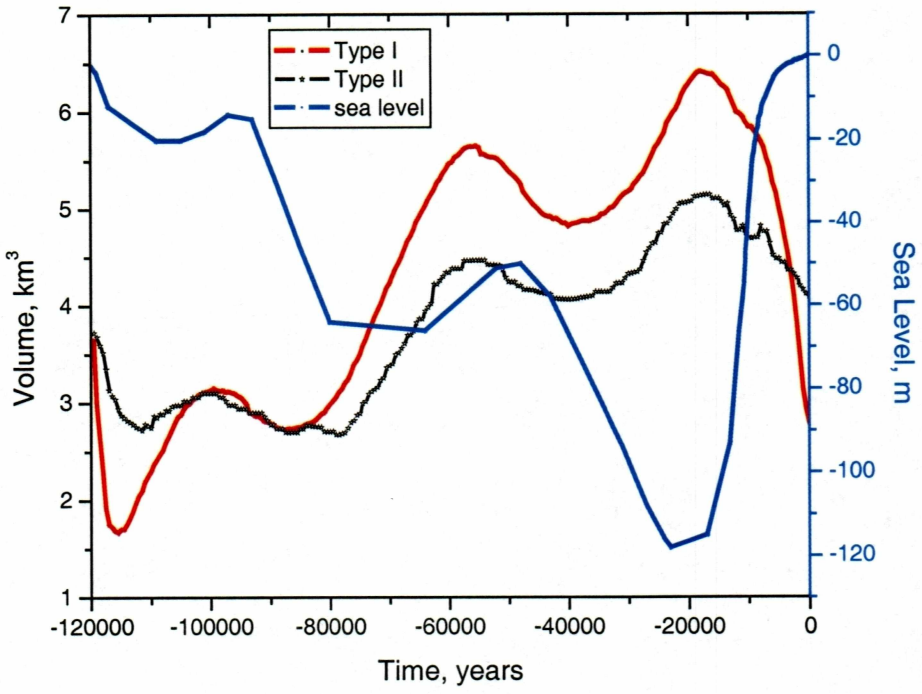

Figure 4.4.2 Dynamics of the volume of gas hydrates along the 1 km wide cross section of shelf zone in comparison with sea level curve, Barrow.

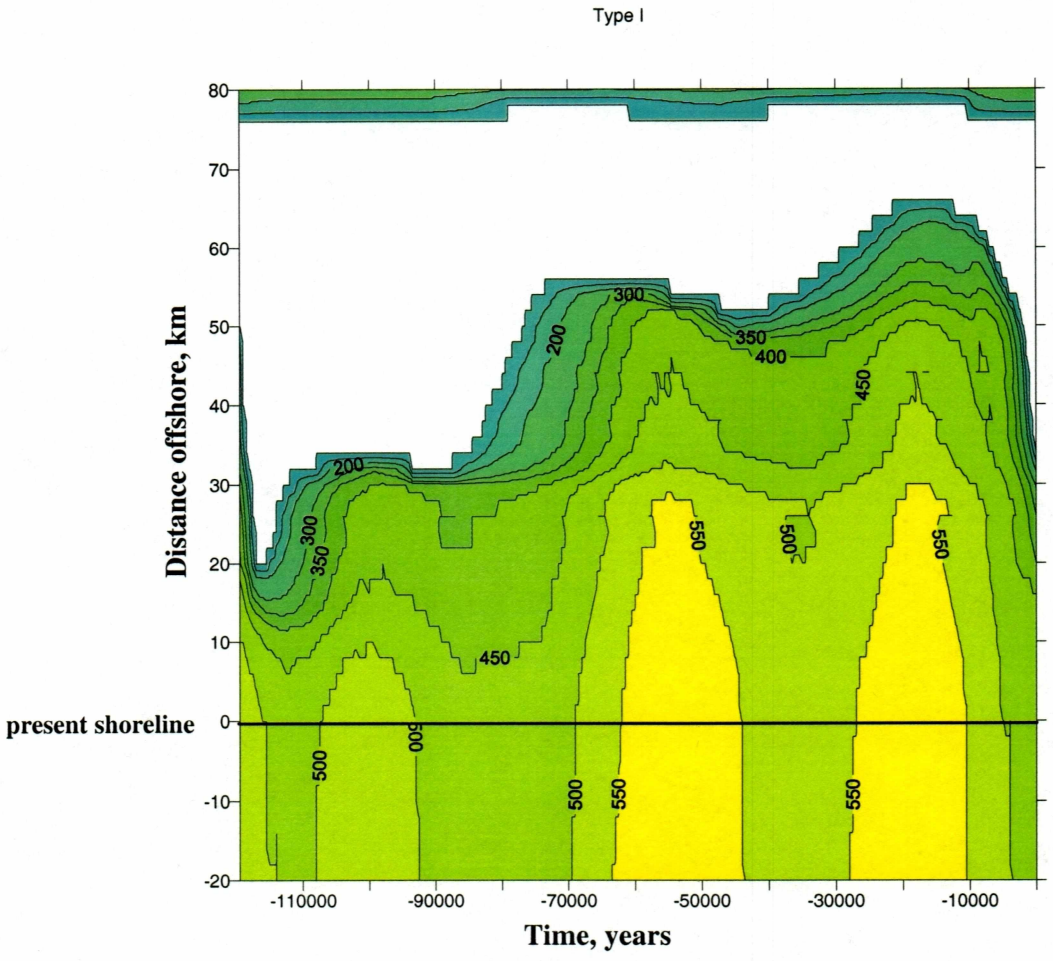

Figure 4.4.3a Dynamics of gas hydrate stability zone thickness over last 120 Kyrs at shelf of Barrow. Isolines show the GHSZ thickness. Results of modeling using Type I program.

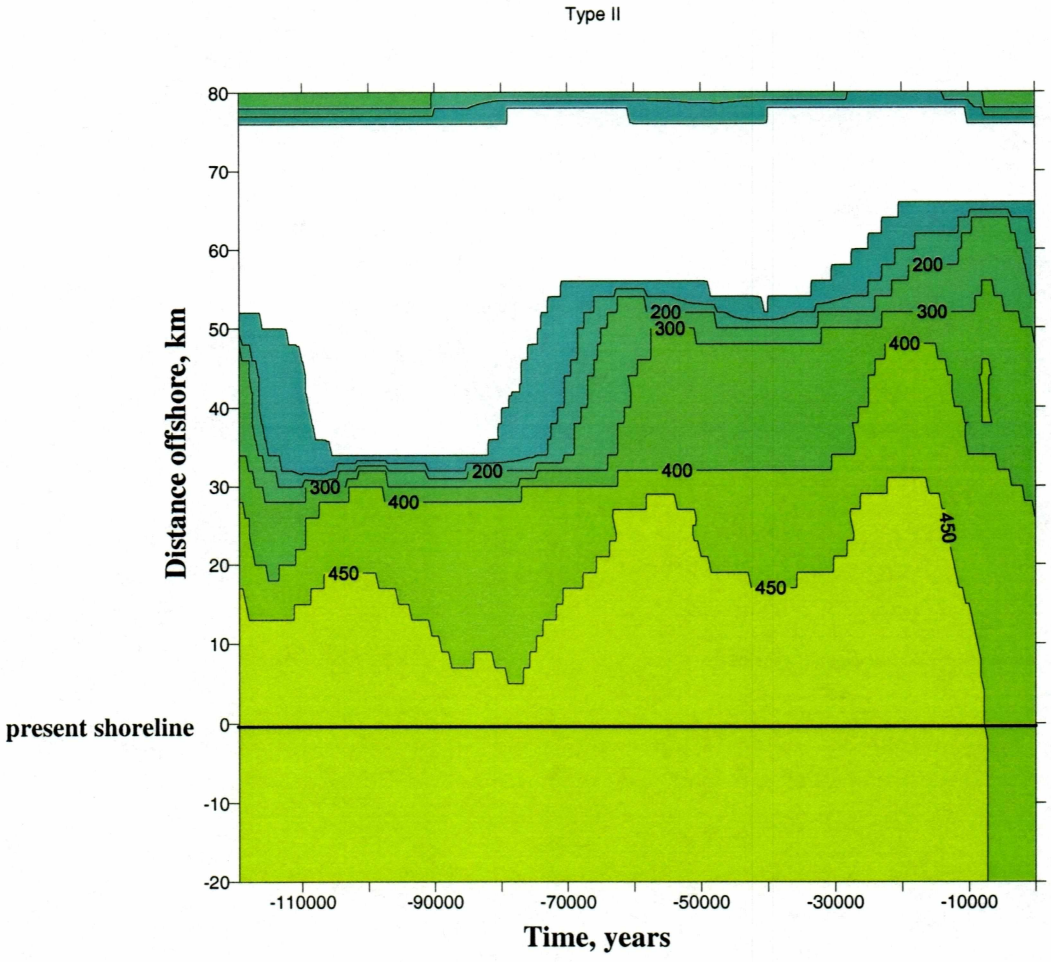

Figure 4.4.3b Dynamics of gas hydrate stability zone thickness over last 120 Kyrs at shelf of Barrow. Isolines show the GHSZ thickness. Results of modeling using Type II program.

4.5 Gas Hydrate Stability Zone at Cape Thompson

Results of modeling using the Type I program are presented in figure 3.4.1a, where the predicted location of the gas hydrate stability zone for the present is shown as a shaded area. The GHSZ is relatively thick onshore. The top of the stability zone is located at 248 m depth; the lower boundary of the stability region is at 970 m below the surface, which gives a total thickness of 722 m. In the offshore region, the GHSZ is almost completely gone; it exists only in the first several kilometers offshore (0.5 – 5.5 km), and the maximum extent is at the depth of 660 m. Figure 3.4.1b shows the temperature distribution and the GHSZ at 18 Kyrs BP at Cape Thompson. The stability region includes the entire shelf. The top of the stability zone is between 220 m and 230 m deep in the permafrost. The bottom depth exceeds 1090 m, so the thickness of the gas hydrate stability zone reaches 860 – 870 m. Sea transgression during the last 18 Kyrs caused the stability zone to disappear offshore and some changes in climate during this period of time affected the onshore position of the stability region. Vertical reduction of the GHSZ onshore is 16.5% over the last 18 Kyrs.

The results obtained using the Type II program are presented in figures 3.4.2a and 3.4.2b, where the predicted GHSZ is shown as a shaded area for the present and for 18 Kyrs BP, respectively. In comparison with the results of the Type I case, the GHSZ onshore has similar thickness (only about 3% more), with the top located at 244 m and the bottom at 993 m. In the offshore region, major differences occur. While in case of the Type I program, the GHSZ offshore almost completely disappeared during the last 18 Kyrs; results of modeling using the Type II program show that gas hydrates can still be stable at the depth range of 400 – 880 m at the

shelf. Comparison of figures 3.4.1b and 3.4.2b (GHSZ at 18 Kyrs BP) does not show significant differences in the GHSZ position; the top of the stable zone is at the same depth and the lower boundary is about 20 m higher in case of Type II program.

Figures 4.5.1 and 4.5.2 reveal the dynamics of the volume of gas hydrates calculated along a 1 km wide profile in comparison with paleotamperature and sea level history. It can be seen from the figures that, in general, both curves showing the volume of gas hydrates look similar. The difference is that the Type II curve has smaller amplitude and some lag. Because of the Type I program's faster reaction to the climate change (due to not taking into account the latent heat of gas hydrate), the Type II curve crosses the Type I curve at about 8 Kyrs BP.

The dynamics of the GHSZ thickness over the last 120 Kyrs are shown on figures 4.5.3a and 4.5.3b for the Type I and Type II results, respectively. The thickness of the GHSZ in the Type II program is slightly smaller overall, and the other difference is that the GHSZ at the far end of the shelf (55 km offshore and farther), disappeared in case of the Type I program at 47 – 45 Kyrs BP, while Type II program results show only the decrease of the stability zone thickness.

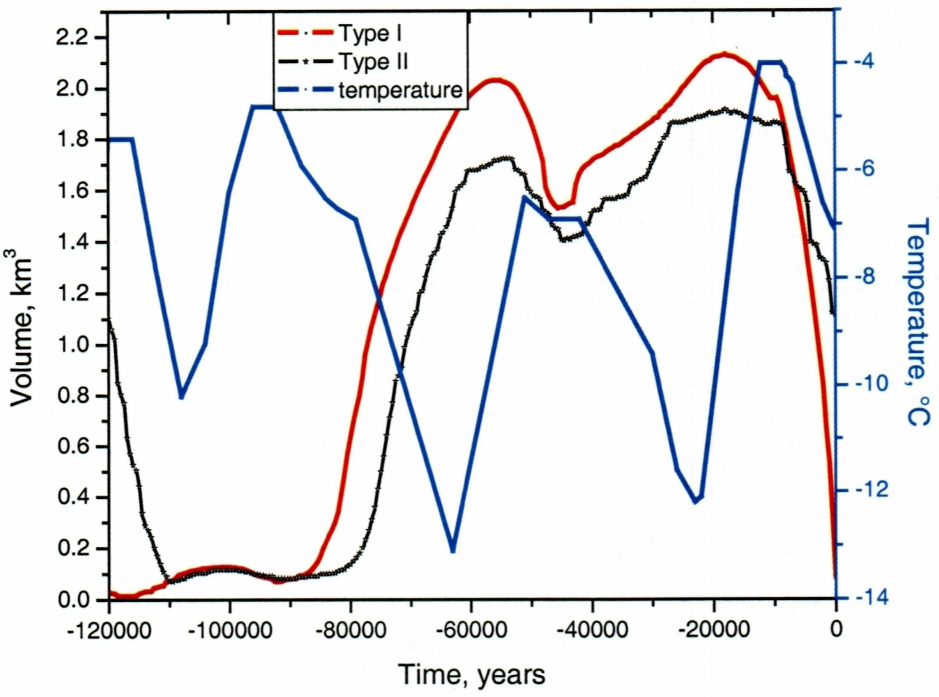

Figure 4.5.1 Dynamics of the volume of gas hydrates along the 1 km wide cross section of shelf zone in comparison with the surface paleotemperature curve, Cape Thompson.

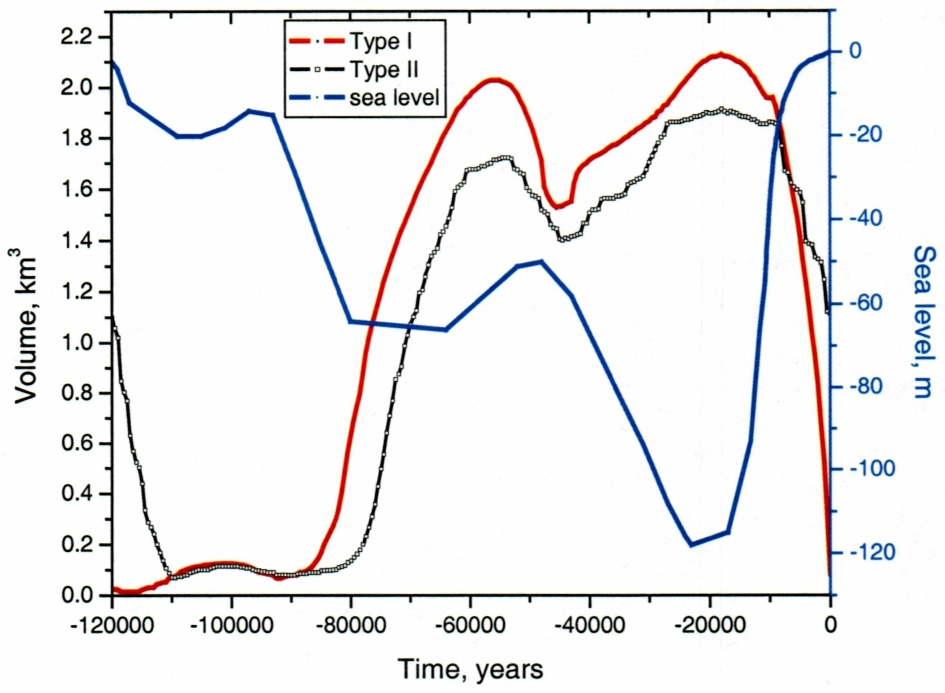

Figure 4.5.2 Dynamics of the volume of gas hydrates along the 1 km wide cross section of shelf zone in comparison with sea level curve, Cape Thompson.

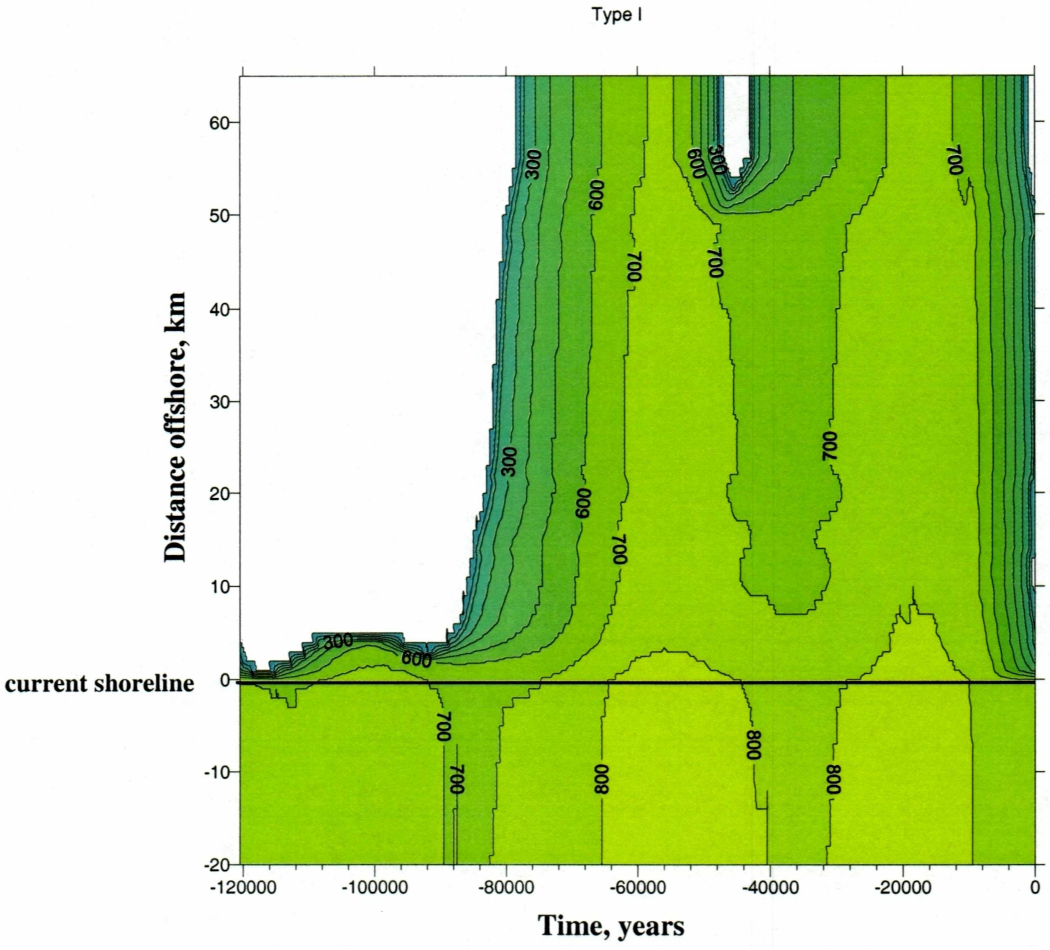

Figure 4.5.3a Dynamics of gas hydrate stability zone thickness over last 120 Kyrs at shelf of Cape Thompson. Isolines show the GHSZ thickness. Results of modeling using Type I program.

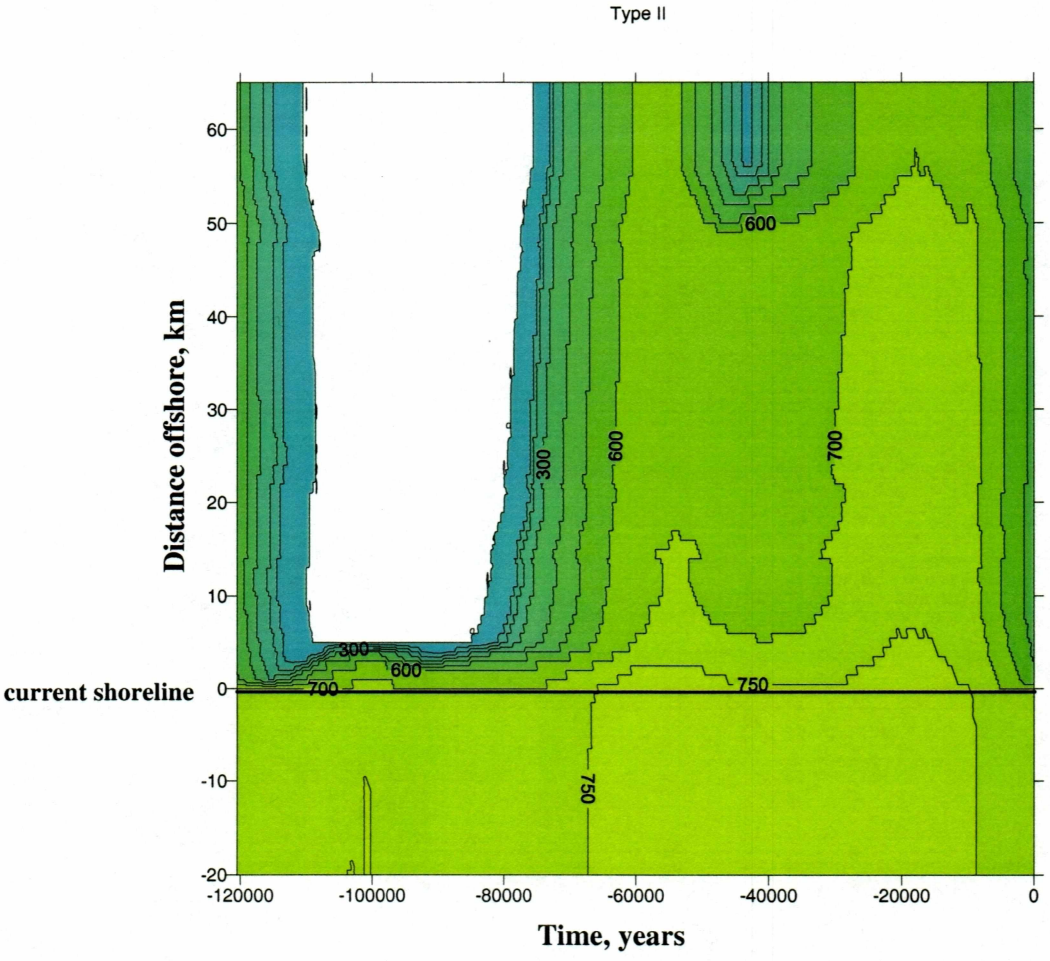

Figure 4.5.3b Dynamics of gas hydrate stability zone thickness over last 120 Kyrs at shelf of Cape Thompson. Isolines show the GHSZ thickness. Results of modeling using Type II program.

CHAPTER 5

Summary and Conclusions

Results of modeling show that the main problem when predicting subsea permafrost and gas hydrate stability zone distribution and dynamics under the present assumption is the correct choice of thermal properties of soils. Since the thermal properties of soils depend on many factors, such as soil structure, porosity, unfrozen water content etc, even small changes in each of these parameters dramatically influence the results of modeling. This effect is amplified even more by long time periods used in simulations (120,000 years). Lower boundary conditions play a significant role too. The values of geothermal heat fluxes as well as the depth where this condition is set can significantly influence the final result.

Calculations were carried out for four different sites along the Alaskan Arctic shelf, and for one of them (Prudhoe Bay) two different types of soils were studied. Different values of geothermal heat flux were applied for each study site to determine the effect of lower boundary conditions on permafrost and gas hydrate stability zone dynamics.

Calculations were made using different programs. Program Type I represents a solution of a quasi-linear heat conductive equation that expresses the energy conservation law through the enthalpy, which takes into account two types of phase transitions: water $\leftrightarrow$ ice + unfrozen water and (water + gas) $\leftrightarrow$ gas hydrate. Thermal properties of soils are calculated in accordance with unfrozen water content. Program Type II is a more complicated version of Type I, in which three kinds of phase transitions are taken into account: (water + gas) $\leftrightarrow$ ice + gas (including unfrozen water content); (water + gas) $\leftrightarrow$ gas hydrate, and (ice + gas) $\leftrightarrow$ gas hydrate. So this

version of the program takes into account the latent heat of gas hydrate formation. Program Type III is a pure Stefan problem, that doesn't take into account the unfrozen water content in soils and that thermal properties of soils remain constant with temperature.

Results of simulations show that for onshore permafrost thickness prediction, the Type III program gives the best results. But to predict the distribution of subsea permafrost, especially the depth of its table, calculations using this approach are not satisfactory. The best way to predict the table of the subsea permafrost is using program Type II or Type III. It is reasonable, because the upper layer of sediments at the sea bed contains salt that dramatically decreases the phase temperature, so using temperature-dependence properties of soils gives better results. Analysis of a gas hydrate stability zone shows that paleotemperature and sea level curve have strong relationships with the GHSZ thickness. During Earth's warming cycles, sea level rise creates more pressure on the sea floor over a wider area, leading gas hydrates to form. However, on land, with the increase of air temperature, hydrates trapped in permafrost can be released into the atmosphere due to permafrost degradation. Modeling shows that during the last 80 – 90 Ka the GHSZ has been growing because of cold temperatures on exposed Arctic shelves. Of course there were some fluctuations, and growing periods alternated with some degrading periods, but still we can clearly see the tendency of the GHSZ to increase.

Fluctuations in volumes of the GHSZ can probably be explained by temperature variations. However the GHSZ is a very inertial system so the local decrease in volume occurs with a lag with respect to decreasing temperature, but still the pattern can be seen (Fig. 4.1.1, 4.1.2, 4.2.1, 4.2.2, 4.3.1, 4.3.2, 4.4.1, 4.4.2, 4.5.1,

4.5.2).

During 20 – 18 Ka B.P. the temperature increased rapidly and sea level started to rise. That increase of temperature could be the reason the volume of the GHSZ decreased during the last several thousand years. The volume of the GHSZ has been decreasing during the last several thousand years over almost the entire Alaskan Arctic shelf, leading us to suspect that it is a result of the last warm cycle (Holocene optimum). At present, the stability zone of gas hydrates exists at a depth of 208 - 220 m at Prudhoe Bay, has a thickness of 320 – 860 m (depending on soil type), and extends up to 90 km offshore; at Lonely it exists at a depth of 210 m, has a thickness of about 370 m and extends up to 25 - 65 km offshore.

The following conclusions can be drawn from two-dimensional modeling of subsea permafrost and gas hydrate stability zone conditions within the Alaskan Arctic continental shelves:

- Results of modeling suggest the presence of subsea permafrost on the continental shelf of the Alaskan Arctic up to 80+ kilometers offshore of Prudhoe Bay, 22 – 36 km offshore near Lonely, and 26 – 48 km near Barrow. At Cape Thompson, subsea permafrost degraded almost completely during last sea transgression and now extends only 0.8 km offshore.

- All models (I, II, III) for both fine- and coarse-grained sediments show an extensive wedge of subsea permafrost for a distance of 22 km to 82 km at present.

- Results of two-dimensional simulations show that for the last interglacial period there is a consistent relationship between climatic changes (sea level and temperature) and existence of subsea permafrost in the continental shelf of the Alaskan Arctic.

- The temperature regime within calculation domain is strongly dependent on soil properties, presence of gases in a pore space, and geometry of the continental shelf.

- The paleotemperature scenario and sea level history indicate that a Gas Hydrate Stability Zone can exist in all four studied sites. The upper boundary of the GHSZ is usually located at the 200 – 220 m depth. The thickness and offshore extent of a GHSZ mostly depends on soil properties and geothermal heat flow. In coarse-grained material, the stability zone is much thicker because of the higher thermal conductivity and lower geothermal gradient.

- Possible formation and presence of gas hydrates in the sediments change the thermal regime significantly; therefore the shape of subsea permafrost depends on whether or not gases are present in the sediments.

- Type I and Type II programs are useful for soil types with high porosity; when the porosity is low, latent heat effect does not play a significant role and the Type III program can give reasonable results.

REFERENCES

- Are, F. E. The Subsea Cryolithozone of the Arctic Ocean, Regional and Thermophysical Studies of Perennially Frozen Rocks in Siberia, USSR Academy of Science, Siberian Branch, Yakutsk Book Publishing House, pp. 3 – 26. (Trans.) Hanover, N. H., U.S. Army Cold Regions Res. And Eng. Lab., Draft Translation 686 1978, 1976.
- Bard, E., Hamelin, B., and Fairbanks, R. G. U-Th ages abtained by mass spectronomy in corals, from Barbados: sea level during the past 130,000 years, Nature, vol. 346, 456-458, 1990.
- Collett, T. S. Natural gas hydrates of the Prudhoe Bay and Kuparuk River area, North Slope, Alaska: American Association of Petroleum Geologists Bulletin 77/5, 793-812, 1993.
- Collett, T. S. and Dallimore, S. R. Permafrost-Associated Gas Hydrate, Natural Gas Hydrate in Oceanic and Permafrost Environment, edited by M. D. Max, Kluwer Academic Publishers, 43-60, 2000.
- Collett, T. S., K. J. Bird, K. J. Kvenvolden, and Magoon, L. B. Map showing the depth to base of deepest ice-bearing permafrost as determined from well logs, North Slope, Alaska, U.S.G.S, Oil and gas investigations, Map OM-222, 1989.
- Davidson, D. W. et al., Natural gas hydrates in northern Canada, Proc. 3rd Intl. Conf. Permafrost, NRC, Canada, Ottawa, Canada, 1978.
- Deming, D., J. H. Sass, A. H. Lachenbruch, and R.F. DeRito. Heat flow and subsurface temperature as evidence for basin scale groundwater flow, North Slope of Alaska, GSA Bull., 104, 528 – 542, 1992.

- Fei, T. A theoretical study of the effects of sea level and climatic change on permafrost temperatures and gas hydrates, M.S. Thesis, 102 pp., University of Alaska, Fairbanks, AK, 1992.
- Harrison, W. D. and Osterkamp, T. E. Heat and mass transport processes in subsea permafrost, I: An analysis of molecular diffusion and its consequences. J. Geophys. Res., 83(C9), 4707-4712, 1978.
- Harrison, W. D. and Osterkamp, T. E. Subsea permafrost: probing, thermal regime and data analyses, Annual report to NOAA, ERL, Boulder, CO, 1981.
- Kachadoorian, R., Lachenbruch, A. H., Moore, G. W., and Waller, R. M. Supplementary Report on Geologic Investigations in Support of Phase II, Project Charioy in the Vicinity of Cape Thompson, Northwestern Alaska. Trace Elements Investigations Report 764, June 1960.
- Kvenvolden, K. A. Methane hydrate – a major reservoir of carbon in shallow geosphere, Chem. Geol., 71, 41-51, 1988.
- Kvenvolden, K. A. and Grantz, A. Gas hydrates of Arctic Ocean region. In: Grantz, A., L. Johnson, and J. Sweeney (eds.), The Arctic Ocean Region, The Geology of North America, 50, Washington DC, Geolog Soc. Am., 1990.
- Lachenbruch, A. H., Thermal Effects of the Ocean on Permafrost, Bulletin of the Geological Society of America, vol. 68, pp. 1515-1530, 1957.
- Lachenbruch, A. H., Brewer, M. C., Greene, G. W., and Marshall, B. V. Temperature in permafrost, *Temperature – Its Measurement and Control in Science and Industry*, vol. 3, pp.791-803, New-York, Reinhold Publication Co., 1962.
- Lachenbruch, A. H.., Greene, G. W., and Marshall B.V. Permafrost and the

Geothermal Regimes. Environment of the Cape Thompson Region, Alaska, United States Atomic Energy Commission, Division of Technical Information pp. 149 – 163, 1966.

- Lachenbruch, A. H., Sass, J. H., Marshall, B. V., and Moses, T. H. Jr. Permafrost, heat flow and geothermal regime at Prudhoe Bay, Alaska, J. Geophys. Res., vol 87(B11), 9301-9316, 1982.
- Lovell, C. W. Temperature effects on phase composition and strength of partially-frozen soil, Highway Res Board Bull., vol. 168, 74-95, 1957.
- MacDonald, G. J. Role of Methane Clathrates in Past and Future Climates, Climatic Change 16, 247-281, 1990.
- MacKay, J. R. Offshore Permafrost and Ground Ice, Southern Beaufort Sea, Canada, Can. J. Earth Sci. vol. 9, 1550-1561, 1972.
- Maximova, L. N. and Romanovsky, V. E. A Hypothesis of the Holocene Permafrost Evolution, Proc. Fifth Int. Conf. on Permafrost, pp. 102-106, Norwegian Inst. Tech., Trondheim, Norway, 1988.
- Molochushkin, E. N. The Effect of Thermal Abrasion on the Temperature of the Permafrost in the Coastal Zone of the Laptev Sea, p. 90 – 93, USSR Contribution, Permafrost, Second Int. Conf., July 13 – 28, 1973, NAS, Washington, D.C., 1978.
- N.A.S. Global change in the geosphere-biosphere; Initial priorities for an IGBP, National Academy Press, Washington DC, 1986.
- Nixon, J. F. Thermal simulation of subsea saline permafrost, Can. J. Earth Sci., vol 23, 2039-2046, 1986.
- Oeschel, W. C. Nutrient and water flux in a small arctic watershed: an

overview. Holarc. Ecol., 12, 229-237, 1989.

- Osterkamp, T. E. Freezing and thawing of soils and permafrost containing unfrozen water or brine, Water Resour. Res., 23(12), 2279-2285, 1987.
- Osterkamp, T. E. Subsea Permafrost. Chapter in, Encyclopedia of Ocean Sciences, p. 2902-2912, J.H. Steele, S.A. Thorpe, and Turekian, K. K. Academic Press, 2001.
- Osterkamp, T. E. and Fei, T. Potential occurrence of permafrost and gas hydrates in the continental shelf near Lonely, Alaska: Proceedings of Sixth International Conference on Permafrost, Beijing, China, July 5-9, 1993: National Academy of Science, Washington, D.C., 500-505, 1993.
- Osterkamp, T. E. and Gosink, J. P. Variations in Permafrost Thickness in Response to Changes in Paleoclimate, J. Geophys. Res., vol. 96, #B3, 4423-4434, 1991.
- Osterkamp, T. E. and Harrison W. D. Subsea permafrost at Prudhoe Bay, Alaska: Drilling report, Sea Grant Report Number 76-5, 1976.
- Osterkamp, T. E. and Harrison W. D. Subsea permafrost: probing, thermal regime, and data analysis, Annual Report to NOAA, ERL, Boulder, CO, 1980.
- Osterkamp, T. E. and Harrison, W. D. Temperature Measurements in Subsea Permafrost off the coast of Alaska, Can. Permafrost Conf., 238-248, 1982.
- Osterkamp, T.E. and Harrison, W. D. Subsea permafrost: Probing, thermal regime, and data analyses, UAG R-301, Geophysical Institute, University of Alaska, Fairbanks, AK, 108 pp., 1985.
- Osterkamp, T. E. and Romanovsky, V. E., Evidence for warming and thawing of discontinuous permafrost in Alaska, Permafr. Pereglac. Proc. 10: 17-37,

1999.

- Osterkamp, T. E., Gosink, J. P., and Kawasaki, K. Measurements of permafrost temperatures to evaluate the consequences of recent climate warming, Final report to ADOTPF, Contract 84 NX 203 F 233181, December 1987a.
- Osterkamp, T. E., Harrison, W. D., and Hopkins, D. M. Subsea permafrost in Norton Sound, Alaska, *Cold Regions Science and Technology*, vol. 14, 173-180, 1987b.
- Osterkamp, T. E., Baker, G. C., Harrison W. D., and Matava, T. Characteristics of the active layer and shallow subsea permafrost, J. Geophys. Res., 94(C11), 16, 227-16, 236, 1989.
- Outcalt, S. A numerical model of subsea permafrost, Freezing and Thawing of Soil-Water Systems, Technical Council on Cold Regions Engineering Monograph, 58-65, 1985.
- Romanovskii, N. N. and Tipenko, G. S. Regularities of Permafrost and Gas Deposits Interaction, Earth Cryosphere, v.II, #1, 3 – 10, 1998.
- Romanovskii, N. N., Kholodov, A. L., Gavrilov, A. V., Tumskoy, V. E., Hubberten, H. W., and Kassens, H. Ice-bonded Permafrost Thickness in the Eastern Part of the Laptev Sea Shelf (results of computer modeling). Earth Cryosphere, v.III, #2, 22 – 32, 1999.
- Romanovsky, V. E., Maximova, L. N., and Seregina, N. V. Paleotemperature Reconstruction for Freeze-Thaw Process During the Late Pleistocene Through the Holocene, 1989.
- Sloan, E. D., Jr. Clathrate hydrates of natural gases, 641 pp., Marcel Dekker,

Inc., New York, NY, 1990.

- Swift, D.W., W.D. Harrison and Osterkamp, T. E. Heat and salt transport processes in thawing subsea permafrost at Prudhoe Bay, Alaska, Proc. of the Fourth Int. Conf. on Permafrost, July 18-23, 1983, Fairbanks, AK, National Academy of Sciences, Washington, DC, 1983.
- Tipenko, G. S., Romanovskii, N. N., and Kholodov, A. L. Simulation of the Offshore Permafrost and Gas Hydrate Stability Zone: Mathematical Solution, Numerical Realization and Records of the Calculation. Earth Cryosphere, v.III, #3, 71 – 78, 1999.
- U.S. Geological Survey, Alaska Topographic Series, 1976.
- United States Department of Commerce National Oceanic and Atmospheric Administration. Bering, Chukchi, and Beaufort Seas Coastal and Ocean Zones Strategic Assessment: Data Atlas. Preliminary Edition 1985.